Active Removal of Space Debris with Space-Based Lasers

Performance and Requirements

A thesis accepted by the Faculty of Aerospace Engineering and Geodesy of the University of Stuttgart in partial fulfillment of the requirements for the degree of Doctor of Engineering Sciences (Dr.-Ing.)

by

Dipl.-Ing. Manuel Schmitz

born in Simmern (Hunsrück)

Committee chair:	Prof. Dr.-Ing. Jens von Wolfersdorf
Committee members:	Prof. Dr.-Ing. Stefanos Fasoulas
	Prof. Dr.-Ing. Roger Förstner
Date of defence:	February 8, 2016

Institute of Space Systems
University of Stuttgart
2016

Acknowledgment

This thesis has been written within the frame of a cooperation between Airbus Defence and Space and the Institute of Space Systems. I would like to thank the Future Programmes department at Airbus Defence and Space in Friedrichshafen for funding this research project.

Moreover, this work would not have been possible without the assistance and support of my supervisor, Prof. Stefanos Fasoulas. I am also indebted to many of my colleagues, most notably (but by no means only) Dr. Jens Utzmann and Dr. Jürgen Wiedmann, who patiently gave me advice and provided suggestions of major importance. Furthermore, my gratitude extends to Klaus Pfefferkorn and Dr. Georg Herdrich, who encouraged me in times of need.

Contents

List of Acronyms

ASAT anti-satellite weapon

AVX Advanced Vector Extensions

BAU business as usual

CHOM Common Heritage of all Mankind

COIL chemical oxygen iodine laser

CPU central processing unit

CW continuous wave

DLR German Aerospace Center

ECI Earth-centred inertial

ESA European Space Agency

FoV field of view

GEO Geostationary Orbit

GPS Global Positioning System

GSO Geosynchronous orbit

IADC Inter-Agency Space Debris Coordination Committee

ICAN International Coherent Amplification Network

IP Internet Protocol

ISS International Space Station

ITP Institute of Technical Physics

LCI laser-centred inertial

LEO Low Earth Orbit

MASTER Meteoroid and Space Debris Terrestrial Environment Reference

MEO medium Earth orbit

MSX Midcourse Space Experiment

NASA National Aeronautics and Space Administration

NORAD North American Aerospace Defense Command

PMD post-mission disposal

PROOF Program for Radar and Optical Observation Forecasting

SGP4 Simplified General Perturbation

SIMD single instruction multiple data

SiS Security in Space

SQL structured query language

SSA space situational awareness

SSDW Space Station Design Workshop

SSN United States Space Surveillance Network

SSO Sun-Synchronous Orbit

TLE two-line element

Nomenclature

(debris) population The set of all debris objects at a given epoch in time.

(space) object An orbital item that is distinguishable from others by a difference in orbital trajectories or regions. This thesis deals with two types of space objects: debris and a laser satellite. The term is used differently in other contexts [1].

ablation threshold The *fluence* at which material ablation is caused by incident laser radiation. Below this threshold only melting occurs. The value depends on the pulse width τ and the irradiated material. It is denoted with the symbol Φ_{th}. (→ Eq. 2.1 on p. 26)

active object An object that is not debris.

catastrophic collision Collision with kinetic energy to target mass $> 40\,J/g$ [2].

coupling coefficient Macroscopic parameter describing *laser-ablative propulsion*: (1) Ratio of momentum change per beamed laser energy or (2) ratio of thrust per incident irradiation power. It is denoted with the symbol C_m. (→ Eq. 2.6 on p. 35)

Crossing Generator Name of the numerical code implementation that simulates the far-field motion of the laser satellite w.r.t. the debris population. It employs a discrete element approach, guiding debris objects and a laser satellite along their orbital trajectories. It supports plug-in routines to handle collisions between debris and satellite in a user-defined way. (→ pp. 55ff)

crossing The passing of a target object flying through the influence sphere of the laser. The influence sphere usually has the radius R_{max}.

debris (object) An anthropogenic object that is either defunct, apparently purposeless, or unintentionally hazardous.

engageable object A *favourable object* that does not exceed an angular velocity limitation while in a favourable position. There is at least one *interaction time* for this object. An engageable object is not necessarily engaged during the mission, because the *engagement policy* may decide against an *engagement*. The set of engageable objects is therefore a subset of the set of *reachable objects* and *favourable objects*.

engagement policy A set of rules that are traversed every time the laser satellite encounters an object during a *crossing* with an *interaction time*. It decides whether or not the laser will irradiate the object, by taking into account technical and operational constraints. Within this thesis, engagement policies have been implemented in a modular way, so that different operational scenarios of the sweeper model can be simulated (→ chapter 3). In a wider sense, it also decides when and why to disengage the laser.

engagement A time period during which the laser satellite irradiates a target object. An engagement can only take place during an *interaction time*.

favourable object A favourable object is a *reachable object* with a perigee above the *target altitude*, which drifts into a favourable position for de-orbitation at least once during the mission. The set of favourable objects is therefore a subset of the set of *reachable objects*.

fluence Deposited laser energy per unit area. It is commonly denoted with the symbol Φ.

graveyard orbit An orbit that keeps sufficient distance from commonly used orbital trajectories, e.g. SSO, MEO or GEO. The IADC suggests two zones to be protected from debris [3, slide 6].

interaction time A time period, during which the laser can engage an object without violating border conditions. Typical border conditions are that

(1) the object must be in range, (2) the object may not exceed an angular velocity limit, and (3) the engagement must reduce the perigee of the object. There can be multiple interaction times for one object during the same mission. There can even be multiple interaction times during the same *crossing*. The duration of the interaction time, in concert with the laser power, determines the maximum impulse that can be imparted. An *engagement policy* decides whether or not the object shall be engaged during an interaction time. If it decides to engage, there will be an *engagement*.

large-sized debris Debris with a reference diameter greater than $10\,cm$. (→ p. 2)

laser-ablative propulsion Propulsive mechanism concept: A high-intensity laser ablates small bits of mass from a target and uses the resulting recoil as thrust. Another term is *laser-impulse coupling*. (→ pp. 6, 11, 34ff, 79ff)

laser-impulse coupling → *laser-ablative propulsion*

lethal collision Collision that ends the satellite's mission [2].

maximum effective range The maximum distance at which a given laser system can effect ablation on a target. (→ p. 26)

maximum operating range The maximum distance at which a given laser system can effect ablation on an average target. It is denoted with the symbol R_{max}. (→ Eq. 2.4 on p. 27)

medium-sized debris Debris with a reference diameter between $1\,cm$ and $10\,cm$. (→ p. 2)

pulse duration → *pulse width*

pulse frequency → *pulse rate*

pulse rate Number of laser pulses per unit time. It is denoted with the symbol f. Other terms are *pulse repetition rate*, *pulse frequency* or *shots per second*.

pulse repetition rate → *pulse rate*

pulse width Duration of a single laser pulse. It is denoted with symbol τ.

reachable object An object that drifts into the *maximum operating range* of the laser satellite at least once during the mission. The set of reachable objects is a subset of the *population*.

relative situation The relative position and velocity vectors of an orbital laser and a target object for a given time epoch. It is denoted with the symbol $\vec{R}$. A *crossing* is a set of relative situations. (→ Eq. 3.13 on p. 70)

RSW-system A coordinate system that is centered in the center of gravity of the orbiting body. The y-axis points radially outward, the z-axis is perpendicular to the orbital plane and x-axis completes the right-handed system. The angle between the x-axis and the velocity vector of the object shall be minimal [4].

shots per second → *pulse rate*

small-sized debris Debris with a reference diameter smaller than $1\,cm$. (→ p. 2)

target altitude An altitude at which debris objects are considered to de-orbit and burn up quickly enough. It is denoted with the symbol r_{Peri}. The orbital laser will attempt to direct debris objects to an orbital arc with this perigee altitude. If nothing else is specified, a value of $200\,km$ is assumed. (→ pp. 48, 65ff)

theoretically reachable object An object that spends some time of its orbital revolution within the altitude range of a debris sweeper. Whether an object is a theoretically reachable object can be tested with eq. 3.5 on page 63. It accounts for the second branching of the mission performance model (→ Fig. 3.26).

Index of Physical Quantities

The units are given in the parentheses after the names of the quantities. Some physical quantities that are not listed in this index are local definitions of the chapter, the section, the subsection or the paragraph (e.g. coefficients in empirical equations).

A_f surface of a focal spot (m^2)

A_{tgt} (mean) cross section of target object (m^2)

a_L semi-major axis of laser orbit (m)

c_e effective exhaust velocity $(\frac{m}{s})$ ($\rightarrow$ [5, Eq.2.10])

C_m laser-ablative coupling coefficient $\left(\frac{N}{W} = \frac{Ns}{J}\right)$ ($\rightarrow$ pp. xi,35)

$D = D_{obj}$ (mean) diameter of target object (m)

d_f diameter of focal spot (m)

d_{Aper} diameter of primary aperture, diameter of focussing element (m)

e_L eccentricity of laser orbit $(-)$

F force, thrust (N)

f pulse rate of laser, shots per second (s^{-1})

$\vec{F}_{Dir} = (X, Y, Z)^T$ direction of the object's Δv, unit length $(-)$

$g_0 = 9.80665\,\frac{m}{s^2}$ (mean) gravitational acceleration

H_L (mean) altitude of laser (m)

I_{sp} specific impulse (s)

i_L inclination of laser orbit $(-)$

M^2 M squared, beam quality factor $(-)$

m_0 (initial) mass of target object (kg)

P power (W)

P_{emit} power of emitted laser light (W)

Q heat (J)

$\vec{R}$ relative situation (state vectors of laser and object at a specific time (→ p. xiv)

$R_{E,eq} = 6378.16\,km$ equatorial Earth radius

R_{max} maximum operating range of laser (m) (→ pp. xiii,27)

r_{Peri} target altitude (m) (→ pp. xiv,48,65ff)

t_i epoch of (arbitrary) time step since begin of mission (s)

t_{i+1} epoch of subsequent time step (s)

W energy, work (J)

W_p energy of a single laser pulse (J)

X first component of $\vec{F}_{Dir}$ $(-)$

Y second component of $\vec{F}_{Dir}$ $(-)$

Z third component of $\vec{F}_{Dir}$ $(-)$

z focal distance (m)

Δt time step increment (s)

Δv change of velocity (of target object) $\left(\frac{m}{s}\right)$

$\Delta\Omega$ change of ascending node parameter $(-)$

$\Delta\omega$ change of periapsis parameter $(-)$

δs misalignment of beam in focal plane (m)

$\delta\Theta$ maximum allowed pointing error $(-)$

η efficiency, overall efficiency of laser $(-)$

λ laser wavelength (m)

μ specific ablation energy $\left(\frac{kg}{J}\right)$

$\pi = 3.14159265358979323846$ ratio of circumference to diameter of a circle $(-)$

σ standard deviation of position knowledge (m)

τ laser pulse duration (s)

Φ laser fluence $\left(\frac{J}{m^2}\right)$

Φ_{th} ablation threshold fluence $\left(\frac{J}{m^2}\right)$ (→ pp. xi,26)

Ω right ascension of the ascending node $(-)$

ω argument of the periapsis $(-)$

ω_{OL} angular velocity of the object w.r.t. the laser $(s^{-}1)$

Abstract

Space debris has recently become a topic of elevated interest. As the threat of an uncontrollable collision cascade among defunct space objects, known as the Kessler syndrome, is being discussed, the stakeholders and decision-makers have begun to consider the active removal of orbital debris. Thus motivated, the space community has begun conceiving and studying technical concepts for the realization. The bulk of them address the removal of larger bodies from orbit. These are catalogued and have the potential of fragmenting into a high number of new, dangerous objects. This thesis, however, treats a concept for the removal of the medium-sized ($1\,cm$ to $10\,cm$) debris objects. These are by far more numerous and are not catalogued. They have a comparable destructive potential but may be even harder to pick from their orbits.

The remediation concept treated herein employs a space-based, high-power laser. By engaging objects in the size regime of $1\,cm$ to $10\,cm$, and causing laser-induced surface ablation on a substantial subset of the debris population, the objects' perigees shall be reduced, so that they will re-enter the atmosphere quickly and eventually burn up.

Although this mission concept has been studied in the past, essential key aspects have not yet been analysed in sufficient depth. In fact, important parts have only been covered by rough estimates and rule-of-thumb calculations. Among these topics are: The number of reachable debris objects, the necessity for orbital manoeuvres to be performed by the laser, the impact of the relative motion between laser and debris in the near field, and the connection between the laser optics and orbital mechanics. This thesis determines the boundaries in which a space-based laser debris removal can be performed. It identifies the necessary assumptions and the prerequisites, and derives technical system requirements for

an implementation.

For this purpose, a generic and comprehensive mission performance model is established. The model employs a discrete element approach, which is implemented as a numerical code. It allows performing case studies of individual missions as well as systematic parameter scans and optimizations. Additionally, it provides insight into the relevant mechanisms that are driving the performance: The user can tell why a particular scenario is strong or weak, and iteratively tune the mission and system parameters of the orbital debris sweeper platform. Three performance-driving quantities have been identified: The laser range, the tracking agility and the laser's power.

This computer-based model is used to identify the constraints and the boundary conditions of the mission concept in general, framing a 'design space' of missions. Finally, three exemplary sweeper missions are presented as a demonstration of the model's capabilities. Requirements for their technical implementation are estimated, along with an analysis of their remediation performance. The balanced scenario is shown to be capable of reducing the debris density in the most polluted orbital regions by 23 % in 10 years.

Zusammenfassung

Das Thema Weltraumschrott hat in den letzten Jahren an Bedeutung gewonnen. Während das Bedrohungsszenario einer unkontrollierbaren Kollisionskaskade, bekannt als 'Kesslersyndrom', diskutiert wird, haben verschiedene Interessensgruppen und Entscheidungsträger begonnen, die aktive Entfernung von Weltraumschrott in Erwägung zu ziehen. Dies motiviert wiederum die Raumfahrtgemeinde, die technische Möglichkeiten einer aktiven Entfernung von Weltraumschrott zu untersuchen. Die Mehrheit der Projekte beschäftigt sich mit der Entfernung größerer Körper aus der Umlaufbahn. Diese Objekte sind katalogisiert und bergen die Gefahr, in eine Vielzahl kleinerer, gefährlicher Teile zu fragmentieren. Im Gegensatz dazu beschäftigt sich die vorliegende Arbeit mit der Entfernung mittelgroßer ($1\,cm$ bis $10\,cm$) Schrottstücke. Davon existiert eine weit größere Anzahl. Sie sind nicht katalogisiert und das Schadenspotential ist vergleichbar. Gleichzeitig erscheint es schwieriger, diese zu beseitigen.

Der vorgestellte Ansatz bedient sich eines satellitengestützten Hochenergielasers. Damit werden die Zielobjekte beschossen, so dass Laserablation stattfindet. Die dadurch verursachten Impulsänderungen verringern die Perigäen der Objekte, welche in der Folge zeitnah in der Atmosphäre verglühen.

Wesentliche Aspekte sind nicht in hinreichender Tiefe abgeklärt, obwohl dieser Ansatz in der Vergangenheit bereits untersucht wurde. Wichtige Teilbereiche wurden bisher nur durch Schätzungen und überschlagsweise Rechnungen abgedeckt. Zu diesen Themen gehören: Die Anzahl der überhaupt erreichbaren Objekte, die Notwendigkeit von Bahnmanövern, die Relativbewegung von Laser und Schrott im Nahbereich und der Zusammenhang zwischen Laseroptik und Bahnmechanik. In der vorliegenden Arbeit wird der Rahmen abgesteckt, in dem eine Entfernung von Schrott mit einem satellitengestützten Laser sinnvoll sein kann.

Die dazu nötigen Annahmen und Voraussetzungen werden identifiziert und Anforderungen an die technische Implementierung werden bestimmt.

Zu diesem Zweck wird ein vollständiges, generisches Modell für die Abräumleistung aufgestellt und validiert. Dieses basiert auf einem Partikelansatz, welcher in einem numerischen Code implementiert wird. Es ermöglicht die Simulation einzelner Szenarien im Rahmen von Fallstudien, aber auch systematische Parameterscans und Optimierungen. Zusätzlich lassen sich Aussagen über die leistungsrelevanten Zusammenhänge des Missionsekonzepts gewinnen: Der Anwender erfährt, warum ein bestimmtes Szenario gut oder schlecht ist und kann iterativ die System- und Missionsparameter anpassen. Drei dominierende Einflussfaktoren auf die Abräumleistung werden identifiziert: Die Reichweite des Lasers, die Agilität der Nachführung des Laserstrahls und die Leistung des Lasers.

Dieses Computermodell wird verwendet, um die grundlegenden Einschränkungen und Randbedingungen des Konzepts zu bestimmen. Dadurch wird ein 'Raum der möglichen Missionen' abgesteckt. Abschließend werden drei exemplarische Missionsszenarien herausgegriffen und zur Veranschaulichung des Modells vorgestellt. Für jedes dieser drei Szenarien wird der Abräumerfolg berechnet und den technischen Anforderungen für die Umsetzung gegenübergestellt. Es wird gezeigt, dass das mittlere dieser Szenarien die Schrottdichte der am stärksten betroffenen Höhenbereiche in 10 Jahren um 23 % senken kann.

1 Introduction and Motivation

Near-Earth space, ranging from its lower border $100\,km$ above the planetary surface up to the Geostationary Orbit (GEO) region, can be considered the most valuable natural resource in space. The majority of our space activities take place there, and these are the ones that affect our everyday life: weather forecasting, communications, satellite television, space-based navigation services (e.g. GPS), Earth sciences, agriculture-related services and arms control.

This natural resource is limited, and it is currently being used up at an alarming rate. Its primary value - besides its closeness to our home planet - lies in its almost perfect emptiness. However, junk objects such as discarded satellites, spent rocket stages and a vast number of smaller fragments fill up this delicate emptiness. The process started with the beginning of the space age in the late 1950s, when there was little concern that the available free space may some day be all occupied.

1.1 Space Debris: An Emerging Problem

Currently, there are more than $17,000$ space objects in the catalogue of the United States Space Surveillance Network (SSN) [6], with only about $1,200$ of them being active satellites [7]. A collision threat emanates from all the other, inactive and uncontrollable objects: The space debris.[1]

The only natural self-cleaning mechanism in the near-Earth space is the residual atmospheric drag. However, the orbital lifetime of objects beyond $400\,km$ is measured in decades or centuries (Fig. 1.1). Therefore, it is likely that an object eventually collides with another object.

[1] The exact definition of 'space debris' is currently under discussion, and the debate is influenced by numerous political interests [1].

Their collision probability per unit time depends on the number of potential collision partners, and each collision generates new objects (fragments), so that the growth of the debris density follows an exponential population dynamics ('snowball effect'). This positive feedback loop of the orbital debris population growth was described first by Donald J. Kessler in 1978, and has become known since then as the Kessler syndrome. He warned that when the density of the debris becomes sufficiently high, a collision cascade is triggered and accidental collisions become the primary source of new space debris [8].

Currently, there is an ongoing discussion in the space community about whether or not the collision cascade has already started. If so, the number of the individual debris objects would keep on growing even if all human space activity stopped tomorrow. Examination of the phenomenon shows that one would have to remove about five to twenty large objects per year just in order to keep the status quo [9, 10].

If nothing is done, the debris density will reach a critical level within a few decades. This means that the risk for a spacecraft of being hit will become unacceptably high.

For reasons rooted in the orbital mechanics, the collisions usually occur at very high relative velocities of up to $14\,km/s$, and a mean value of roughly $10\,km/s$. At those velocities, even an object as small as $1\,cm$ can pass straight through the body of a satellite or rocket (Fig. 1.2). The object's specific kinetic energy is up to 23 times the specific energy of dynamite [11]. This type of impact will be catastrophic. Only impacts to peripheral elements such as solar array wings or radiators can be tolerated to a certain degree.

The space debris is categorized by object size in this thesis:

- Large-sized debris: $\geq 10\,cm$
- Medium-sized debris: between $1\,cm$ and $10\,cm$
- Small debris $\leq 1\,cm$

There are different coping strategies for these three types of debris: Satellites can be shielded against objects up to a size of $1\,cm$; the International Space

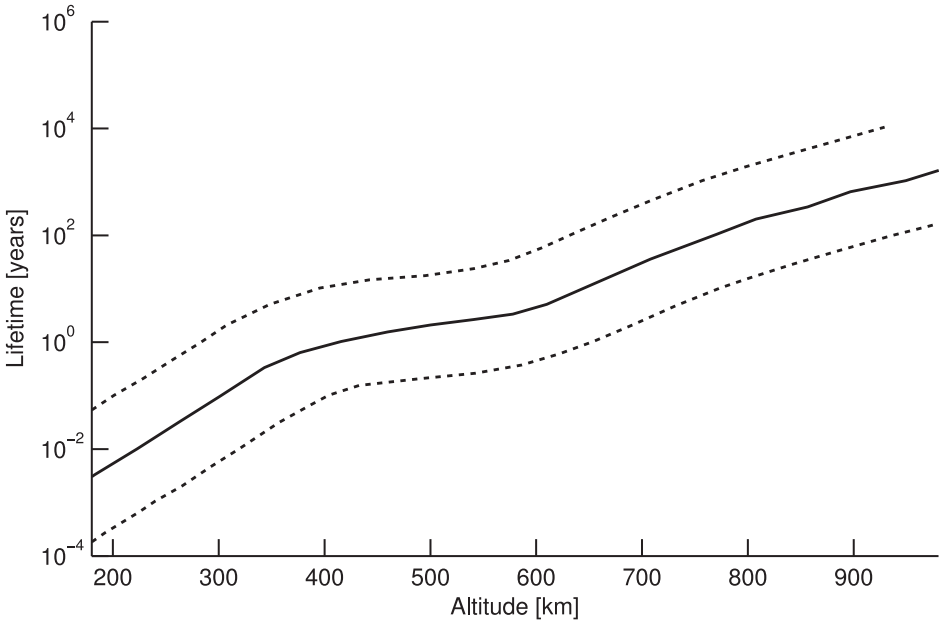

Figure 1.1: The lifetimes of orbital objects over the altitudes. The dotted lines show the possible deviations due to the influence of secondary influence factors, such as the ballistic coefficient or the solar activity [12].

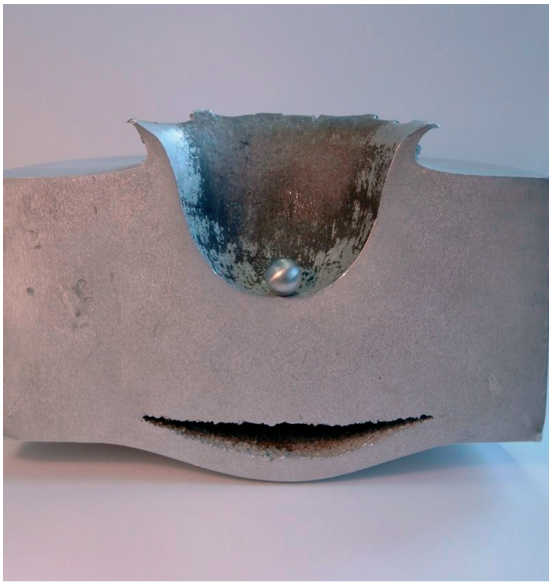

Figure 1.2: A hypervelocity impact sample [13]: This picture illustrates the destructive potential of small, but fast impactors.

Station (ISS) is shielded against objects of up to 1.4 cm [14, p.101]. The large debris $> 10\,cm$ is being tracked so that satellites can perform evasive manoeuvres and avoid collisions with them. The subset of the medium-sized objects is the most problematic, because their number is relatively high and so is the collision probability. Evasive manoeuvres are not possible, because the objects cannot be systematically catalogued and tracked. And at the same time, they are too large for efficient shielding against them.

Overall, satellites are very vulnerable and completely defenceless against the medium-sized debris. At the same time, the space debris has a high damage potential and has become one of the top hazards in space.

Since the risk of collision between debris objects and an active satellite cannot be neglected any more, the topic has found its way into the space security community. Incidents such as the collision of Cosmos-2251 with Iridium-33 on February 10th 2009 have raised awareness among the stakeholders and the decision-makers. Their natural concern is the protection of multi-billion dollar space assets. A preliminary assessment showed that the heavily used Sun-Synchronous Orbit (SSO) region between 700 km and 1200 km altitude is 'unstable' [15]. This means that the collisional cascade could be about to start, or could have already started there. In this region, the vast majority of active systems are owned by governments.

1.2 Active Space Debris Removal

In the view of the current threat, one might ask for the right course of action. During the past decades, the dominant space-faring nations have tried to mitigate the problem, mainly by limiting the creation of new debris. Codes of conduct have been established, calling for the mandatory implementation of post-mission disposal (PMD) [16, 17, 18, 19]. On national levels, the adherence to these codes has been enforced. However, the growth of the debris population still could not be prevented because, first, the mitigation codes are being fulfilled only partially, with some actors even deliberately creating additional junk. The most prominent example might be the test of a Chinese anti-satellite weapon (ASAT) [20]. Sec-

ondly, some satellites inevitably fail before their planned PMD. The breakdown of Envisat is one example among many.

It is too late for simply stopping the littering, as it will not necessarily stop the debris population from growing. Moreover, launching heavily armoured satellites is impractical for a variety of reasons: Shielding increases the systems' complexity, the launch masses and the costs. Not all parts of a satellite can be shielded for technical reasons, and a lethal collision can never be ruled out. Besides, the additional shielding mass could end up as additional debris when the satellite fails to perform PMD manoeuvres.

Finally, there are two options left: Actively clean up space, or be prepared to live with a high collision risk for spacecraft. There is a common understanding that natural resources should be used in a sustainable manner, which implicitly demands that near-Earth space should be preserved in a usable state at least. Conclusively, debris must be actively removed.

In this light, it does not surprise that the active removal of space debris has advanced to an essential part of the Security in Space (SiS) field within the last few years. SiS is a term that has been coined and used by Airbus Defence and Space, and refers to the complex of topics related to the protection of space assets against all types of potential threats. With space debris being one of these threats, the subject is a subtopic within SiS. Figure 1.3 shows how the battery of the SiS methodologies can approach the debris populations in different size regimes [21].

The necessity and the effectiveness of active debris removal has been affirmed by a majority of researchers [22, 23, 24]. However, the task of removing a piece of junk, regardless of its size, has unique characteristics: The target is uncooperative and, to a certain extent, unpredictable. There is a very high diversity in the object properties, such as size, shape, chemical composition, optical and electromagnetic properties, rotation velocity and orbit. A removal mission must not leave behind more debris than it removes. The legal requirements and implications are unclear, if not confusing, inconsistent or disputed [25, 26, 27]. There is no political framework yet where such a mission could be performed. Finally,

it has never been done before. The removal of individual or multiple objects from orbit appears to be an extraordinary challenging task.

Although there is no historical reference for an active removal mission, and there is not even a convincing technical concept, a variety of approaches have been suggested and discussed: the de-orbitation by a one-shot chaser [28, 29], the attachment of drag enhancement devices, electrodynamic tethers [30, 31], motor-driven slingshot tethers, booster packages [32], expanding foam [33], and ion-beam shepherds [34], among others. All of these concepts have one thing in common: They target the removal of individual, large objects such as decommissioned satellites or burned-out rocket stages.

Less attention has been spent on the removal of medium-sized debris, ranging from $1\,cm$ to $10\,cm$ in size, of which there are more than 20 times as many objects. They are particularly dangerous to active spacecraft, because the collision probability is relatively high due to their large number (Fig. 1.4). One of these objects can destroy a space asset just as a larger object can. In fact, some have argued that the immediate, short-term threat to satellites originates from these medium-sized objects, while the large-sized debris will become medium and small-sized debris in the future. Therefore, remediation efforts should not only be directed exclusively towards the removal of large objects, but must also consider the removal of medium-sized debris [23].

It might surprise that ideas and concepts for the removal of these particularly dangerous, medium-sized debris objects are so rare. Maybe, this is because the

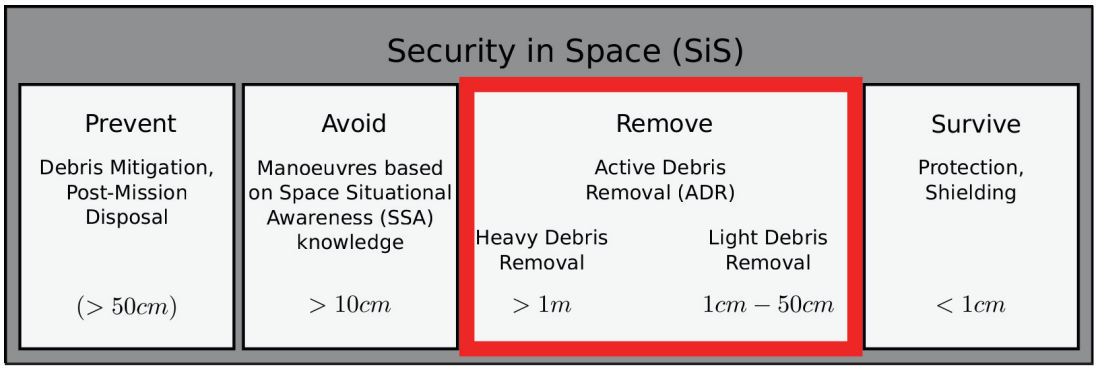

Figure 1.3: Active debris removal in the SiS context (inspired by [21])

task appears even more difficult:

Removal concepts for larger junk usually require rendezvous operations with each targeted object. This is costly in terms of fuel and time, and therefore impractical when dealing with a high number of smaller objects. The use of high-power lasers appears to be one of the (very) rare means by which the medium-sized debris can be addressed: When a high-intensity pulsed laser engages an object, it ablates small bits of mass. The resulting recoil will change the velocity of the targets, lowering the perigees, so that the objects' orbital lifetimes are reduced (Fig. 1.5). Sometimes, this interaction mechanism is called 'Laser-ablation propulsion' [36] or 'Laser-impulse coupling' [37].

Laser ablation is a widely used industrial process [38, 39], and devices harnessing the generated recoil have already been developed to the maturity of engineering models [40, 41]. Although the effectiveness of the mechanism in the context of space debris has not yet been ascertained on an experimental level, laser-based debris sweeper systems have been suggested.

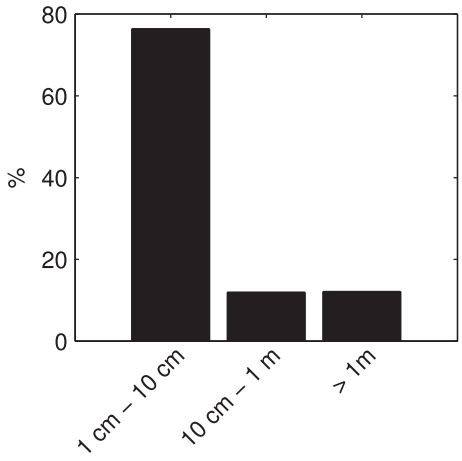

Figure 1.4: Relative collision probability for a 767 km SSO satellite with debris of different size regimes. Data calculated by MASTER [35].

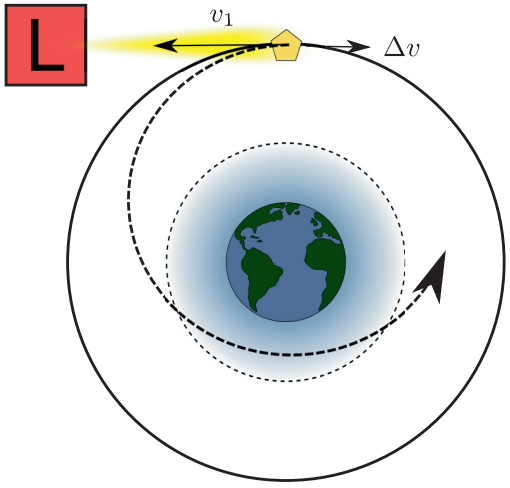

Figure 1.5: The laser shall lower the target objects' perigees

The laser can be placed on the ground or in orbit. So far, ground-based concepts have been studied [42, 43, 44, 45, 46], most notably within the ORION study in the 1990s [47, 48]. Since June 2011, there is a European project to pursue the idea of a ground-based laser debris removal system. It is named CLEANSPACE, and aims at defining a global architecture for the removal of medium-sized debris, including the topics surveillance, identification and tracking [49, 50]. Much less work has been done investigating the possibility of placing the laser into space. There may be considerable advantages compared to a ground-based solution, most notably a reduction of the firing distance, resulting in a much smaller laser, and the absence of atmospheric interference.

So far, all publications until now are case studies. They aim at proving the feasibility by providing a viable mission example [51, 52, 53]. However, they may not represent a favourable or optimal design point.

1.3 Thesis Objectives

It is the objective of this work to determine the boundaries in which space-based laser debris removal can be performed. More precisely, the interplay between the removal strategy, the mission profile, the key system figures and the removal performance is to be unravelled, so that the 'space of possible mission variants' can be explored and outlined.

With this in mind, the debris sweeper's mission will be described in a mission model, so that the remediative impact on the debris population can be predicted. Besides the prediction of the removal performance, the model shall assess the technical and the technological requirements for the implementation of the mission. In other words: 'To what extend can a sweeper relieve the debris problem, and how complex would the necessary system be?'

The predictive model shall be generic in nature and accept the broadest sensible set of input parameters. Once the model is established and validated, it can be used to conduct case studies for different variants of the sweeper. Having a parametric model would also allow for the optimization of mission scenarios and permit systematic parameter studies. Such parameter scans can be used to

probe the input parameter ranges for boundary conditions. Since the model is generic, these boundaries would be the fundamental limitations of the mission concept.

As a first step, the current state-of-the-art of science and technology will be reviewed, and the relevant key aspects will be collated and examined (sec. 2.1). Some points will require further in-depth analysis, which will be performed over the course of this thesis (sec. 2.2 to 2.7).

Then, the mission performance model will be developed, which incorporates the extracted relationships between the removal strategy, the mission profile, the key system parameters and the remediation performance (chapter 3). By using the model, boundaries for the mission parameters can be obtained, as well as information on the technical and the technological requirements of a space-based debris sweeper (chapters 4 and 5).

2 Mission Concept and Relevant Aspects

The mission concept examined herein aims at the removal of medium-size debris, although this concept could theoretically also be used for the removal of larger or smaller objects [11]. Judging from the distribution of the debris density over altitude (Fig. 2.1), the demand for an active removal is the highest in the Low Earth Orbit (LEO) region from 600 km to 1200 km.

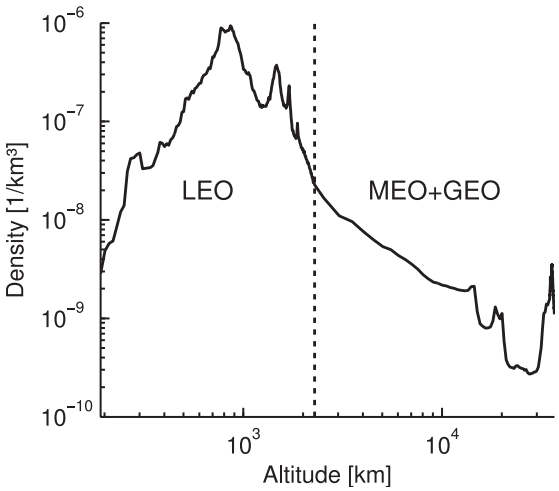

Figure 2.1: Debris density 1 cm to 10 cm

The proposed mission removes debris objects by using laser-ablative propulsion: The targeted objects are illuminated with a very high-intensity laser beam, leading to ablation. The ablated vapour or plasma expands into space, acting like a thruster and changing the target's trajectory. The basic idea is to change the trajectory of a high number of objects, so that they will cross denser atmospheric layers during their orbital revolutions ('aerocapture').

Before one can start assembling the mission model, one must be aware of the mission concept's primary driving mechanisms; one needs to know its fundamental logical relationships, its underlying working principles, and its immanent problems.

This chapter will start with a review of the pertinent scientific publications, and provide a chronological synopsis of laser debris sweeper studies. From these exemplary studies, the relevant mission aspects will be extracted. Afterwards, these aspects will be detached from the context of previous studies and elaborated on in a more generic context. An attempt will be made to strip the individual facets down to their essence. The generalized relationships will then serve as building blocks for the performance model in chapter 3.

2.1 Review of Historical Debris Sweeper Studies

2.1.1 Nuclear-Powered Space Debris Sweeper (1988)

Summary

One of the first suggestions for an orbital laser debris sweeper has been published in 1988 by John Metzger et al. [51]. The paper outlines a debris sweeper with a total mass of around $6300\,kg$, which roams the LEO region and engages debris objects in the $1\,cm$ to $5\,cm$ size range. Their number is estimated to be around $40,000$.

The publication first drafts a mission concept, then recapitulates the relevant facts about laser-ablative propulsion, derives requirements for the laser, and finally sketches a possible system design.

The paper describes a mission profile, in which the laser performs one target engagement every hour. Frequent orbital manoeuvres of the laser platform guarantee a corresponding supply with fresh targets. A target object can be completely de-orbited in one pass, so that the laser platform can clean up the entire near-Earth space within five years.

The publication also summarizes the relevant facts about laser-ablative propulsion: The interaction between the laser beam and a target object is modelled by a macroscopic coupling coefficient C_m. It provides the link between optics and mechanics by describing the ratio of the generated momentum per incident laser

energy. In theory, this coefficient depends on the laser wavelength, the pulse duration, the intensity and the target material.

There is an intensity when the C_m becomes maximal, called the 'point of optimum coupling'. Figure 2.2 illustrates the trend of C_m over the intensity. For intensities below the optimum coupling, the ejected vapour is not given enough energy for high exhaust velocities. On the other side, for intensities above the optimum coupling, there are energetic losses due to photochemical dissociation and ionization.

For the debris sweeper concept study, a simplified version of the interaction model is used. The provisional assumption is made that all debris objects consist of aluminium. Experimentally determined C_m data is available for aluminium. The targets are spherical in shape, they are always hit at their centre, and the laser has a Gaussian beam profile. The imparted velocity change vector is parallel to the laser beam, and the system operates near the intensity of optimum coupling.

The authors have picked three representative debris objects from $0.5\,cm$ / $0.027\,g$ to $2.5\,cm$ / $0.675\,g$ and calculated the imparted velocity change Δv per

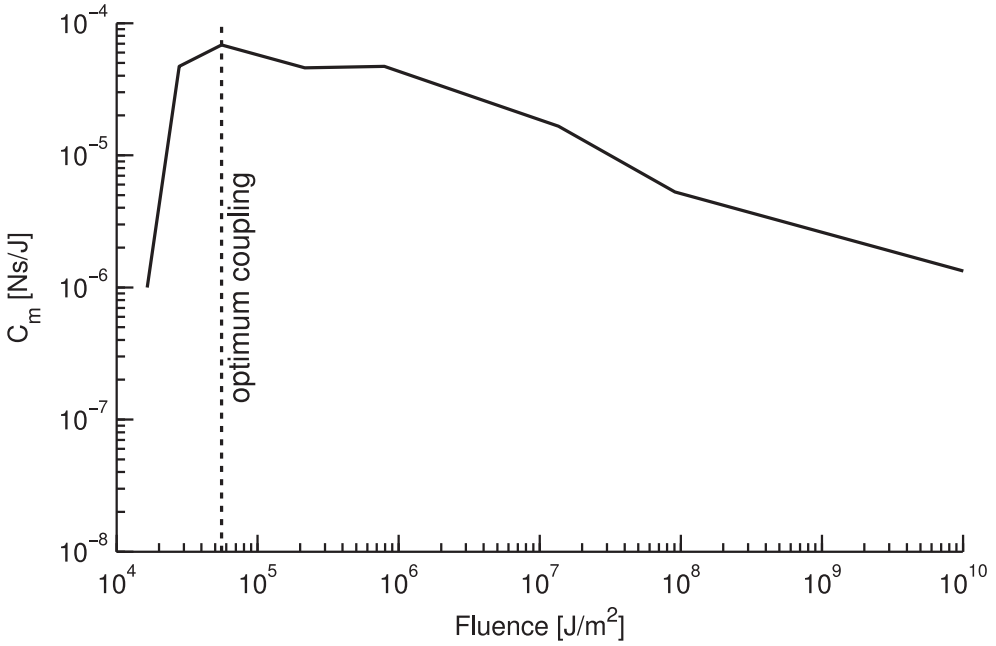

Figure 2.2: Coupling over intensity [51]

laser pulse. Showing that sufficient Δv can be transferred with a realistic pulse count, the viability of the concept is demonstrated.

Through the analysis of the interaction model, the paper derives four requirements for the laser: First, the laser shall be able to deliver short, intensive pulses. The shorter the pulse duration, the less energy is thermally conducted away from the zone of ablation, which would curtail the efficiency. For the same reasons, continuous wave (CW) lasers would be impractical. Secondly, short wavelengths are favourable for a number of reasons. Wavelengths in the lower visible or ultraviolet region are closer to the photochemical absorption bands of the target material. Apart from that, shorter wavelengths penetrate deeper into the material, and are easier to focus. Thirdly, the pulse rate shall be moderate, and fourthly, the beam quality should be high for good focussing.

Based on these requirements, a laser for the sweeper is selected. Solid-state sources, such as Nd:YAG lasers, are dropped from further consideration because sufficiently high pulse energies cannot be achieved. CO2 lasers have an excessive wavelength. Apart from free electron lasers, which are deemed adequate, excimer lasers are considered favourable. A KrF laser with $248\,nm$ wavelength is suggested as a baseline, because they can generate pulse energies as high as $10\,kJ$ and have an efficiency of $10\,\%$.

The operational range of the laser is determined by the size of the focal spot, which shall be nearly equal to the size of the target. One would increase the sweeper's range by enlarging the focussing mirror.

A firing range of up to $10\,km$ is chosen, at which the laser fires $10\,kJ$ pulses at a repetition rate of about $1\,Hz$. The laser engages its targets when they are in the lower hemisphere as seen from the laser, and the applied impulse change is always retrograde with respect to the target. Judging from the estimated debris flux and the surface area of the $10\,km$-hemisphere, the laser needs to perform orbital manoeuvres in order to reach enough debris objects.

The laser platform's orbit adjustments are both in-plane and off-plane. In-plane manoeuvres are performed to reach and sweep additional altitudes, while plane-changing firings are conducted to shorten the interim time between the

engagements. Chemical and electrical propulsion are considered, concluding that an electrical arcjet system with a power consumption of about 100 kW is likely to be the favourable choice. In any case, a SP-100 type nuclear reactor is believed to be the optimum source of energy for the sweeper. The 3800 kg nuclear reactor also dominates the sweeper's overall mass.

The time-averaged required laser energy is calculated to be 55 W. Two hundred kilojoules need to be generated between two engagements and stored until the next firing phase.

Comment

When outlining the debris sweeping satellite, the authors have been relying on a number of assumptions.

First, the assumed debris population is based on the 1976 North American Aerospace Defense Command (NORAD) debris census, and a 5 % population growth over 20 years. This information is outdated, although it had been a valid presumption back in 1989. Nonetheless, a contemporary examination of the mission concept must take into account more recent models of the debris population.

Furthermore, it is assumed that the debris objects are on nearly circular orbits. Because the bulk of the medium or the small sized objects has been generated by explosions or collisions, at least some of them will have a substantial eccentricity. Whether or not eccentric target orbits have a relevant impact on the mission concept remains to be investigated.

The laser-induced velocity changes are always retrograde, regardless of the relative position of the laser w.r.t. the object. In practice, the relative position can have a considerable impact on the direction of the laser-ablative force that is imparted onto the target. It is yet unclear how this affects the removal performance: there may be situations in which the object's perigee is increased instead of lowered, or at least the necessary Δv for a de-orbitation is substantially higher.

Moreover, a target perigee of 300 km for the debris is claimed to be sufficient. While this assumption is certainly suitable for a first-shot evaluation of the mission concept, there is no supporting rationale that the atmospheric drag will then cause a prompt re-entry. This leaves the particular value for this quantity open

for debate.

The available interaction times have not yet been considered. It could be possible that debris objects will be passing by so quickly that objects will have to be engaged multiple times, especially when the pulse rate of the laser is as low as $1\,Hz$. Given the maximum operating range of the laser of $10\,km$ and relative velocities in the domain of kilometres per second, only few pulses can be delivered to the objects.

Just as the interaction times, the number and the magnitude of the orbital manoeuvres of the laser depend on a more detailed picture of the debris population. This is a far-reaching statement, considering that the orbital manoeuvring dominates the power requirements and the mass budget of the system.

In the Metzger study, the operational range of the laser is determined by the size of the primary aperture. But how large would the mirror have to be? And how fast does it need to be rotated in order to keep track of the passing objects? For very high power lasers with good beam quality, the optical destruction threshold of the optical components can represent an additional limitation.

If both, the focal spot and the target, were only few centimetres wide, then the pointing accuracy of the beam would be in the microradian domain or smaller. This would imply that the object's position will have to be known with millimetre precision. However, the detection of targets, the tracking or the cueing requirements remain to be analysed and discussed.

Moreover, the laser selection argumentation has been obsoleted by technical progress since 1989. Today, solid-state disc lasers feature a firm development perspective towards high pulse energies, short pulses and a fair beam quality. A reconsideration of the laser selection, respecting today's leading-edge technologies, would be justified.

There are also far-reaching assumptions in the field of the laser-debris interaction. First, it is said that the focal spot size should be as large as the target. However, there might be circumstances under which a certain beam overspill seems acceptable or even desirable. For example, the assumption that the beam is always centred on the target may not hold for a finite pointing accuracy of the laser beam. A focal spot that is larger than the target allows for a slight misalignment of the beam without cutting the laser-ablative thrust.

Secondly, if the focal spot were allowed to be larger than the target, then the beam would not be strong enough to ablate at large distances. Then, one would have to consider the ablation threshold of the target material as an additional constraint for the laser's operating range.

Thirdly, a Gaussian beam profile has been assumed, but the selected KrF laser is likely to have a rectangular beam profile. (This approximation will yield smaller inaccuracies if the focal spot is allowed to be larger than the object.)

Fourthly, the targets are treated as spherical objects in order to keep the model complexity manageable. At the same time, the authors recognize correctly that the coupling depends on the angle of the surface normal w.r.t. the laser beam. Conclusively, irregularly shaped targets should at least exhibit different coupling characteristics. However, the influence of the target shape still needs to be investigated and taken into account.

Fifthly, the laser shall operate in the intensity of the optimum coupling, but no reason is given. Maybe it would be beneficial to relax this constraint in favour of other advantages. In view of the unknown shapes of the targets, it seems difficult to tune the laser intensity for the optimum coupling anyway. Moreover, most of the objects pass with high relative velocities, and the available interaction time is limited. Delivering a high amount of energy in a short time frame could be more important than a high coupling.

Finally, it is not explained why objects passing below the sweeper would be engaged, but objects above would not. This appears to be a rather arbitrary choice.

Overall, the 1989 proposal is a typical first-order analysis of the concept, and therefore based on numerous non-trivial assumptions. This is why the sensitivities of the design w.r.t. key parameters or assumptions are left in the dark. Additionally, some presuppositions are outdated today. Nonetheless, reviewing the publication revealed that there are at least two cruxes. One is the kinematics of the mission, which is governed by the laws of orbital mechanics. The other is the interaction between the laser and the debris.

A sound investigation of the first issue, the mission kinematics, would have required a detailed picture of the orbital properties of the debris population, but sufficiently advanced debris models have not been available 25 years ago. For this reason, John Metzger and his colleagues were forced to conclude that the

'mode of operation will require extensive study'.

2.1.2 Space Station Protection Study by the DLR (1998)

Summary

In 1998, nine years after the nuclear-powered sweeper had been proposed, Wolfgang Schall of the German Aerospace Center (DLR) has published a paper suggesting an orbital laser platform to protect the ISS against debris impacts [52]. Besides the protection option, the proposed system would also be capable of cleaning up the LEO.

The paper begins with the introduction of a few assumptions (debris population, laser, coupling, ...) and then calculates the performance and the limits of a possible laser station.

His sweeper system targets objects between $1\,cm$ and $10\,cm$ in size. Eccentrically orbiting the Earth between $400\,km$ and $1200\,km$ altitude, a gas laser with an operating range of $100\,km$ sets out to clean the LEO within a few years. In contrast to the nuclear-powered debris sweeper, orbital manoeuvres do not play a key role. Instead, two natural effects feed new objects to the laser: the relative drift of the orbital planes, which is caused by the Earth's oblateness, and the residual atmospheric drag.

Schall considers using an ArXe-laser with $1\,kJ$ pulse energy and a $100\,Hz$ repetition rate. It has $2\,\%$ efficiency, and one engagement is planned for every 12 minutes. He has calculated that there is a roughly $4\,kW$ average power consumption, assuming that the focal spot generally has the same size as the targets.

The rate of five engagements per hour is estimated by calculating the volume of a 'hose' along the laser's orbital trajectory. By multiplying its volume with the expected density of the debris, the number of engagements per unit time is determined.

When the laser engages the debris objects, the thrust vector is always parallel to the beam. Therefore, the retrograde, perigee-lowering component of the transferred momentum varies, depending on the relative position of the object w.r.t.

the laser. This means that the smaller the retrograde vectorial component, the more total momentum must be transferred in order to achieve the de-orbitation (or the deflection). Motivated by the debris deflection scenario, Schall performs an in-depth analysis of the influence of the relative positions of the laser and a target. Flanked by analytical considerations, a numerical approach has been employed to simulate a large number of encounters. Although the results are mostly relevant to the deflection mode of operation, they point out that the available interaction time depends on the relative geometry.

The laser, being nearly diffraction limited, has a wavelength of $1\,\mu m$ to $2\,\mu m$. It requires a primary aperture of $2.5\,m$ for reaching a maximum firing range of $100\,km$. A coupling coefficient of $20\,Ns/MJ$ is assumed, which indicates a set point near the intensity of the optimum coupling. The coupling figure is complemented with an ablation rate of $80\,\mu g/J$, which allows the estimation of the effective exhaust velocities and the ablated mass fractions. Indeed, some target objects may be evaporated completely, especially when they are crossing with an adverse relative trajectory. A minimum of $37\,\%$ of the mass is ablated in every case.

In the time between 1989 and 1998, the use of ground-based lasers for space debris remediation had been examined. The most notable effort has been the ORION study [44, 54, 55, 56] in the 1990s. The Schall paper highlights some of the advantages of a space-based laser compared to a ground-based station: There are no atmospheric distortions and no beam attenuation and the range of the laser can be substantially lower. Moreover, the space-based laser can de-orbit an object in one pass, while ORION would require multiple passes, including intermediate tracking or re-detection.

Comment

Schall has recognized the importance of the relative positions of an object and the laser. This aspect has a major impact on the direction of the laser-ablative recoil and, in consequence, on the post-engagement orbit of the object. However, the effects of the radial and the off-plane components of the imparted Δv still need to be added to the model. Both can contribute relevantly to the specific

orbital energy, depending on the geometry of the crossing. Additionally, the radial component should cause in-plane changes to the orbital eccentricity.

Moreover, he introduces an ablation rate. Until here, the laser ablation has been described by the C_m quantity only. Adding the ablation rate allows not only the calculation of a mass loss, but also the specification of an effective exhaust velocity or specific impulse I_{sp}. However, the objects should be shrinking over the course of an engagement and change their ballistic coefficient. This effect is not yet taken into account in the analysis, as well as a possible change of the geometrical shape due to the ablation.

The publication points out the advantages of the space-based sweeper compared to the ground-based variant. However, the ground station also has its undeniable advantages, e.g. the provision of electrical energy is much cheaper. Maybe both concepts are to be favoured in different fields of application. Or they could work hand-in-hand as part of an integrated concept. It must still be determined whether such a scenario is feasible.

Another completely new aspect has been brought into play by Wolfgang Schall: The laser may require service, including the exchange of wear parts. For the gas laser, one must replenish leaked gas or remove the products of unwanted chemical reactions. Other types of laser have comparable requirements, e.g. the periodical exchange of pumping diodes. This problem of wear is generic to the mission concept, regardless of a specific technology.

An average time interval between the engagements of the targets is specified. Of course, the encounters will not be evenly spaced. Some encounters may take place well before that average idle time has elapsed. Encounters could also temporally overlap. The sweeper would then have to either fire at two objects at the same time, or prioritize targets.

The paper is more specific on the durations of the engagements, or ‘available irradiation times’, than the 1989 article. It provides a distribution of the interaction times, which are in the order of seconds. This has probably been the reason for giving the laser a repetition rate of $100\,Hz$, in contrast to the $1\,Hz$ of the nuclear-powered sweeper.

The Schall study shows some of the same problems as the paper of the nuclear-

powered debris sweeper. First, the overall number of the debris objects is based on estimations, but twice as high as in the 1989 publication. The requirement for frequent orbital manoeuvres can be dropped when extending the operating range to 100 km, which is ten times the range of the nuclear-powered sweeper. This relieves the design of a far-reaching constraint.

At the same time, however, this relief adds another assumption: It is presumed that two effects would constantly be bringing new debris objects into the laser's range. One of them is the drift of the orbital planes, which is caused by the Earth's oblateness. The other one is the residual atmospheric drag. However, there is no evidence yet that these two effects can feed sufficient new objects to the laser. Especially the drift of the orbital planes depends on the distributions of the inclinations and the eccentricities of the debris. However, these distributions are unknown.

It seems that the reliable calculation of a potential removal performance can only be based on a detailed model of the debris population. Only with the knowledge of the distributions of the orbital elements of the debris one can calculate a more accurate rate of encounter. The need for such a model has been affirmed by both, Metzger and Schall.

Such a higher-definition model of the debris population could also shed light on other aspects of the mission concept. The DLR sweeper must be injected into an eccentric orbit, so that it roams a larger range of altitudes. But what if the majority of the debris objects already had eccentric orbits? Then, the laser could remain at a circular orbit with a fixed altitude and expect the objects to drop by.

Moreover, one could also determine the available interaction times and the relative geometries of the crossings with higher precision. This would also cast light on the distribution of the time intervals between the engagements, et cetera.

The topics of the detection, the tracking and the cueing of the objects will need further investigation. It is argued that the ground-based laser remediator would require a 'formidable detection and acquisition system'. Yet, there is neither an elaboration nor a quantification of some kind, nor a comparison to the requirements of a space-based sweeper.

Just as in the nuclear-powered sweeper paper, it is assumed that the thrust vector

is parallel to the beam. It is claimed that this assumption will hold if the targets are tumbling, and the number of pulses is high. This sounds sensible, but then the Δv components, which are normal to the beam, will cancel each other out after many pulses. Conclusively, there would be a penalty to the magnitude of the overall imparted Δv, which must be accounted for with an efficiency factor.

Moreover, the objects may 'jump' in the beam, because the velocity component normal to the beam changes from pulse to pulse. Generally, a discussion of the pointing accuracies would reveal additional information on the boundary conditions of the space-based sweeper concept.

Another commonality between both publications is the calculation of the operating range of the laser. Both studies maintain that the focal spot should have the same size as the target. Therefore, the range of the laser would be determined by the focussing aperture. The DLR study judges beam overspill to be a waste of energy. Again, this disregards the pointing accuracy problem and the inevitable misalignment of the beam.

The operating range of the DLR laser is ten times as high as the range of the 1989 nuclear-powered sweeper. This is curious, because its pulse energy is one tenth smaller, and the focal spot size is equal. To some extent, this can be explained by the pulse width. Schall assumes $100\,ns$, while the nuclear-powered sweeper has probably been based on the Nike laser (though not explicitly mentioned). The pulse durations of the Nike are a multiple of $100\,ns$ [57].

A tilted target surface will experience lower illumination intensity. This effect, usually referred to as 'cosine-factor', alters the coupling characteristics. The 1989 paper accounts for intensity variations, which are caused by inclined target surfaces, but the DLR paper does not explicitly mention this aspect.

The bottom line is that the DLR study sheds light on additional aspects, which had been omitted by John Metzger et al. in favour of other aspects. Most notably, the impact of the relative position of the object w.r.t. the laser has been examined by Wolfgang Schall. Some other questions remain open, such as the characteristics of the real debris population. In a few points, interestingly,

both studies contradict one another.

The most striking difference between the nuclear-powered sweeper and the DLR debris deflector is the rate of reached objects. While the nuclear-powered sweeper performs orbital manoeuvres in order to reach enough objects, Schall argues that natural perturbations can do the job just as well. It seems impossible to resolve this contradiction without a detailed model of the debris population: Only the inclination, altitude and eccentricity distributions of the debris population can describe the relevant dynamics of the debris, which includes the azimuthal plane drift. Conclusively, a realistic assessment of the performance of a debris sweeper will require a higher-accuracy modelling of the orbital debris environment.

Furthermore, the number of encountered objects per unit time depends on an interplay between the debris population, the laser range, and the orbital manoeuvres performed by the laser. A systematic, parametric and generic modelling of that relationship would reveal a central part of the mission's kinematics.

The remaining part of the mission kinematics is the relative motion of the debris objects w.r.t. the laser. The Schall study puts an emphasis here, but makes some non-trivial assumptions and leaves aside the radial and the off-plane components of the laser-ablative recoil. These simplifications are unproblematic in the context of a protection/deflection scenario. Yet, they deserve a more elaborate assessment for the debris de-orbitation case, where the longer-term post-engagement trajectory is most important.

This aspect is linked to the choice of a target altitude. The Schall paper aims at reducing the perigees of the targets to below $100\,km$, while Metzger and his associates have deemed a perigee of $300\,km$ as sufficient. Generally, the post-engagement altitude determines the residual orbital lifetime of an object. The acceptable value for the residual lifetime depends strongly on an individuals' perspectives, so that choosing a particular value should be avoided. Ideally, the quantity would be a free parameter of a more versatile mission model.

Another fundamental difference between both studies is the selection of the laser. According to the DLR paper, there would be multiple alternatives for the gas laser. From today's perspective, even the limitation to gas lasers seems questionable. There has been a substantial technical progress, e.g. in the domain of disc or fibre lasers. In the view of the rapid technical development, any laser

choice of today might be outdated again after few years. It would be desirable to make the laser a parameter of a more generic mission model. This way, one could study the performance and the limitations of the mission concept independently from the selection of a particular laser.

However, this complicates the modelling of the ablative propulsion process. So far, coupling coefficient (C_m) data has been specified only for individual laser types. When the laser is parametric, the coupling model will have to be generic in order to accommodate different wavelengths, pulse widths and intensities.

Besides its actual findings, the DLR paper introduces numerical methods to the topic. It demonstrates that the numerical simulation of the encounters can yield valuable results. At the same time, the approach and the realization of the method remain well understandable, and the effort seems to be within reasonable limits.

2.1.3 Generalization

The two studies represent the cornerstones of investigations until now in the field of space-based laser debris sweepers. Other publications have not revealed game-changing findings, but have instead restated or confirmed the already known.

Now, one needs to distil the key aspects out of the antecedent review. The first key aspect is certainly the reachability topic. It determines the number of objects that come into the range of the debris-clearing laser. An object must come into range at least once, or it cannot be de-orbited. Therefore, the reachability defines an upper boundary for the removal performance per unit time. This aspect has been the weakest link in the argumentations of all previous investigations, caused by the lack of a high-definition model of the debris population.

The second key aspect is the relation between the relative motion in the near field and the trajectory change of the target. Wolfgang Schall has elaborated on this matter, but his approach was originally motivated by the deflection scenario. It should not be too hard to derive a similar geometrical relationship, which does not reveal the near-linear, short-term trajectory, but the post-engagement orbital elements. From them, one can determine the (perigee) altitudes of the targets. This new relationship should then be put into the context of a high-definition debris model, because there might be preferential crossing geometries.

Preferential crossing geometries could have an impact on the required momentum for de-orbitation, or on the overall removal performance of the sweeper.

Thirdly, it seems prudent to review the requirements for a modelling of the laser-ablative propulsion mechanism. A new, consolidated interaction model is to be created or adopted. After that, one can simulate individual engagement phases, just as Wolfgang Schall did for the deflection mission. Now, the focus would be on the changes of the orbital elements. This ought to bring light into the relationships between the overall debris problem, the laws of orbital mechanics, the interaction times between the laser and the debris objects, the parameters of the clearing laser and resulting remediation performance.

All aspects should be investigated in a most general manner, so that the results will reflect the prospects of the pure mission concept. Otherwise, it would be just another case study of a particular system design. For this reason, it will be tried to relax as many assumptions and constraints as possible, and introduce new ones only when deemed absolutely necessary.

For example, no particular laser will be assumed. Instead, the laser is kept as a free parameter. Neither will the rotational movement of the sweeper be restricted, nor will a definite target altitude be specified.

2.2 Reachability

The orbital laser can only de-orbit objects that are encountered during the mission. Some objects may pass by multiple times, while others are never seen by the sweeper. Therefore, the number of the reached objects quantifies a theoretical upper limit of the remediation performance.

Previous studies have employed a ‘gas kinetics’ approach, where a swept volume has been multiplied with a number density of debris objects. Then, the number of de-orbitable objects depends on the size of the swept volume, which in turn depends on the maximum effective range of the laser.

This section will analyse the impact of the range on the number of reached objects. However, before this, we need to define the term ‘sweeper range’ more precisely, and discuss how it relates to technical properties of the laser.

The *maximum effective range* is defined as the largest distance at which the laser can effect an ablation on a target. An ablation can be effected if and only if the fluence at the focal distance is equal or greater than the ablation threshold. So there are two ingredients: the ablation threshold and the fluence at focal distance.

The ablation threshold Φ_{th} is usually defined as a fluence, and its value is higher than the melting threshold for the same material. It depends on the target's material as well as on the pulse duration. An approximate ablation threshold for metallic targets, such as the bulk of the space debris objects, would be $28\,kJ/m^2$ at a $10\,ns$ pulse width [58]. The quantity scales with the square root of the laser pulse width $\sqrt{\tau}$. This relationship accounts for the thermal penetration depth at the target surface, because energy is thermally dissipated into the body of the target. Therefore, an approximate value for Φ_{th} in the range between $100\,ps$ and $1\,ms$ can be estimated by the following equation:

$$\Phi_{th}(\tau) = 28\frac{kJ}{m^2}\sqrt{\frac{\tau}{10ns}} \qquad [58,\ 59] \tag{2.1}$$

The second ingredient is the laser fluence at focal distance. A good approximation for the focal spot diameter at a distance z can be given by

$$d_f \approx \frac{4}{\pi}\frac{M^2 \cdot z}{d_{Aper}}\lambda \tag{2.2}$$

with z being the focal distance, M^2 the beam quality, d_{Aper} the diameter of the primary aperture and λ the laser's wavelength.

The maximum firing range can be related to the laser parameters by putting both ingredients together. The laser pulse fluence at a distance z is

$$\begin{aligned} \Phi(z) &= \frac{W_p}{A_f(z)} \\ &= \frac{4}{\pi}\frac{W_p}{(d_f(z))^2} \\ &= \frac{\pi}{4}W_p\left(\frac{d_{Aper}}{M^2\,\lambda\,z}\right)^2 \qquad \text{with Eq. 2.2} \end{aligned} \tag{2.3}$$

when W_p is the pulse energy of the laser and A_f is the area of the focal spot. The focal distance z at which the laser fluence is exactly the ablation threshold is named *maximum operating range* R_{max}. By rewriting the above equation and substituting z with R_{max} and $\Phi(R_{max}) = \Phi_{th}$, one gets

$$R_{max} = \sqrt{\frac{\pi}{4}\frac{W_p}{\Phi_{th}}}\left(\frac{d_{Aper}}{M^2\,\lambda}\right) \tag{2.4}$$

This equation links the size of the swept orbital volume to some fundamental, generic laser parameters.

While the *maximum effective range* depends on the material of the individual target, the definition of the *maximum operating range* R_{max} neglected the dependency on the material. R_{max} is a mean value for multiple materials with a comparable ablation threshold. It serves as a constructed, approximative key figure to describe a mission scenario.

For a given laser, one can now calculate the volume in space that is swept per mission time. The greater this volume, the more objects are reached and the higher the removal performance can be. Before we attempt to obtain practical figures from this equation, let us examine the key equation 2.4 in greater detail: The laser technology will most likely be selected out of qualitative considerations, such as the maturity of the technology, the reliability or the amount of necessary maintenance. There will probably be limited room to adjust λ or M^2. The same applies for τ, which dictates Φ_{th} by Eq. 2.1. The primary aperture d_{Aper} is determined by the required size of the focal spot. So finally, the pulse energy W_p is left as free parameter for tuning the range of the sweeper. Equation 2.4 can be rewritten to provide the necessary pulse energy for a desired R_{max}:

$$W_p = \frac{4}{\pi}\left(\frac{M^2\lambda}{d_{Aper}}\right)^2 \Phi_{th} R_{max}^2 \tag{2.5}$$

Figure 2.3 shows the pulse energies that would be required to achieve different R_{max}. One can see that in order to double the operating range, one must quadruple the energy per pulse. Every increase of the operating range must be paid

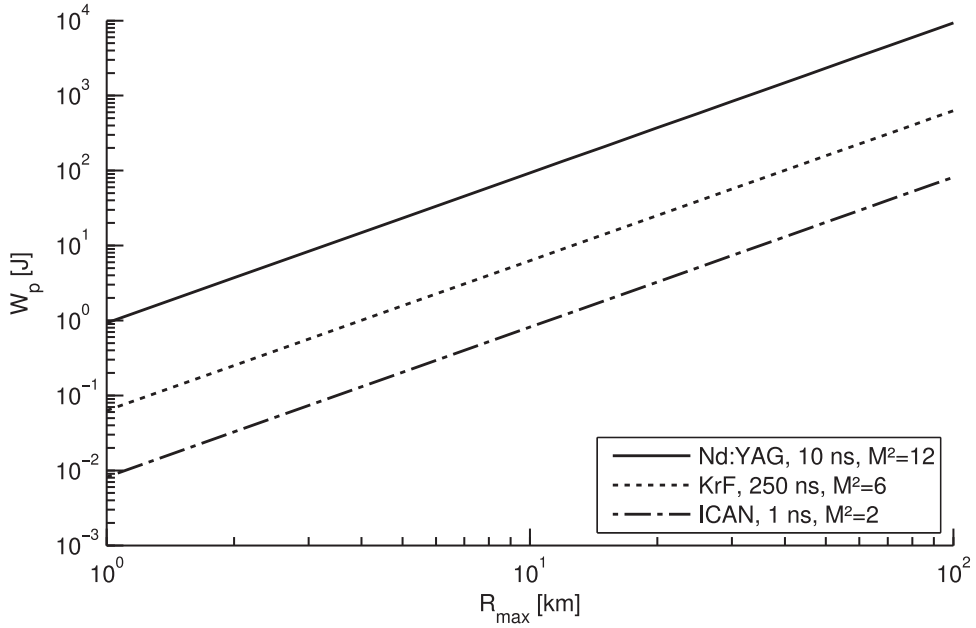

Figure 2.3: Required pulse energies for three selected lasers, when the primary aperture has a diameter of $2.5\,m$. The third laser is a fibre laser based on a suggestion by [60].

for with a disproportionately larger laser. Because W_p, in turn, is proportional to the power consumption of the laser, an increased R_{max} also requires a disproportionately larger power generator, more energy storage and more waste heat removal. For this reason, increasing the operating range of the sweeper R_{max} is very expensive in terms of system size and launch mass. Any mission design should attempt to minimize R_{max}.

This consideration also illustrates the advantage of an orbiting sweeper compared to a ground-based laser broom. The ORION system would engage debris targets at distances of $800\,km$ to $1500\,km$ [44, 54, 55, 56]. This would be 8 to 150 times as far as the space-based sweeper. Consequently, a ground-based laser would have to be 64 to $22,500$ times as large, including the proportionately scaled energy supply and waste heat removal.

Even if it turned out that a space-based sweeper could not exhibit a satisfactory removal performance, it could still shove debris to lower orbits, so that the

necessary range of a ground station can be reduced. The ground and space based laser remediator concepts do not necessarily compete against each other. They might as well complement one another.

Moreover, Equation 2.4 does not assume an equality between the size of the focal spot and the size of the target. This is a major difference to the works of Schall and Metzger et. al [51, 52]. One could introduce such a boundary condition at any time and, by doing so, restrict generality.

Not only the pulse energy, but also the primary aperture d_{Aper} could be tuned to increase R_{max}. A larger d_{Aper} increases the range over which the beam is well focussed, so that the fluence will exceed the ablation threshold of a target at a greater distance. However, the focal spot cannot be made indefinitely small, because there is an upper limit for d_{Aper}, which is determined by the pointing accuracy (subsection 2.6.1).

In reality, the beam will not point exactly at the centre of a target object. Instead, the direction of the beam will deviate by a small angle because of various distortions and uncertainties. If the focal spot is larger than the target, then the target will still be illuminated, even if there was a small misalignment. The larger the ratio of the diameter of the focal spot to the diameter of the object d_f/D, the more misalignment (pointing error) can be tolerated. This comes at the cost of beam overspill, which means that some laser energy is not absorbed by the target but radiated into the empty space. For this reason, one would make d_{Aper} as large as possible but as small as required by the beam pointing subsystem.

There is an additional, hard lower limit for d_{Aper}: The laser fluence incident to a mirror or a lens shall not exceed its optical destruction threshold. Typical destruction thresholds will be reached only when d_{Aper} is below $50\,cm$. For larger mirrors, there should be no concern.

After the above chain of thought, one can now assume an arbitrary pulsed laser source, then use the R_{max} equation (Eq. 2.4) to calculate its operating range, and finally estimate the swept volume in space. However, this does not yet provide a quantification of the actual objects reached. A model of the debris density or flux must be added to the consideration, so that the rate of encounters with a sphere of radius R_{max} can be calculated. This model must account for the

anisotropic distribution of the debris in space *and* for the azimuthal drift of the orbital planes. This means that the number of reached objects will not only depend on R_{max} but also on the orbital path of the sweeper.

Conclusively, one needs a methodical technique that can take an R_{max}, an orbital path of the laser and a complex debris model, and then determine a number of reachable objects for a specified mission duration.

2.3 Relative Geometry

The DLR sweeper study has performed an analysis of the flyby geometries [52], but its methodical approach was tailored towards a deflection or a protection scenario. The post-engagement long-term trajectories have not been studied. For the investigation of a laser broom scenario, one needs to relate the geometrical circumstances of an encounter to the post-engagement orbital elements of the target.

The question is, how the remediation performance impact that is caused by the different flyby geometries can be quantified. Two measurable quantities, which can be defined for relative trajectories, will be introduced and discussed in this section. The first one is the post-engagement orbit, and the second one is the angular velocity of the object about the laser. By systematically aggregating these figures for a mission scenario, one should be able to measure the impact of the flyby geometries on the remediation performance.

It has already been pointed out that the direction of the beam has an impact on the direction of the laser-ablative recoil. For example, Schall and Metzger et al. have assumed that the recoil is parallel to the beam [51, 52]. Therefore, the post-engagement orbits of the targets depend on the relative motion of the laser w.r.t. the target object (and on the magnitude of the imparted velocity change, of course). This means that the direction of the imparted velocity change cannot be completely controlled, because it is predetermined by the proper motion of the objects (Fig. 2.4a).

In some cases, the laser-ablative velocity changes may adversely increase the perigee altitude of an object, and prolong its orbital lifetime (Fig. 2.4b). It is necessary to analyse the passing of the objects in this regard, and determine when

to engage and when to disengage the laser. Some objects may never acquire a favourable relative position, although they come into close range of the laser one or multiple times. This effect cuts the remediation performance of the sweeper, and therefore it is necessary to analyse and quantify it.

The direction of the laser-ablative force, which is influenced by the direction of the laser beam, does not only determine whether an engagement would be productive or not. In the favourable case, it also affects the magnitude of the necessary velocity change for reaching a specific target altitude. In order to illustrate this effect, one can split the laser-ablative force into three vectorial components: along-track, radial and off-plane.

The along-track component will reduce the orbital energy and lower the orbit as long as it is retrograde. Since the thrust component directly counteracts the orbital velocity, it is the most efficient way of reducing the orbital altitude of the target.

The radial component adds energy to the orbit, increasing the velocity. However, it also changes the direction of the orbital velocity vector. This means that the shape of the orbit is changed, and with it the altitude of the perigee. If the shape-changing effect of the radial thrust component outweighs its energy-adding effect, then the target will still end up with a reduced perigee (Fig. 2.4c). For example, imagine a particle on a circular orbit. Now, we apply an Earth-directed velocity change in the order of magnitude larger than the original orbital velocity. The post-engagement orbit would be a nearly straight line, passing close by the centre of the Earth. Although this example has been exaggerated, it illustrates the general effect. This example also illustrates that the post-engagement orbit can be parabolic or hyperbolic in extreme (but not ill-conceived) cases.

The third, off-plane component of the laser-ablative thrust will add orbital energy and make the object faster. However, it also changes the orbital plane and affects the chances of encountering the object a second time. In an advanced sweeper scenario, the laser could, for example, aim at the aggregation of non-de-orbitable objects on the same inclination. This would reduce their rate of fragmentation and increase the available interaction times for future encounters with a laser sweeper.

The perigee-changing effects of all three vectorial components of the laser-

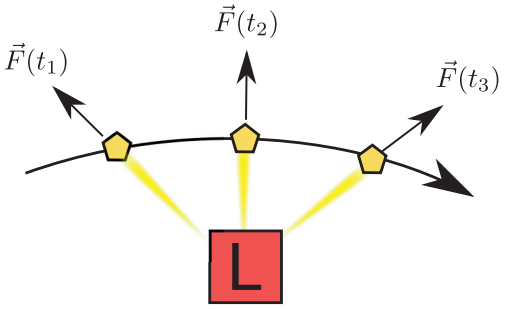

(a) The direction of the laser-ablative thrust depends on the proper motion of the object w.r.t. the laser.

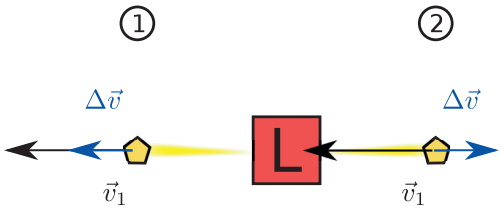

(b) Unfavourable (1) and favourable (2) relative geometries

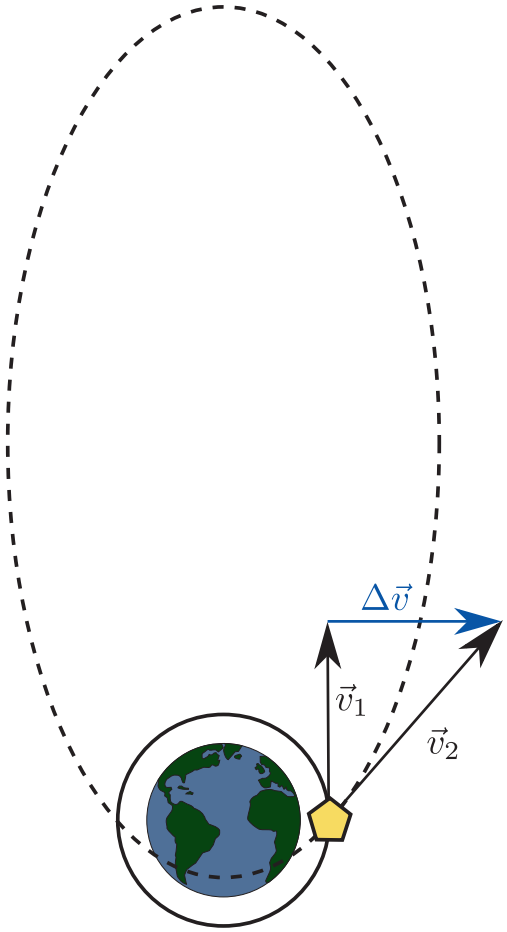

(c) Radial manoeuvres can lower the perigee, although the object becomes faster.

Figure 2.4: Selected aspects of relative flyby geometry

ablative thrust are to be quantified on general grounds. As a next step, one can analyse an individual engagement by summing up these effects, and specify the magnitude of the required velocity change to impart. Alternatively, one can reverse the process and calculate the lowest reachable perigee altitude for a given crossing geometry and velocity change.

However, the post-engagement orbits are not the only concern when analysing the crossing geometries. In the DLR sweeper study, the primary aperture of the laser would have a diameter of up to $2.5\,m$ [52]. This means that the focussing mirror can be as large as the mirror of the Hubble space telescope. In contrast to the telescope, the sweeper must track targets that are moving quickly. Keeping the beam pointed on a target with sufficient precision and stability will be increasingly demanding for faster moving objects. It is by no means guaranteed that the mirror of the sweeper can track objects with an arbitrary velocity. Therefore, it would be prudent to analyse the angular velocities of the objects passing about the laser.

There is also a logical conjunction between the angular velocity and the post-engagement orbit: The target can only be engaged when the engagement would decrease the perigee *and* the object moves with a velocity that is low enough for the beam tracking.

On the mission level, a technique is required to quantify the losses of the remediation performance that are caused by the constraints imposed by the crossing geometries. The first step would be to accurately model or reproduce these geometries. Since the relative motion is determined by the orbits of the debris objects, a debris population model must be the basis. Then, one needs a method or an algorithm that evaluates the relative trajectories regarding the post-engagement orbit and the angular velocity, then aggregates the results, and eventually concludes on the impact on the overall remediation performance. This method must not depend on a specific target altitude but accept a target altitude value as a parameter.

2.4 Laser Debris Interaction

In the two previous sections, only kinematic aspects of a sweeper mission have been covered: How many objects come into the interaction range, and how does their flyby geometry affect the performance of the mission? However, the causal relationship between the sweeper and the velocity change of a passing debris object has been omitted until here. This section will address the transfer of momentum to the targeted objects, which is caused by the high-intensity laser of the sweeper.

From the flyby geometry, which has been discussed in the previous section, one can derive the available interaction time frames. During such a time window, the relative trajectory meets the following conditions: The object is within range, it does not exceed angular velocity limitations, and an engagement would lower the perigee. Within a mission scenario, there can be one or multiple of these interaction time frames, even for the same object, even within the same crossing.

The sweeper must decide whether to use such a time window for actually firing at the object. There may be situations when the laser cannot engage because of technical, operational or other restrictions, although the situation would be favourable from an orbital dynamics point of view. For example, the laser would not fire if there was a chance of accidentally hitting another active satellite. A set of rules that decides whether an interaction window is used is named *engagement policy*.

For cases when the sweeper has decided to engage the object, the velocity change of the object must be determined. Generally, the laser-ablative momentum transfer can be characterized by the coupling coefficient C_m, which is the ratio of

transferred momentum per absorbed laser energy:

$$C_m = \frac{m_0 \cdot \Delta v}{W} = \frac{F}{P}$$

m_0	mass of the object
Δv	velocity change
W	absorbed laser energy
F	thrust
P	absorbed laser power

(2.6)

The value of C_m depends on the intensity, the pulse duration τ, the wavelength λ of the laser and the material of the target. However, there is limited information available on the chemical composition of space debris objects, particularly in the $1\,cm$ to $10\,cm$ size regime. The C_m values, which have been used in the 1989 sweeper study, are for aluminium only and appear to be rather chunky (Fig. 2.2). It would be desirable to procure more experimental data, and synthesize a more accurate model for the C_m.

The C_m function for a specific material has a global maximum value. It is called the *point of optimum coupling*. In this point, the returned momentum per invested laser energy is maximal. The naming suggests that the sweeper should attempt to operate the laser system at this set point. However, this is not necessarily true. If not the supply with laser power but the available interaction time confined the sweeper's performance, then a high laser power would be favoured over optimum coupling. In other words, effectiveness could be more important than efficiency.

Besides, in order to control the coupling set point, the sweeper must be able to technically control the intensity at the target. However, a system design could cut this ability in favour of other, more important features.

Therefore, a generic modelling of the sweeper mission should not rely on the assumption that the coupling is at its optimum. Instead, it must include the C_m function for a broad range of intensities.

Apart from C_m, there is another macroscopic parameter, which characterizes the interaction process: The specific ablation energy μ. For example, aluminium

ablates with $\mu = 80 \cdot 10^{-9}\, kg/J$ [52]. The quantity relates C_m to the effective exhaust velocity c_e and the specific impulse I_{sp} of the propulsive process [36]:

$$\begin{aligned} c_e &= C_m\, \mu \\ I_{sp} &= c_e / g_0 \end{aligned} \tag{2.7}$$

It quantifies how efficient the ablated material is used to create an impulsive effect. If the I_{sp} is higher, the object loses less mass for the same propulsive effect.

Indeed, the objects will shrink while the laser is firing on them and mass is being ablated. Their surface to mass ratio tends to increase, and so does the laser-ablative acceleration. The overall mass loss during an engagement can be substantial, especially when the thrust is directed suboptimally and a high velocity change must be imparted to put the object onto its targeted orbit. Some objects can be evaporated completely [52]. Making things even more complicated, the objects will not simply shrink, but they can also change their geometrical shape.

Previous laser-broom studies, ground-based as well as space-based, have been assuming planar or spherical ablation targets. The underlying physics and the driving mechanisms are relatively well understood in these cases. Yet, quite little is known about the influence of irregularly shaped or non-cooperative targets on the remediation performance. As it has already been explained in subsections 2.1.1 and 2.1.2, there is reason to believe that both, the magnitude and the direction of the velocity change, can be affected by the shape of the target.

In a previous study, it has been assumed that the targets are rotating. For many pulses, the velocity increments normal to the beam will cancel each other, so that the mean $\Delta\vec{v}$ points into the same direction as the beam [52]. The cancellation losses could be accounted for with an efficiency factor between 66% and 100% [53].

Now, how can these rather specific effects contribute to the bigger picture of the performance of the mission? Based on a model for C_m (and μ), one can calculate the magnitude of the imparted $\Delta\vec{v}$ for a single engagement phase. This also

requires, of course, the specification of a laser system and the distance between the laser and the object. Together with the relative geometrical situation, one obtains the vectorial velocity change and therefore the post-engagement orbit of the object.

Each object can be engaged one or multiple times during the mission. A change of the orbit can be calculated for every engagement by using the ablation model, so that the orbits of the objects can be determined for every moment in time during the mission. If this is done for all population objects, then the state of the entire population can be aggregated for every time of the mission. This includes the post-mission state of the orbital debris population, from which one can draw conclusions on the overall removal performance of the mission.

Altogether, one cannot seriously conclude on the remediation performance of a debris sweeper without taking into account a model of the laser-debris interaction. Because a generic model would not depend on a particular laser technology, the interaction model must also be generic in this regard. It shall accept all relevant laser-related quantities, e.g. λ, τ, M^2, as free parameters.

Moreover, this model must be integrated into the orbital mechanics-based, kinematic models (sections 2.2 and 2.3). This is necessary, because there is a feedback dependency between the orbital dynamics of the mission and the laser-ablative velocity changes: The interaction model will dictate the post-engagement orbit of an object. Then, the reachability model will use this post-engagement orbit to determine whether there will be a second encounter during the remaining time of the mission. If there is one, then the model for the relative geometry will provide an interaction time for a subsequent engagement, and so forth.

With a coherent, integrated modelling that takes into account the reachability, the relative crossing geometry and the laser-material interaction it should be possible to provide a credible and well-founded picture of the mission concept in general. It would be possible to find out the post-mission debris population, and to state a total number of removed objects.

2.5 Scheduling of Engagements

So far, the mission as a whole has been considered. It has been attempted to find aggregate quantities, which summarize aspects of the mission as a whole, and it has been tried to conclude on the overall performance.

To a certain extent, it can be useful to take a look at the mission timeline. It is, of course, impossible to predict the de-orbitation of an individual real-world debris object in this study. For that, one would at least need an object catalogue, which is not available for medium-size debris. However, since the population follows a statistical model that is believed to be representative, it should be possible to draw statistical conclusions on the scheduling of the engagement phases:

The first question concerns the concurrency of engagement opportunities. Concurrent opportunities lead to scheduling conflicts. Since there is only one laser, only one object can be engaged at a time. A high number of concurrent engagement possibilities throughout the mission indicate that a design with additional lasers could be considered.

Another aspect is the rate of engagements. Maybe there are times, when the laser is busy, and there are other times, when the laser is nearly idle. An idle laser would be a waste of resources. Conclusively, the mission should be balanced towards a nearly stationary workload.

Two more features of interest are the average duration of an engagement and the average time between two engagements. Both quantities should follow a distribution with an expectancy value for both time figures. The laser may need a minimum time between two engagements in order to realign the mirror or perform other preparatory work for the next engagement phase. Without a system study, it is impossible to predict how long that re-orientation phase would be. However, with the distribution of the idle phase durations, one could estimate how many engagements could not take place because operations overlap. The design-specific minimum duration of a preparation phase would be used as a free parameter.

Finally, it would be interesting to know what reasons would prevent the laser from firing, or why the laser would abort a firing and disengage.

2.6 Debris Detection, Cueing and Accuracies

2.6.1 Pointing Accuracy

In this subsection, the minimum required pointing accuracy for the laser will be explored. For the sake of simplicity, a nearly rectangular profile of laser beam will be assumed. (This means, the areal intensity is constant in every plane traverse to direction of the beam propagation.)

At a large distance from the laser, the focal spot may be larger than the target object. This leads to a 'beam overspill'. At a smaller distance, the focal spot size can be equal to the cross section of the object. For even lower distances, the spot could be smaller than the object.

In the first case, a loss of laser energy due to the beam overspill is inevitable. When the position of the focal spot has an error of

$$\delta s \geq \frac{d_f - D_{obj}}{2} \tag{2.8}$$

some part of the target will not be illuminated any more (Fig. 2.5). And for a greater deviation of the focal spot

$$\delta s \geq \frac{d_f + D_{obj}}{2} \tag{2.9}$$

the target will not be illuminated at all. Consequently, there would be no photoablative propulsion.

Taking the maximum allowed misalignment δs, one can write the maximum allowed pointing error

$$\delta\theta(D_{obj}, z) = \frac{\delta s}{z} = \frac{d_f(z) + D_{obj}}{2\,z} \tag{2.10}$$

with z being the distance between the object and the laser source. Therefore, the minimum required beam pointing accuracy for targets from $1\,cm$ to $10\,cm$ is

$$\delta\theta_{min} = min[\delta\theta(D_{obj}, z)] \quad \forall \quad 0.1\,m > D_{obj} > 0.01\,m,\ z > 0 \tag{2.11}$$

and with Eq. 2.2 finally:

$$\delta\theta_{min} = \frac{2\,M^2\,\lambda}{\pi\,d_{Aper}} + \frac{0.01\,m}{2\,R_{max}} \tag{2.12}$$

So far, it has been assumed that the position of the object is exactly known. When that is not the case, there will be a position knowledge error, which is described by a standard deviation σ. Assuming that the error is normally distributed, and the object shall be hit with a 99.7 % probability, the maximum deviation is

$$\delta s = \frac{d_f + D_{obj} - 6\,\sigma}{2} \tag{2.13}$$

and the required pointing accuracy is therefore

$$\delta\theta_{min} = \frac{2\,M^2\,\lambda}{\pi\,d_{Aper}} + \frac{0.01m - 6\,\sigma}{2\,R_{max}} \tag{2.14}$$

It is important that $d_f + D_{obj}$ must always be greater than $6\,\sigma$. If that cannot be guaranteed, the cueing system (sec. 2.6.3) must be improved so that the position is known with a smaller deviation at the time of the engagement.

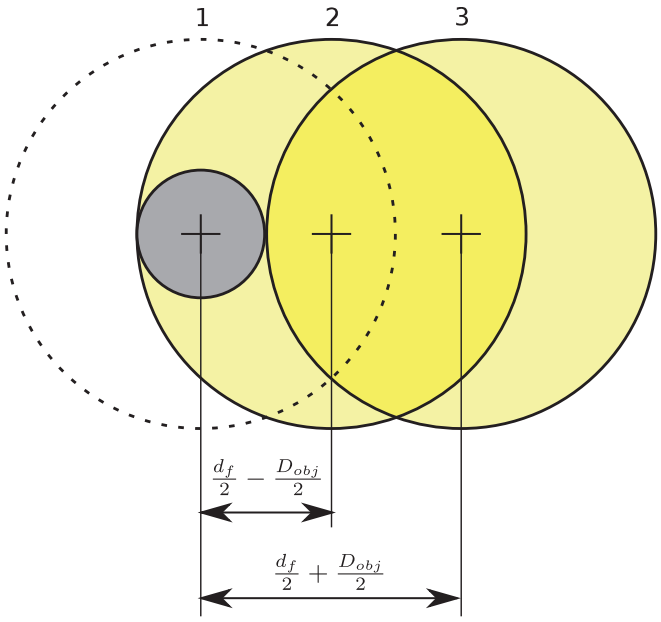

Figure 2.5: Focal spot and target in the focal spot plane

Required pointing accuracies for a minimal cueing system ($6\sigma = d_f$) will be presented in Table 4.3 in chapter 4 for three reference mission scenarios. For better cueing systems with a smaller measurement deviation, the allowed deviation of the beam pointing would be higher (Eq. 2.13) and the pointing accuracy requirement would be relieved.

2.6.2 Detection

In this subsection, it will be explained why the laser debris sweeper can only engage catalogued objects.

Let us assume, that the laser would have no knowledge of the targeted population of objects whatsoever. In order to gain knowledge of potential targets, the debris sweeper would have to scan its environment for passing objects.

Let us further assume that this scanning system would have a range of $200\,km$ and that the closing velocity of many objects is in the range of $10\,km/s$. This would mean that there would be few seconds between the detection and the engagement. Within this time, the laser sweeper would have to plan the engagement, rotate the platform and align the laser. There can be no doubt that this process would have to be performed automatically, because a human reaction would take too much time. This implies that the laser would have to decide about the engagement of unknown objects autonomously. Such a scenario will not be taken further here, due to the far-reaching legal, political and ethical problems, let alone the technical challenges.

An object with a relative velocity of $10\,km/s$ travels $1200\,km$ in two minutes. It is believed that a human operator requires at least two minutes to check the data of a detected object against the United Nations registry [61], the US Space Surveillance Network catalogue and other sources, and then make a reliable decision. This means that the object must be detected before it reaches a distance of $1200\,km + R_{max}$ in order to give the operator enough time to decide, while the orbital platform would be already preparing for the engagement.

An omnidirectional active detection system with a range beyond $1200\,km$

would, among other technical challenges, require large amounts of energy.

Based on these considerations, one must catalogue the targeted objects well in advance. Ground personnel can categorize the objects, and identify the ones cleared for removal. The legal and the political uncertainties regarding the removal of particular objects can be resolved well before the first engagement.

Engagements of objects can be planned in advance, which is particularly useful when two objects are crossing at the same time or in short sequence. In this case, the operations can be prioritized. A criterion could be the maximization of the debris-clearing effect. A ground crew can monitor the activities of the orbital laser and intervene when necessary.

2.6.3 Cueing

In order to point the laser on the target, the position of that target must be known with sufficient accuracy: The predictive position error must be smaller than (roughly) the radius of the focal spot. However, the catalogue data will most likely be not good enough:

The accuracy of a catalogue entry depends on a variety of influence factors, such as the axis (along-track, radial or cross-track), the re-visit frequency, the duration and the method of measurement. For the preliminary design of the debris sweeper, a rather conservative accuracy figure should be used, which is the along-track deviation after few weeks without a measurement.

Available two-line element (TLE) catalogue entries have an error of up to $2\,km$ ($3\,\sigma_{catalogue}$) for objects of $10\,cm$ or larger [62]. Taking into account an optimistic ablation threshold of $10\,kJ/m^2$, the laser would have to generate more than $1.2\,GJ$ per pulse to illuminate a spot with a radius of $2\,km$. For a pulse rate of only some $10\,Hz$ and an efficiency factor below $50\,\%$, the required electrical power would easily end up in the terawatt domain.

Though hard to predict, a future catalogue may optimistically have an accuracy of $100\,m$ for objects in the centimetre range [63]. Even in that case, the required laser pulse energy would be at least $314\,MJ$.

No doubt, the pure accuracy of the catalogue is insufficient. There is a delta between the catalogue accuracy and the accuracy that is required for engaging

the object. There must be a cueing system that bridges this delta and refines the position knowledge immediately before an engagement.

A ground-based cueing is impractical for a number of reasons. First, one would need multiple tracking stations around the world. Secondly, there are atmospheric distortions, which must be compensated. Thirdly, the refined position and velocity of the object would have to be uploaded, which involves latency and possibly interference. Finally, the measured data would be available in inertial or Earth-fixed coordinates, while the laser needs the relative motion. The necessary transformations take time and involve additional uncertainties. Therefore, it seems reasonable to assume a cueing system on board the sweeper.

The cueing system should be active, so that it can work during the eclipse phase. Depending on the delta between the accuracy of the catalogue and the required accuracy, and the quality of the cueing system, a number k of individual measurements (pulses, echoes, ...) is required. With every individual measurement, the accuracy is improved. The required accuracy must be reached, when the object enters the firing range of the laser (R_{max}). Therefore, the measurement phase must begin at a distance R_0:

$$R_0 \geq R_{max} + v_c \frac{k}{f} \tag{2.15}$$

v_c is the closing velocity of the object, which is about $14\,km/s$ in the worst case, and f is the measurement rate (pulse rate, PRF, ...) of the cueing system.

For high pulse rates, the measurements can become ambiguous: The echo of an earlier measurement pulse may be mistaken for the echo of a later pulse. Depending on the assumed catalogue accuracy, a maximum possible pulse rate of $37.5\,kHz$ can be calculated. For higher rates, echoes from individual measurements may overlap on the time axis.

It should be noted that this limitation is not carved into stone. Some technologies, such as radar systems employing waveform diversity, can ease or omit this requirement. However, these technologies are more challenging and may come at the cost of other limitations.

2.6.4 Summary

Summarizing all the side aspects in this section, it is clear that the laser debris sweeper will require a catalogue of the targeted objects and an active cueing system, which augments the catalogue data immediately before an engagement. The cueing system must be capable of

- finding an object as small as 1cm
- within a field of view (FoV) $2n\sigma_{catalogue}/R_0$ (e.g. $6\sigma_{catalogue}/R_0 = 4\,km/R_0$),
- correlating the object to an entry in the catalogue (matching),

and then to

- determine the relative trajectory of the object
- with an accuracy of the focal spot radius at R_{max} ($\approx$ few centimetres) while
- the object can be as far away as R_0.

2.7 Required Power Supply and Waste Heat Removal

Eventually, different system designs of the sweeper will be developed in a trade study. It will be necessary to quantify the amounts of the required energy, the required power and the waste heat, which must be removed. When the output power of the (operating) laser is constant, it can be written as

$$P_{emit} = W_p\, f \tag{2.16}$$

Together with an overall efficiency of the laser, its electrical power consumption can be given to

$$P_{el} = \frac{W_p\, f}{\eta} \tag{2.17}$$

and the waste heat is approximately

$$\dot{Q} = \frac{1-\eta}{\eta}\, W_p\, f \tag{2.18}$$

One can calculate the mean electrical power by summing up the required energy of all engagements and dividing it by the mission duration. Theoretically, generating this power would suffice to run this mission. However, there may be times when the laser is unusually busy, or the durations of the engagements are particularly long. The energy to bridge these more demanding times of the mission would have to be generated in advance, and stored. If the required storage turned out to be disproportionally large, it might be sensible to generate extra energy, shunt it when not needed, and go with a smaller storage.

The rate at which the energy can be drained from the storage is another aspect to consider. It equals the electrical power consumption of the laser (Eq. 2.17). This maximum discharge power can be quite high, and not all storage technologies may be equally suited for the needs of this particular application.

3 Mission Performance Model

To assess the potential performance of the proposed mission, all relevant effects must be reproduced in a mission model. But what are the figures of merit? The answer to this question will determine the required output of the model.

The remediation performance of the sweeper can be measured in various ways. The most straightforward measure is the number of de-orbited debris objects. Being a single scalar quantity, it will be easy to compare different variants of the mission. But it might also oversimplify the situation. Sometimes, measuring densities at orbital altitudes, which are decreased, could be relevant.

Therefore, a second and more informative measure of the remediation performance is the post-mission distribution of the density of the orbital debris over the altitude. It shows, which altitudes have been relieved the most, and which altitudes have received additional debris.

This implies that some objects will not be de-orbited, but merely moved to a lower altitude band. Although these objects are not entirely purged from orbit, their remaining in-orbit lifetime will be considerably shortened. Their number is a figure of merit, which complements the number of removed objects.

At this point, it is clear that the performance model shall predict the post-mission debris population. The question is, which analytical method would be the most suitable.

The largest 'grid cell' of interest is a sphere around the sweeper with a radius in the order of $R_{max} = 100\,km$. It would statistically contain fewer than four debris objects. This number is insufficient for representatively sampling the debris population at the present location. Therefore, a continuum model would not be suitable. The Program for Radar and Optical Observation Forecasting (PROOF) software demonstrates that a discrete element approach does not exceed the computing power of today's workstation computers. Such a technique would be both,

productive and conceptually facile, as has been demonstrated more than 15 years ago [52]. Hence, a deterministic, discrete element approach is chosen in favour of a statistical mechanics method. This, of course, implies the development of numerical algorithms, flanked and supported by analytical considerations.

Figure 3.1 shows how the chosen deterministic method is used to simulate the sweeper mission: First, one needs to generate a representative set of discrete debris elements, a population. This preparatory part is shaded yellow in Fig. 3.1, and will be covered in the next section of this thesis (sec. 3.1). The second step, shaded in red, implements the equations of motion for the population elements. It forms the basis of the actual performance model, and is discussed in subsection 3.2. Afterwards, section 3.3 will deal with the analysis of collisions between the debris elements and the range sphere of the laser (green part in Fig. 3.1). The actual interaction is then modelled in section 3.4 (blue part in Fig. 3.1).

For the remainder of this thesis, it is assumed that objects with a perigee altitude below $200\,km$ have a short orbital lifetime. It is safe to say that these objects will have a residual lifetime of a few weeks in the worst case (Fig. 1.1). In most cases, the object will de-orbit within hours, or within a few days. In any case, the probability of such a particle harming an active satellite or colliding with another object is negligible. Judging from that, debris objects with a perigee altitude below $200\,km$ are considered to be 'removed'. If a debris object has been engaged by the laser, but the perigee still remains above $200\,km$, the lifetime of the object has merely been shortened.

Nonetheless, this assumption does not restrict the generality of the performance model. In fact, the value has been implemented as a free parameter, named r_{Peri}, which can be chosen at one's convenience.

3.1 Debris Population

Throughout chapter 2, it has been repeatedly pointed out that a serious investigation of the laser debris sweeper concept can only be based on a representative and detailed model of the orbital debris situation. There exists a high-definition synthetic population model, which is widely accepted. That population has been

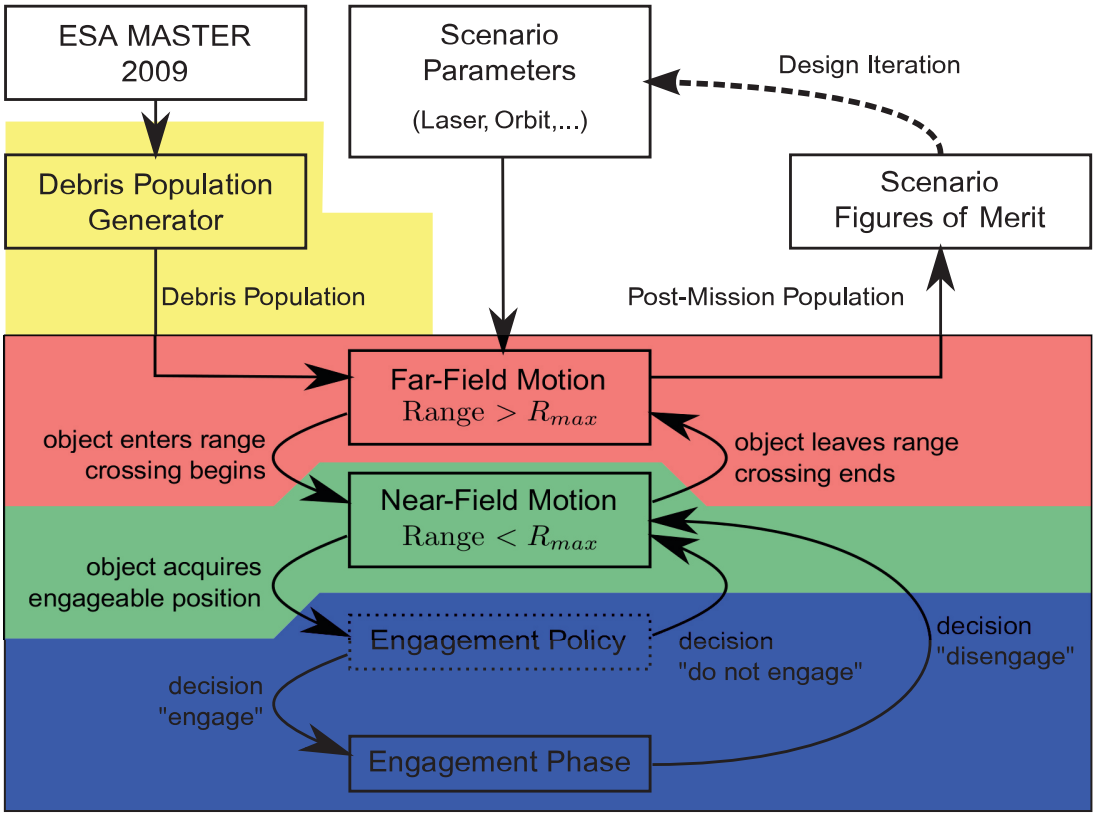

Figure 3.1: Overview of the performance model

generated as a data basis for the European Space Agency (ESA) MASTER debris model at the TU Braunschweig [35]. The population itself, which is a set of discrete objects, has not been available to this research project. That is why a new population had to be derived from the statistical data that is contained within MASTER.

It must be mentioned that the MASTER model employs 'statistical objects' with non-integer representation factors. One statistical object represents a (non-integer) number of real-world particles. Such factors could be problematic in a deterministic numerical simulation. Therefore, the generated population has been created without representation factors; every object represents exactly one real-world object. Although this trait is favourable for the simulation, it inevitably leads to minor deviations between the generated population and the original MASTER population.

3.1.1 Population Generator

This subsection describes the process that has been used to generate the debris population. First, the probability tables of the ESA MASTER 2009 model must be available for the desired reference epoch of the population. Then, debris particles are generated. This basically reverses the process in which the MASTER 2009 probability tables have been generated. A more detailed description of the process can be found in appendix A.

The data of the MASTER 2009 model is contained in so-called 'probability tables'. They are multidimensional arrays of object densities. There are, for example, three spatial dimensions. The array item at given coordinates then contains the predicted debris density at the corresponding location in space. However, those tables do not only resolve spatially, but they also contain extra dimensions for the time, the orbital parameters, the size and the type of the debris. This means that one array item contains the density of debris with a given (a) orbit, (b) size and (c) type at (d) a given location in space for (e) a given epoch. Mathematically speaking, the probability tables are discrete, multidimensional probability density functions (with independent variables).

In order to generate a population from those tables, they are treated as a 'debit side'. At the same time, the (initially empty) population is treated as the 'credit side'. The algorithm tries to minimize the debit side, while increasing the credit side:

1. Obtain an adequate probability table, e.g. by using the MASTER software. Multiple runs of the MASTER executable may be necessary in order to extract sufficient data points.

2. Scan this auxiliary probability table, and find the entry with the highest density.

3. Generate a debris particle that corresponds to this entry in the table. Add it to the population.

4. Calculate the new particle's statistical contribution to the debris densities. (The 'statistical footprint' of this particle in the probability table.)

5. Subtract the statistical contribution from the auxiliary probability table.

The steps two to five are repeated until the auxiliary probability table contains only zeros. An illustration of the algorithm is shown in Figure 3.2. A more detailed description of the population generator tool can be found in the appendix (appendix A).

The algorithm has been used to generate a debris population for the May 2009 epoch. This means that the following mission performance investigation will take into account the 2009 debris situation.

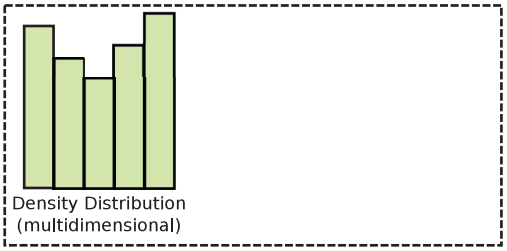

(a) At the beginning, there exists a multidimensional probability table. Each entry contains the density of a debris component with a specific orbit, size, and type at a given point in time and space.

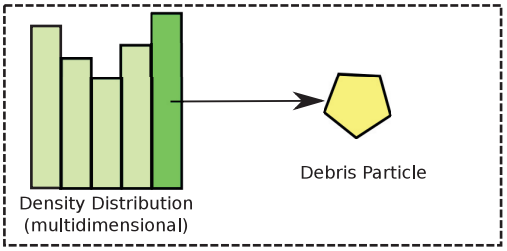

(b) First, the entry with the highest density is chosen. A debris object is generated, according to the orbit, size and type corresponding to the entry in the probability table.

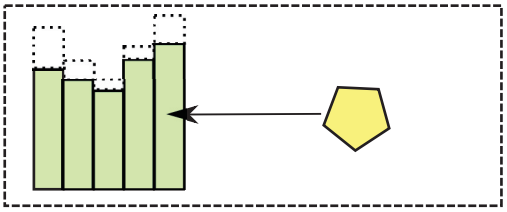

(c) Then, the contribution of the new object to all probability density entries is calculated. This contribution is subtracted from the probability table. The table contains only the density that is not accounted for by the generated objects.

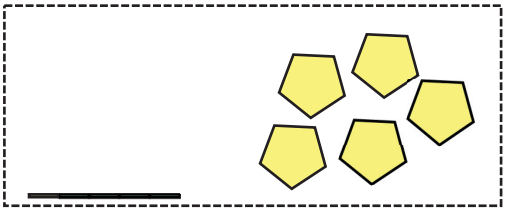

(d) The process is repeated until the complete probability table has been converted into population objects.

Figure 3.2: Working principle of the population generator

3.1.2 Validation of the Population

Before the newly generated population can be used, it must be validated. Only a valid debris population will lead to a correct reproduction of real-world effects in a simulation. For this reason, the population is compared against the original MASTER 2009 data.

The most pivotal property of the debris population is its density. It determines the probability of an encounter between an orbital laser and a debris object. Therefore, it also determines the total number of objects that can be reached during a given mission, and for a given mission orbit.

Figure 3.3 shows the density resulting from the generated population in comparison to the MASTER 2009 prediction. It is slightly higher than predicted by MASTER, but still well within one order of magnitude. It seems that the deviation is the highest for areas where the density is low: The highest deviation is in the medium Earth orbit (MEO) altitude range, which is not of interest for this study anyway.

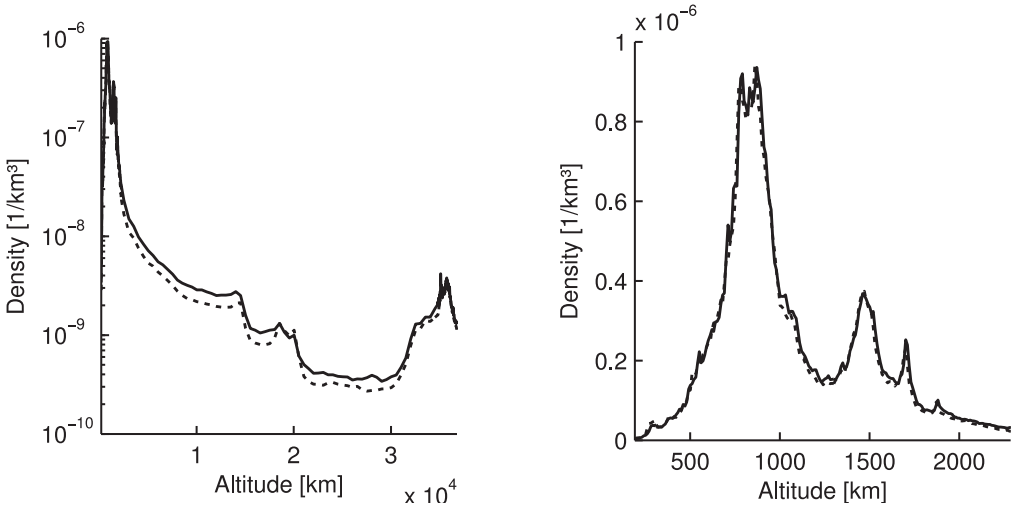

(a) Complete near-Earth space (b) LEO only

Figure 3.3: Debris density resulting from generated population. Dashed lines represent the MASTER 2009 reference population for comparison.

The orbital planes of the debris particles are defined by the combination of the inclination and the longitude of the ascending node Ω. The latter are uniformly distributed. The orbital plane is the dominant influence factor on the relative geometry between the laser and its targets. For that reason, it is important that the inclination is correct in the generated population.

Two most different source types have been selected for the validation of the inclinations. The coolant droplets have the most distinct inclination distribution. The MASTER final report states that the coolant was released at altitudes from $900\,km$ to $950\,km$ [35, p.105]. Since then, the droplets should have descended to lower orbits as a result of orbital perturbations. The MASTER report additionally says:

> *"NaK releases are restricted to a very narrow region near* $65°$ *inclination."*

Although the inclinations of the droplets may have changed as well, this change is probably in the range of few degrees. Figure 3.4a shows a scatterplot of the inclinations of the droplets over the semi-major axis. It can be seen that the distribution is as expected.

Figure 3.4b shows the same plot for the explosion fragments. One can clearly see that the bulk of the objects concentrate about the inclinations and altitudes of frequently used orbits. However, there is one exception: There seem to be far too many explosion fragments on Tundra orbits. (A Tundra orbit is a Geosynchronous orbit (GSO) with a Molniya inclination.) This feature has been investigated, and it turned out that there are actually relatively few, but evenly distributed objects.

The shape of the orbital ellipse is determined by the combination of the semi-major axis and the eccentricity. It has a secondary influence on the relative geometries between an orbital laser and the debris particles. There should be few particles with perigee altitudes below $200\,km$, because these are short-lived trajectories. Also, there should be no particles with a perigee above the upper GEO graveyard (GEO + $235\,km = 42,487\,km$ [3]). Additionally, the sodium-potassium droplets must be expected on a circular trajectory, because they have

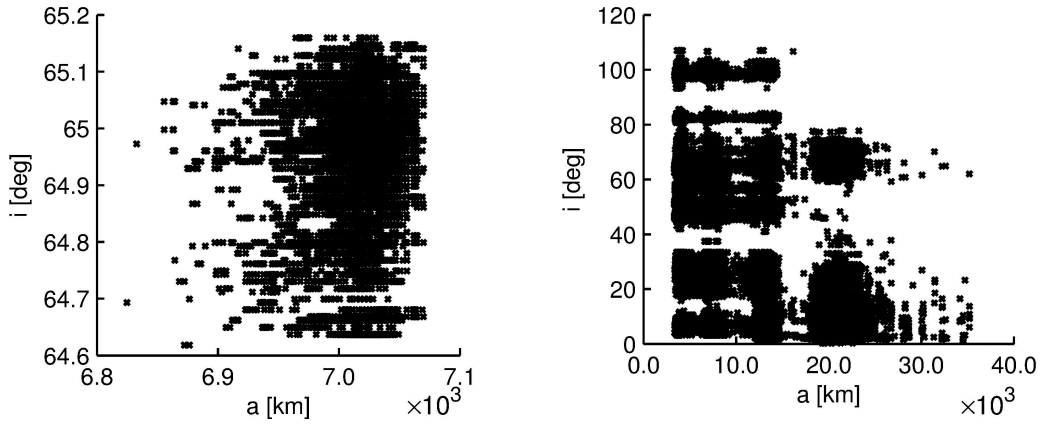

(a) Sodium-potassium droplets (b) Explosion fragments

Figure 3.4: Distribution of debris particle inclinations

leaked out of a circular-orbit satellite.

Figure 3.5a confirms that the sodium-potassium droplets are on near-circular orbits. Figure 3.5b shows that collision fragments tend to have high eccentricities, which also seems plausible. Furthermore, the (a, e)-distributions of other debris subsets are showing similar, credible characteristics.

Finally, the MASTER model assumes three parameters to be uniformly distributed among debris objects: the argument of the ascending node Ω, the perigee angle ω, and the mean anomaly M. For the generated population to be correct, these parameters must be sufficiently randomized. Scatter plots of these three parameters have been generated. They showed no concentrations of values.

Overall, it can be said that the generated debris population shows the characteristics that have been predicted by the MASTER 2009 model. There are slight deviations, but those can be considered irrelevant to this type of concept study.

3.1.3 Impact on the Performance of the Mission

The mission concept has been limited to the removal of LEO objects in the $1\,cm$ to $10\,cm$ regime. From these two constraints, first conclusions can be drawn on the removal performance:

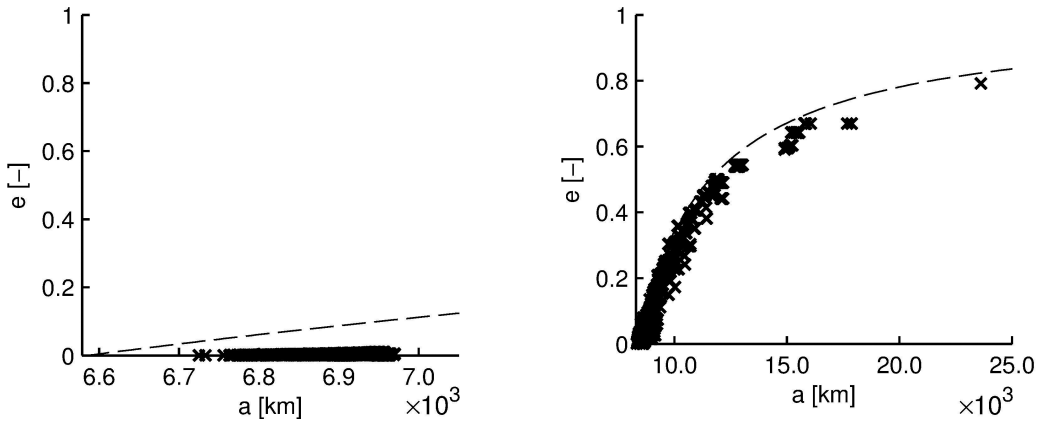

(a) Sodium-potassium droplets (b) Collision fragments

Figure 3.5: Scatter plots of orbit shape parameters

The population contains roughly $830,000$ objects with a diameter from $1\,cm$ to $10\,cm$. This includes objects from all regions of near-Earth space, including - for example - objects roaming only the MEO or the GEO regions. Only about $572,000$ objects spend at least part of their time in the LEO region. (Fig. 3.6)

The remaining $258,000$ objects follow trajectories that will never lead them to altitudes below $2200\,km$. This means that those objects will never come into the range of the space-based laser, and will not be de-orbited. One can drop them from further analysis.

Although this figure may not be directly associated with the sweeper, it provides a first, fundamental limit to the performance prospects of the mission. Therefore, it may be regarded as a constant term in the performance model. The next sections will add additional, parametric terms to the performance equation.

3.2 Reachability

As already discussed in section 2.2, an object must drift into the operating range of the laser; otherwise, it cannot be de-orbited. Reachability of a particle is a necessary condition for its de-orbitation.

This section will describe a numerical technique that allows isolating the subset

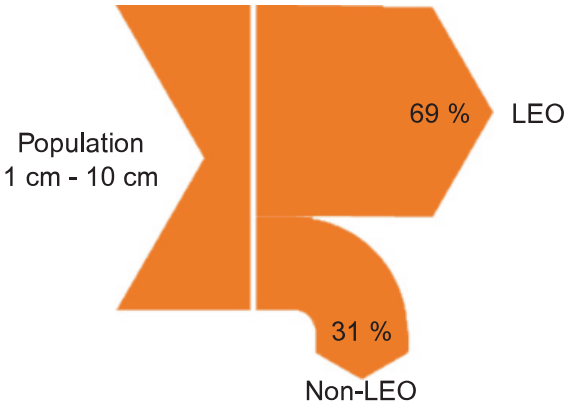

Figure 3.6: Relation between LEO and non-LEO objects

of reached objects from the LEO objects for a specific mission. It will demonstrate how the reachability aspect affects the parameters of the mission. Additionally, the influence on the overall performance of the mission will be derived.

3.2.1 Description of the Crossing Generator

The implementation of the numerical technique that determines the subset of reached objects has been named *crossing generator*. Its task is the determination of all collisions between the range sphere of the orbital laser and all debris particles. (Fig. 3.7) Such a collision is called a 'crossing'. As part of a crossing, a debris object enters the range sphere of the laser, then reaches a point of closest approach, and finally leaves the range sphere.

For one object, there can be zero, one or multiple crossings during a mission. For a constant debris population, the number of crossings for each object depends on the range of the laser R_{max} (sec. 2.2), the duration of the mission and the orbit of the laser. The problem is purely kinematic.

The presented solution determines the crossings individually for every object: All crossings between one object and the laser are calculated. When this has been done, the next object is processed, and so forth. This allows for a very efficient parallelization, because the processing of all population objects are mutually independent subtasks.

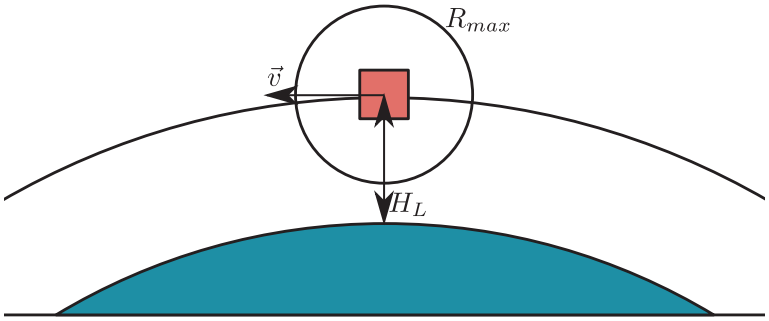

Figure 3.7: Concept of the reachability analysis: The laser (red) has an associated maximum operating range R_{max}. It sweeps around Earth and registers all debris objects that pass through the influence sphere.

First, the trajectories of the laser and the object must be known. From both trajectories, one can - either analytically or numerically - determine the intersections between the object trajectory and the range sphere of the laser.

It has been decided to guide both collision partners along Kepler ellipses, but with an additional drift of the nodal line and the apsis:

$$\Delta\Omega = -\frac{9.96\,\pi}{1.5552 \cdot 10^7} \left(\frac{R_{E,eq}}{a_L}\right)^{3.5} \frac{\cos(i_L)}{(1-e_L^2)^2} \tag{3.1}$$

$$\Delta\omega = \frac{4.98\,\pi}{1.5552 \cdot 10^7} \left(\frac{R_{E,eq}}{a_L}\right)^{3.5} \frac{5\,\cos(i_L) - 1}{(1-e_L^2)^2} \tag{3.2}$$

These modifications account for the most dominant orbital perturbations in the LEO region, which are mostly due to the oblateness of the Earth ('J2'). Both equations have been taken from the PROOF final report [64, Eq.2.22f]. A more accurate trajectory determination would be the Simplified General Perturbation (SGP4). However, the 'modified conics' approach above is deemed sufficient for the present analysis.

The next question is the determination of the intersections between the laser and the object. A hybrid between numerical and analytical methods has been chosen, mainly because it maximized the calculation performance. The algorithm begins with the calculation of the positions of the laser and the debris object. Depending

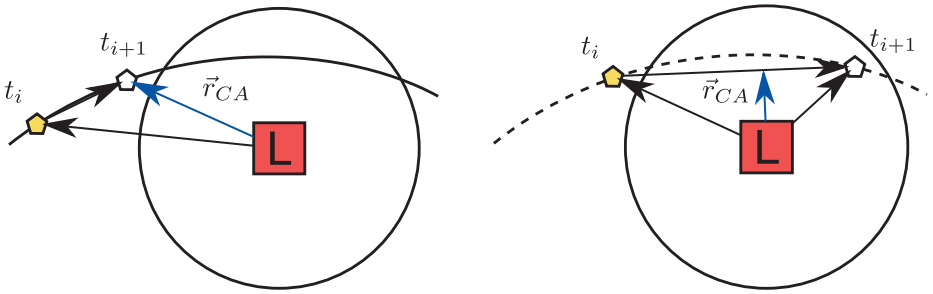

(a) Time step without crossing detection

(b) Time step that leads to the detection of a crossing

Figure 3.8: Working principle of the crossing detection: The laser is the red box. The blue arrow is the closest distance of the debris particle during the depicted time step. (The curvature of the particle's relative trajectory is exaggerated.)

on their distance d, the next time step is chosen:

$$t_{i+1} = t_i + \Delta t(d) \tag{3.3}$$

$$\Delta t(d) = max\left(c_1 \quad , \quad \frac{d - c_0\, R_{max}^{0.25}}{25 \cdot 10^5\, m/s}\right) \tag{3.4}$$

This equation has been determined empirically; its results are very satisfactory for $c_0 = 1681.79\, m^{0.75}$ and $c_1 = 0.2\, s$ when $R_{max} \leq 200\, km$. It leads to a fast (but less accurate) propagation when the object is far away from the laser, and ensures an accurate trajectory resolution when the object is close to the laser.

In the next step, the relative position of the object w.r.t. the laser is calculated for both time steps. The relative trajectory in between is approximated as a straight connecting line, which is acceptable for short sections of the trajectory. Then, the point of the connecting line that is closest to the laser is calculated. If the relative distance of this point is smaller than R_{max}, then there must be a crossing. (Fig. 3.8)

One can now calculate the times when the debris enters or leaves the range sphere of the laser. Additionally, the time and the state vectors of the closest approach are determined. This is done by using an iterative, numerical algorithm that is

based on the bisection method. This additional information will be useful later in this study, although it is not needed for the analysis of the reachability.

Three aggregates are generated for every scenario simulation run: The distinct list, the first encounter rate and the summary record.

Distinct List The distinct list contains one line for every encountered object. Each line contains the object's unique ID, the number of detected crossings for this object, its diameter, its source type and its Kepler elements. An example of the distinct list is shown in Fig. 3.9. The file is written as in a semicolon-separated csv format, angles are given in degrees, diameters in metres and semi-major axes in kilometres.

First Encounter Rate The first encounter rate file contains the number of newly encountered objects over time. It contains one line for every week in the mission. One line contains the total number of first-time encounters of objects during that particular week. The file is written as a semicolon-separated csv file; an example is depicted in Fig. 3.10.

Summary Record Finally, the summary record summarizes a scenario into a single line. This aggregate is meant for the comparison of multiple scenarios against each other. It contains three types of information: The scenario description (input), some execution data, and a summary of the results (output).
In detail, the input parameters are

```
Id; # Cross; Diameter; Source type; SMa; Inc; Ecc; APe; RAAN; TAn
13182; 1; 6.6e-2; coll; 7722.6; 86.47;0.06;  17.3;  24.2;  55.1
03410; 1; 1.0e-2; coll; 7320.5; 74.10;0.03; 221.2; 153.7; 204.5
91660; 1; 1.5e-2; coll; 8848.6; 73.81;0.19; 206.0; 242.7;  63.7
28645; 1; 1.5e-2; coll; 7661.9; 72.66;0.08; 323.4;  41.4; 206.9
[...]
```

Figure 3.9: Example of a distinct list. (The number of decimal places (precision) has been shortened here; in reality, there are six decimal places for all Kepler elements and four decimal places for the diameter.)

```
01.05.2009;07.05.2009; 3424;
08.05.2009;14.05.2009; 3365;
15.05.2009;21.05.2009; 3191;
22.05.2009;28.05.2009; 2936;
29.05.2009;04.06.2009; 2847;
05.06.2009;11.06.2009; 2791;
12.06.2009;18.06.2009; 2562;
19.06.2009;25.06.2009; 2422;
26.06.2009;02.07.2009; 2263;
03.07.2009;09.07.2009; 2194;
10.07.2009;16.07.2009; 2128;
[...]
```

Figure 3.10: Example of a first encounter rate file

- The debris environment into which the laser has been placed. This implies the starting epoch for the propagation.
- The number of total debris population objects (LEO, MEO and GEO). The value is always $827,955$ in this study.
- The number of objects that cross the LEO region (below $2286\,km$); the value is always $571,907$ in this study.
- The maximum operating range of the laser R_{max}.
- The maximum number of theoretically reachable objects. (Objects that cross the laser's altitude band, Eq. 3.5)
- The duration of the simulated mission.
- The orbit of the laser.

The execution data contains the start date and the end date of the simulation run, and its duration. The simulation of a single scenario took 6 to 24 hours, mainly depending on the clock frequency and the type of the central processing unit (CPU), and the number of theoretically reachable objects. As output data, the following values are added to the summary record:

- The total number of crossings.
- The number of distinct objects that have been reached.

The whole tool chain has been extensively validated against the PROOF 2009 software. There have been no differences of any significance. All (minor) differences can be explained by the fact that PROOF 2009 has been compiled by the Intel Fortran compiler, which handles floating point numbers in a different way [65], leading to different rounding errors.

The technical details of the implementation are documented in a separate report [66].

3.2.2 Parameter Study and Results

The orbital laser must reach a meaningful fraction of the debris population. Otherwise, the number of possible engagements would be small, and it would be impossible to generate a noticeable impact on the debris situation.

For this reason, a parameter scan has been performed in order to identify an initial set of promising mission scenarios. When assuming a circular orbit for the laser, a mission scenario can be characterized by only three parameters: the laser's orbital inclination i, its altitude H and its maximum operating range R_{max}.

Using the crossing generator tool, every mission scenario between $600\,km$ and $1300\,km$ altitude has been simulated. The altitude step width has been $100\,km$ (Fig. 3.11a), and the inclination step width has been 20°. A number of different laser ranges R_{max} from $2\,km$ to $200\,km$ has been probed. Only the first year of each mission scenario has been simulated.

Figure 3.11b shows the results of the parameter scan. It can be seen that most objects will be reached at altitudes where the debris density is highest. This is true for all laser ranges between $2\,km$ and $200\,km$. Conclusively, the preferred orbital altitude of the space-based laser is determined at $871\,km$, where the reference population has the maximum debris density.

The real-world debris population, which is largely unknown yet, may have a slightly different altitude of maximum density. For this reason, the choice of the $871\,km$ value has a somewhat provisional character, but it is accurate enough for

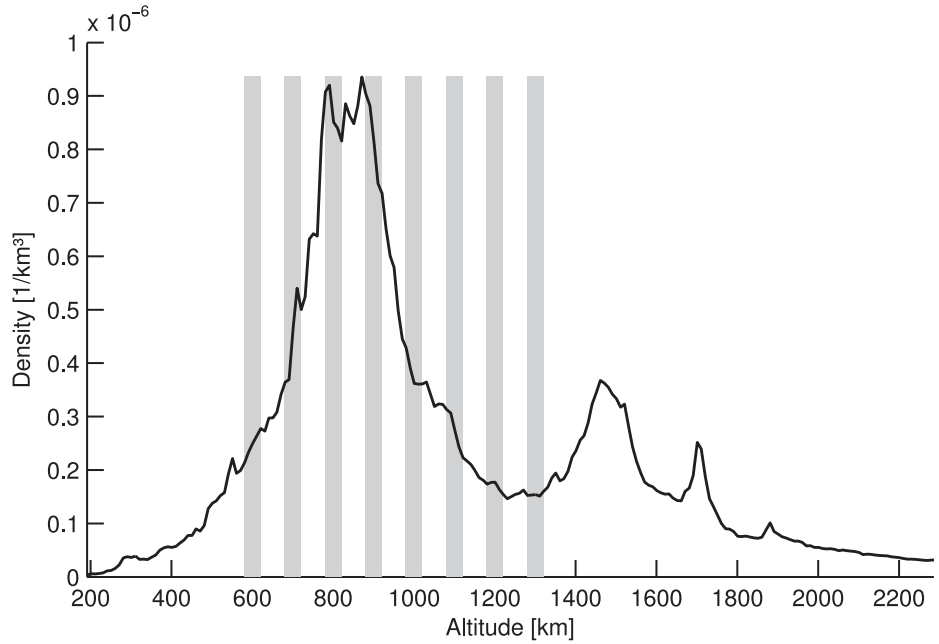

(a) Altitude discretization. Every vertical bar represents a simulated altitude.

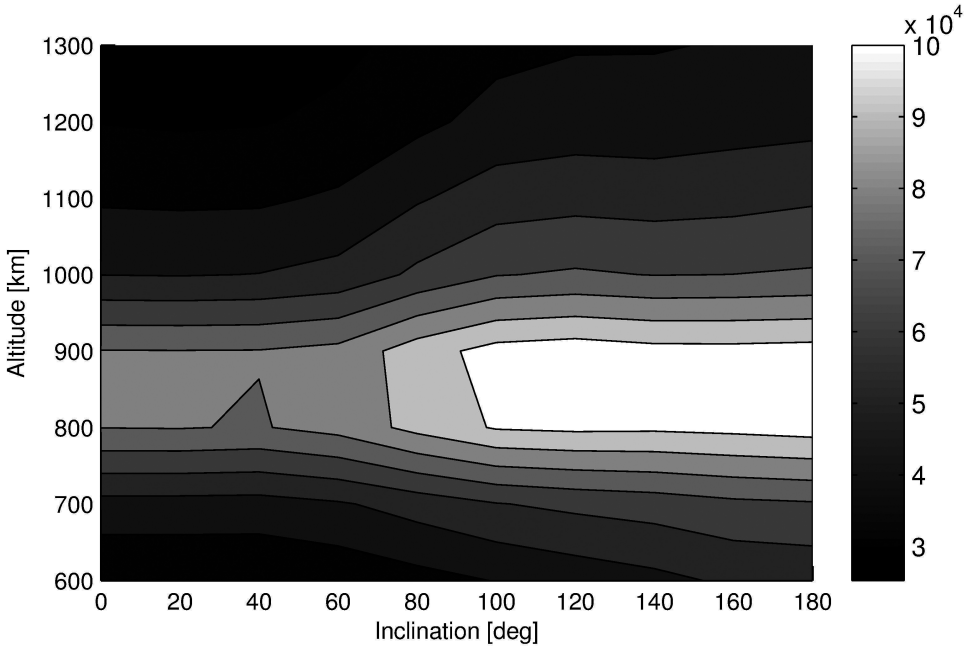

(b) Reached objects over a one-year mission ($R_{max} = 20\,km$)

Figure 3.11: Scanned altitudes and results of the parameter study

the purpose of this study.

Judging from the number of reachable objects (Fig. 3.11b), retrograde orbits ($i \geq 90°$) seem to be slightly better than prograde ones. The root cause of this effect is the increased debris flux, caused by the higher relative velocities between the mostly prograde debris and a retrograde laser. However, it must be suspected that the operational disadvantages of high relative velocities (e.g. short interaction times) will outweigh the advantage of reaching more objects. This hypothesis will be tested in the next section.

Furthermore, the subsets of reached or not reached objects showed no noticeable characteristics in terms of their size, their orbital parameters or their composition. It seems to be a more or less randomly drawn subset of the total population.

3.2.3 Impact on the Performance of the Mission

Now, that a mean laser altitude of 871 km has been selected, further conclusions can be drawn on the performance of the mission. Figure 3.12 shows that the laser sweeps a fixed altitude band. Debris objects that never enter this altitude band cannot be de-orbited.

The highest and the lowest reachable geocentric radii are

$$\begin{aligned} r_{highest} &= \underbrace{a_L(1+e_L)}_{r_{L,Apo}} + R_{max} \\ r_{lowest} &= \underbrace{a_L(1-e_L)}_{r_{L,Peri}} - R_{max} \end{aligned} \tag{3.5}$$

For moderate eccentricities ($e_L \leq 0.02$) and $R_{max} \approx 20\,km$, one can generally drop roughly $153,000$ objects from further analysis (Fig. 3.13).

Afterwards, a full reachability simulation can be performed to determine the number of objects actually reached. The main influence factors are R_{max} and the mission duration. If both parameters have high values, then the number of 'unreachable' objects in Figure 3.13 (red branching) will drop to nearly zero.

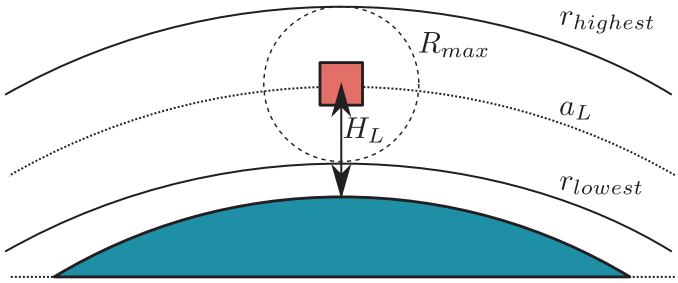

Figure 3.12: Altitude band swept by an orbital laser

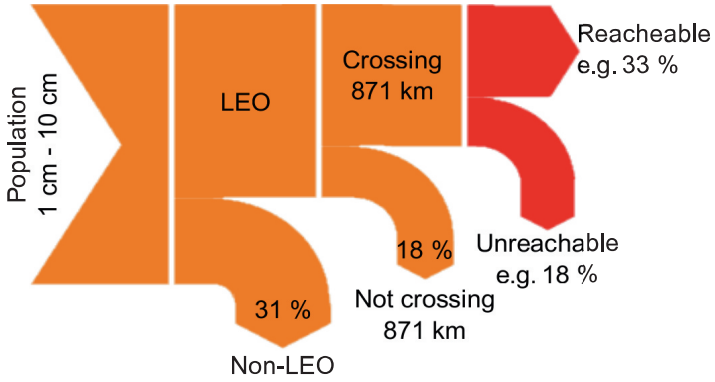

Figure 3.13: Influence of a 871 km mission altitude and reachability

3.2.4 Summary

In this section, a numerical technique has been introduced, which determines the number of reachable objects. It has been implemented into a tool named crossing generator, which requires the following input parameters: A debris population, the orbit of the laser sweeper, a mission duration, and a value for R_{max}. The implementation has been validated against the ESA PROOF software, showing only negligible deviations.

Moreover, a mean orbital altitude of 871 km has been selected for the sweeper. The value is determined by the altitude of maximum density of the debris population. Finally, there has been a better estimation for the performance of the sweeper. It takes into account the reachability of objects as an additional boundary condition. In the next section, this estimate will be refined further.

3.3 Relative Geometry

When the orbital laser engages a target object, laser-ablative recoil is generated. As a result, the orbital trajectory of the target object will change. However, not all types of trajectory change are desirable. For example, the transfer to an orbit with an increased orbital lifetime would be counterproductive.

The mission concept aims at the reduction of the orbital lifetimes of debris objects. The main influential factor on the debris lifetime is the perigee altitude: An object with a low perigee will pass through lower and denser layers of the atmosphere, where it dissipates orbital energy during each passage. Eventually, the object will burn up.

Conclusively, a change of the orbital trajectory is *favourable* when it lowers the perigee of the target object. Otherwise, it is *unfavourable*. If the trajectory change depends on the laser-ablative recoil, then how is the correlation between the recoil and the 'favourableness'? This question will be answered in this section. An equation will be derived, which gives the necessary velocity change for reaching a lower perigee. The returned velocity change depends on the direction of the recoil, and therefore on the relative position of the object w.r.t. the laser. If the equation returns a meaningful result, then the targeted perigee can be reached and the situation is favourable.

An additional aspect of the relative geometry is the angular velocity of the object w.r.t. the laser. During the engagement, the laser beam must be directed towards the object and track it along its path.

3.3.1 Theoretical Background

Two common assumptions are made. First, the transfer of momentum is impulsive. This means that the total recoil is always applied instantaneously in an infinitesimally short time. Strictly speaking, this implies a laser with unlimited power. Secondly, it is assumed that the recoil is directed towards the same direction as the laser beam (Fig. 3.14a). This is the connection to the relative geometry between the laser and the object. Both assumptions are an approximation of the real situation. Their influence will be reviewed and discussed in sections 3.4.3 and 6.1.

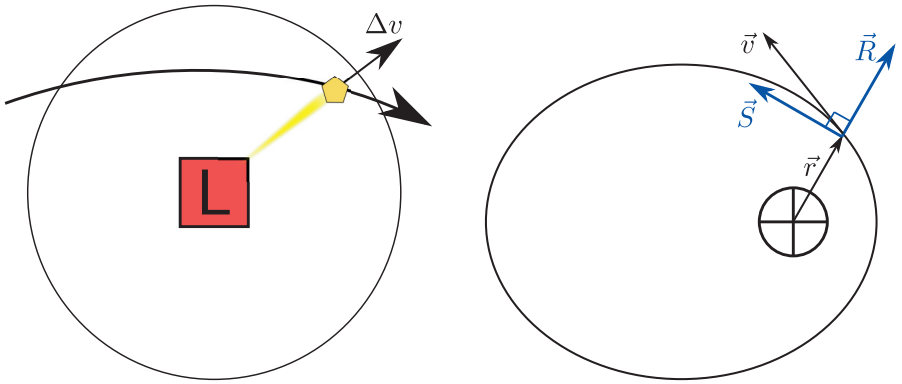

(a) The direction of the applied Δv is determined by the relative position between the laser and the target.

(b) The RSW coordinate system from [4]: The R axis points radially outward, the W axis is perpendicular to the orbital plane and the S axis is $\vec{W} \times \vec{R}$.

Figure 3.14: Direction of the recoil and the RSW coordinate frame

Initial Situation A debris object is on an initial orbit with a perigee larger than r_{Peri}. It is encountered by the orbital laser at a given Earth-centred radius r, when the initial velocity of the object is $\vec{v}_1$. The task is to change the trajectory of the object, so that its perigee becomes r_{Peri}. No doubt, the manoeuvre can be described by a single (vectorial) velocity change.

Furthermore, there is a constraint that a velocity change Δv can be applied only towards a given direction $\vec{F}_{Dir} = (X, Y, Z)^T$. This vector is given by the relative position of the object w.r.t. the laser. (Fig. 3.14a)

Definitions and Nomenclature An index of 1 indicates the orbit of the object *before* the velocity change. An index of 2 indicates the orbit of the object *after* the velocity change.

r	geocentric radius at which the target object is encountered, and at which the Δv is applied
r_{Peri}	desired perigee of the target object (perigee after the Δv has been applied), e.g. $R_{Earth} + 200\,km$
v_{Peri}	velocity of the object at the desired perigee r_{Peri} after the velocity change

ϕ_2	flight angle at radius r after the velocity change
$\vec{F}_{Dir}$	direction of the applied Δv in the RSW system as defined in [4, p.42] (Fig. 3.14b)
$(X, Y, Z)^T$	components of $\vec{F_{Dir}}$ in the RSW system
v_1	velocity of the target at the geocentric radius r (just before the velocity change)
$(v_{1R}, v_{1S}, v_{1W})^T$	components of v_1 in the RSW system

Fundamental Conditions The thrust direction vector has unit length

$$\sqrt{X^2 + Y^2 + Z^2} = 1 = |\vec{F}_{Dir}| \tag{3.6}$$

The off-plane component of the initial velocity is, by definition of the RSW system, always zero:

$$v_{1W} = 0 \tag{3.7}$$

The initial velocity is determined by the vectorial sum of its components:

$$\sqrt{v_{1R}^2 + v_{1S}^2} = v_1 \tag{3.8}$$

The scalar velocity change must always be positive; reverse impulse changes would be expressed by a mirrored $\vec{F}_{Dir}$:

$$\Delta v \geq 0 \tag{3.9}$$

Derivation The square of the specific orbital angular momentum of the target orbit is

$$h_2^2 = r_{Peri}^2 \, v_{Peri}^2 = r^2 \, v_2^2 \, \sin^2 \phi_2$$

The conservation of energy (Vis-Viva) between the same two orbital points is:

$$\frac{1}{2} v_{Peri}^2 - \frac{\mu}{r_{Peri}} = \frac{1}{2} v_2^2 - \frac{\mu}{r}$$

Together, one can write

$$\frac{r_{Peri}^2}{r^2}\left(1-\frac{2\mu}{v_2^2}\left(\frac{1}{r}-\frac{1}{r_{Peri}}\right)\right)-\sin^2\phi_2=0 \tag{3.10}$$

In the next step, Δv, $\vec{F}_{Dir}$ and v_1 are introduced into the equation, substituting ϕ_2 and v_2. Exploiting geometrical relationships (Fig. 3.15), one can find

$$v_2^2=(\vec{v_1}+\Delta v\vec{F_{Dir}})^2$$

and

$$\sin^2\phi_2=\frac{(v_{1S}+\Delta vY)^2+\Delta v^2Z^2}{v_2^2}$$

Both relationships are put into Equation 3.10. Together with the binomial theorem for $(\vec{v_1}+\Delta v\vec{F_{Dir}})^2$, one finally finds:

$$a\Delta v^2+b\Delta v+c=0$$

with

$$\begin{aligned}a&=r_{Peri}^2\,r-r^3(Y^2+Z^2)\\ b&=2\,r_{Peri}^2\,r\,(v_{1R}X+v_{1S}Y)-2\,r^3\,v_{1S}Y\\ c&=r_{Peri}^2\,r\,v_1^2-2\,\mu\,(r_{Peri}^2-r\,r_{Peri})-r^3v_{1S}^2\end{aligned} \tag{3.11}$$

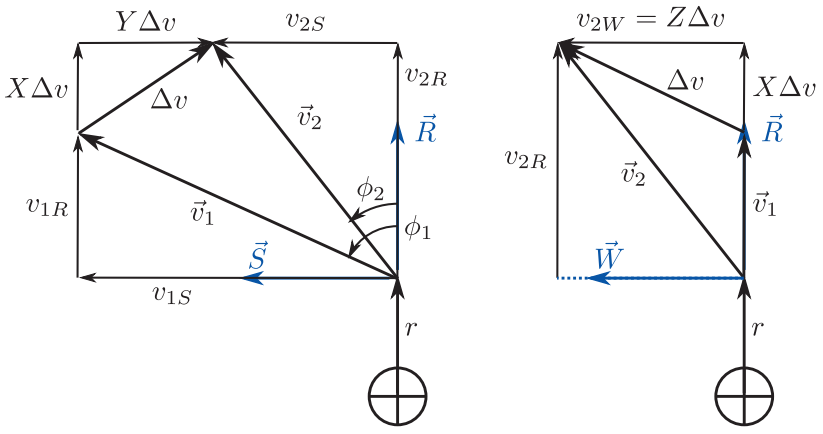

Figure 3.15: Geometrical relations between v_1, v_2 and Δv

Mathematically, this equation can have either zero, one or two real, positive solutions for Δv. Negative Δv are not allowed and must be interpreted as a false/no solution (Eq. 3.9). How many of the solutions are positive? It shows that there are three domains:

$$\begin{cases} D < 0 & \text{no real solutions} \\ D > 0 \ \wedge \ N < \dfrac{r_{Peri}}{r} & \text{one positive } \Delta v \\ D > 0 \ \wedge \ N > \dfrac{r_{Peri}}{r} & \text{both } \Delta v \text{ have the same sign} \end{cases} \tag{3.12}$$

$$\text{with} \quad N = \sqrt{Y^2 + Z^2} \quad \text{and} \quad D = b^2 - 4\,c\,a$$

However, the necessary Δv can be extremely high in some cases. Then, one could decide against a de-orbitation although it would be theoretically possible.

3.3.2 Implementation

A relative geometry is favourable if the laser could engage the object and bring it to a sufficiently low perigee. In this case, there is a real, positive solution for equation 3.11. An object is *favourable* if it acquires a favourable relative position at least once during the mission.

A relative situation between the laser and the object is called *engageable* if the object is in a favourable position and the angular velocity of the object w.r.t. the laser is below an upper limit. An *engageable object* is a debris object that acquires an engageable situation at least once during the mission. Consequently, the engageable objects are a subset of the favourable objects. (These relations are visualized in Figure 3.22 on page 78.)

In order to determine the number of favourable or engageable objects for a given scenario, the crossing generator tool has been extended. Instead of simply counting the crossings, they are analysed in depth: The relative trajectory of the object is resolved into a sufficiently large number of individual relative situations (Fig. 3.16). The kinematic state of each relative situation is then analysed with regard to its favourableness and the angular velocity. All relative situations of

all crossings for one mission are stored in a database. From this database, one can determine the number of favourable or engageable objects (Fig. 3.17).

A *relative situation* is described by the position and the velocity of both, the laser and the target object, in combination with a reference epoch:

$$\begin{aligned}\vec{R} &:= (\vec{S}_{laser},\ \vec{S}_{obj},\ t)^T \\ &= (\vec{r}_{laser,ECI},\ \vec{v}_{laser,ECI},\ \vec{r}_{obj,ECI},\ \vec{v}_{obj,ECI},\ t)^T\end{aligned} \tag{3.13}$$

For the description of the relative motion of the object w.r.t. the laser, it is necessary to transform the object into the accelerated laser-centred inertial (LCI) frame:

$$\begin{aligned}\vec{r}_{obj,LCI} =& \vec{r}_{obj,ECI} - \vec{r}_{laser,ECI} \\ \vec{v}_{obj,LCI} =& \vec{v}_{obj,ECI} - \vec{v}_{laser,ECI} - \vec{\omega}_{laser} \times \vec{r}_{obj,LCI}\end{aligned} \tag{3.14}$$

With the angular velocity of the laser motion around the Earth:

$$\vec{\omega}_{laser} = \frac{\vec{r}_{laser,ECI} \times \vec{v}_{laser,ECI}}{|\vec{r}_{laser,ECI}|^2}$$

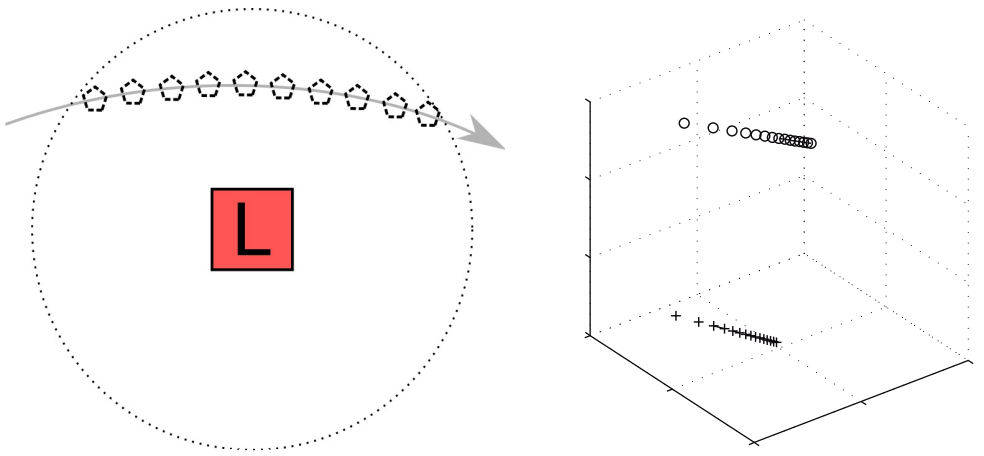

(a) Schematic drawing

(b) Example taken from an actual calculation: Every circle is an object position, every cross a laser position.

Figure 3.16: How a crossing is resolved into individual situations

```
ObjID |  SimT      | SV L  | SV O  | Range | AVel  | favourable
      |  [s]       |       |       | [km]  | [°/s] |
-------------------------------------------------------------
30782 |  484086.1  | [...] | [...] | 14.9  |  33.0 | No
30782 | 3425947.9  | [...] | [...] | 14.9  |  40.2 | Yes
30786 | 3707774.7  | [...] | [...] | 14.8  |  11.7 | Yes
[...]
```

Figure 3.17: Example of the relative situation database: The first entry shows object 30782 in situation in which de-orbitation is not possible ('unfavourable'). However, there is an opportunity to de-orbit the same object later, although the angular velocity may be challenging.

Then, the angular velocity of the object w.r.t. the laser (beam tracking velocity) can be computed:

$$\omega_{OL} = \frac{|\vec{r}_{obj,LCI} \times \vec{v}_{obj,LCI}|}{|\vec{r}_{obj,LCI}|^2}$$

The determination of the favourableness of a situation is more complicated than the computation of the angular velocity. There is a matrix that rotates from the LCI system into the RSW system of the target:

$$\bar{R} = (\vec{e}_R, \vec{e}_S, \vec{e}_W)^T$$

$$\vec{e}_R = \frac{\vec{r}_{obj,ECI}}{|\vec{r}_{obj,ECI}|} \quad , \quad \vec{e}'_W = \vec{e}_R \times \vec{v}_{obj,ECI} \quad , \quad \vec{e}_W = \frac{\vec{e}'_W}{|\vec{e}'_W|} \quad , \quad \vec{e}_S = \vec{e}_W \times \vec{e}_R$$

It allows to calculate

$$\vec{F}_{Dir} = \bar{R}\,\frac{\vec{r}_{obj,LCI}}{|\vec{r}_{obj,LCI}|}$$

and

$$\vec{v}_1 = \bar{R}\,\vec{v}_{obj,ECI}$$

The overall algorithm for the analysis of a single relative situation is depicted in Figure 3.18. If it returns $\Delta v = 0\,\frac{m}{s}$, then the situation is unfavourable. The evaluation of the favourableness has been done in a subroutine, because of its complexity. Despite the fact that it merely implements Equation 3.11, there are two challenges involved: First, the correct solution out of two possible must be

selected. The following rule has been derived:

$$\begin{cases} D < 0 & \text{return 0 (unfavourable)} \\ D > 0 \ \wedge \ N < \dfrac{r_{Peri}}{r} & \text{return } max(\Delta v_1, \Delta v_2) \\ D > 0 \ \wedge \ N > \dfrac{r_{Peri}}{r} & \text{return } max(0, min(\Delta v_1, \Delta v_2)) \end{cases} \tag{3.15}$$

$$\text{with} \quad N = \sqrt{Y^2 + Z^2} \quad \text{and} \quad D = b^2 - 4\,c\,a$$

Secondly, there is a singularity for $a = 0$, which is removable is many cases. Then, a is replaced by a very small value δ in order to return the closest numerical approximation for Δv. The algorithm is depicted in Figure 3.19. It has been proven to be very fast, robust and sufficiently accurate.

The technical details of the implementation are documented in a separate report [66].

3.3.3 Selection of Inclination and Eccentricity

Within the previous parameter study (sec. 3.2.2), it has been claimed that mission scenarios with retrograde laser orbits will have worse performance than prograde ones. This hypothesis can now be tested, using the tool for the analysis of the relative geometry.

Ten scenarios with different inclinations and a common altitude of 871 km have been simulated (Fig. 3.20a). The results of the simulations are shown in the diagram 3.20b. They present the number of the engageable objects for different upper limits of the angular velocity. It can be seen that more agile mirrors can engage a much higher number of objects.

Moreover, the curves are smoother for higher angular velocities: The main influential factor on the relative velocity is the difference between the orbital plane of the laser and the orbital planes of the objects. For low tracking velocities, only coplanar objects with the same inclination as the laser can be engaged, and the curve follows the distribution of the objects over the inclination. The more

function EvalSituation($\vec{r}_{laser,ECI}$, $\vec{v}_{laser,ECI}$, $\vec{r}_{obj,ECI}$, $\vec{v}_{obj,ECI}$, r_{Peri}, μ)
  $\vec{r}_{obj,LCI} \leftarrow \vec{r}_{obj,ECI} - \vec{r}_{laser,ECI}$
  $R \leftarrow |\vec{r}_{obj,LCI}|$

  if $R < 2m$ **then**
    $\omega_{OL} \leftarrow 2\pi$
  else
    $\vec{\omega}_{laser} \leftarrow \vec{r}_{laser,ECI} \times \vec{v}_{laser,ECI}$
    $\vec{\omega}_{laser} \leftarrow \vec{\omega}_{laser}/|\vec{r}_{laser,ECI}|^2$
    $\vec{v}_{obj,LCI} \leftarrow \vec{v}_{obj,ECI} - \vec{v}_{laser,ECI} - \vec{\omega}_{laser} \times \vec{r}_{obj,LCI}$
    $\omega_{OL} \leftarrow |\vec{r}_{obj,LCI} \times \vec{v}_{obj,LCI}|$
    $\omega_{OL} \leftarrow \omega_{OL}/R^2$
  end if

  $\vec{e}_R \leftarrow \vec{r}_{obj,ECI}/|\vec{r}_{obj,ECI}|$ ▷ Construct RSW of object
  $\vec{e}_S \leftarrow \vec{v}_{obj,ECI}$
  $\vec{e}_W \leftarrow \vec{e}_R \times \vec{e}_S$
  $\vec{e}_W \leftarrow \vec{e}_W/|\vec{e}_W|$
  $\vec{e}_S \leftarrow \vec{e}_W \times \vec{e}_R$
  $\bar{R} \leftarrow (\vec{e}_R, \vec{e}_S, \vec{e}_W)^T$ ▷ from ECI to RSW

  $F_{Dir} \leftarrow \bar{R} \cdot \vec{r}_{obj,LCI}$
  $F_{Dir} \leftarrow F_{Dir}/|F_{Dir}|$
  $(v_{1R}, v_{1S}, v_{1W}) \leftarrow \bar{M} \cdot \vec{v}_{obj,ECI}$
  $\Delta v \leftarrow \text{DeltaV}(|\vec{r}_{obj,ECI}|, r_{Peri}, v_{1R}, v_{1S}, F_{Dir}, \mu)$ ▷ (p. 74)

  return $(\Delta v, \omega_{OL})$
end function

Figure 3.18: Algorithm for Υ

function DELTAV($r, r_{Peri}, v_{1R}, v_{1S}, X, Y, Z, \mu$)
  $r_3 \leftarrow r^3$ ▷ Useful values
  $r_{p2} \leftarrow r_{Peri}^2$
  $v_{12} \leftarrow v_{1R}^2 + v_{1S}^2$

  $a \leftarrow r_{p2} * r - r_3 * (Y^2 + Z^2)$
  if $a = 0$ **then** ▷ Catch singularities
    $a = sqrt$(minimum positive value)
  end if
  $b \leftarrow r_{p2} * r * (v_{1R} * X + v_{1S} * Y) - r_3 * v_{1S} * Y$
  $b \leftarrow 2 * b$
  $c \leftarrow r_{p2} * r * v_{12} - 2 * \mu(r_{p2} - r * r_{Peri}) - r_3 * v_{1S}^2$

  $p \leftarrow b/a$
  $q \leftarrow c/a$
  $D \leftarrow p^2/4 - q$
  $\Delta v_1 \leftarrow -p/2 + sqrt(D)$ ▷ Calculate solutions
  $\Delta v_2 \leftarrow -p/2 - sqrt(D)$

  if $\Delta v_1\ \Delta v_2 < 0$ **then** ▷ Which solution is correct?
    return $max(\Delta v_1, \Delta v_2)$
  else
    return $max(0, min(\Delta v_1, \Delta v_2))$
  end if
end function

Figure 3.19: Algorithm for Δv

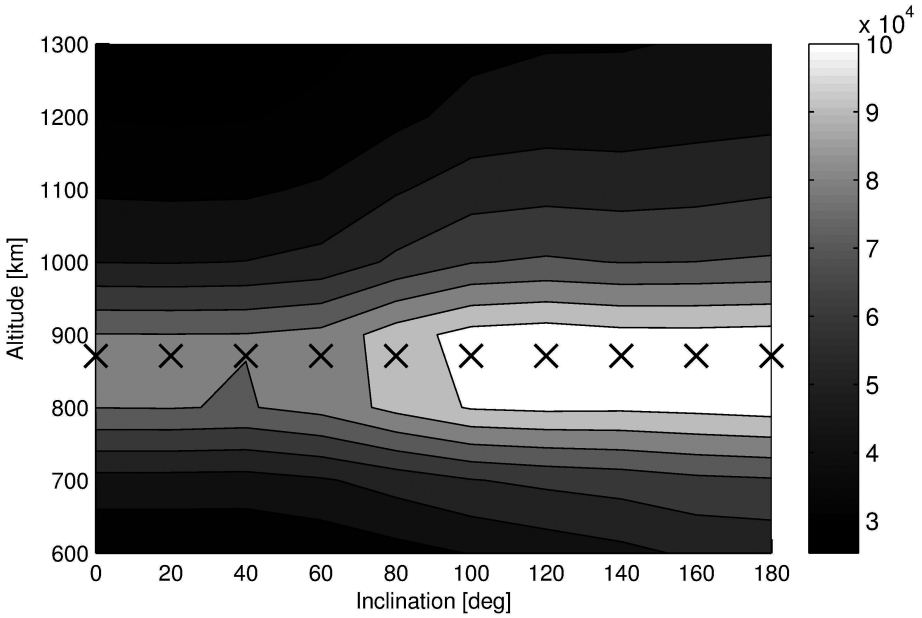

(a) The simulated scenarios are marked by crosses. (The greyscale is the number of reachable objects from Figure 3.11b.)

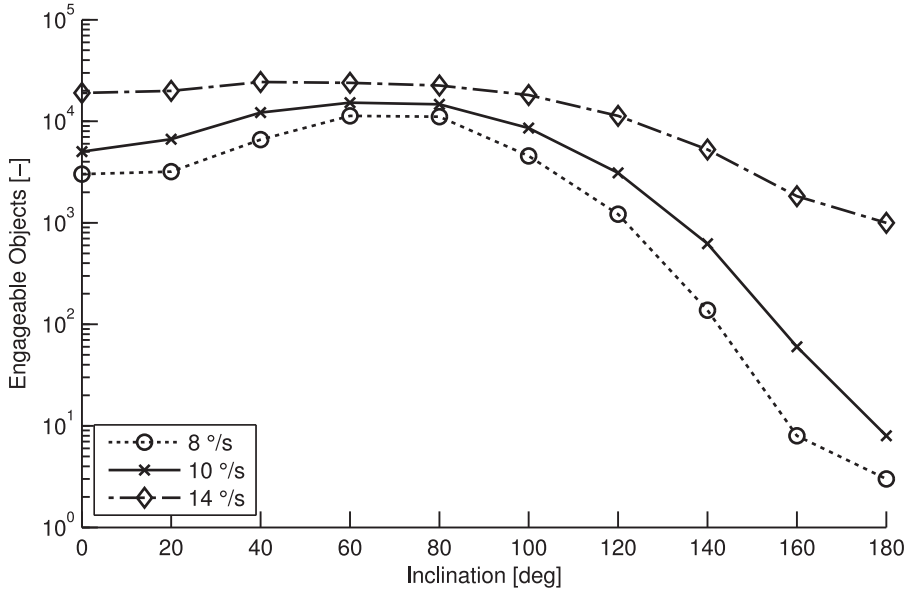

(b) Engageable objects for $R_{max} = 20\,km$ and different tracking agilities of the laser.

Figure 3.20: Selection of an orbital inclination for the laser (scenario with $R_{max} = 20\,km$ at $871\,km$ altitude)

agile the laser is, the more inclination difference it can tolerate.

This also explains why retrograde orbits are worse than prograde ones, except for very agile lasers, which can track practically every particle regardless of its velocity. However, the available time for the interaction would still be very short then.

One can perform the same simulation for R_{max} other than $20\,km$. Although the number of engageable objects will be different, the same qualitative relationship will be found for all $2\,km \leq R_{max} \leq 200\,km$. It can be said that putting the laser on a highly inclined orbit (near-polar) will maximize the number of engageable objects.

Until now, the laser has been assumed on a circular orbit. On one hand, a nonzero eccentricity might guide the laser to orbital altitudes where the debris density is lower, thus reducing the number of the reached objects. On the other hand, additional objects may be encountered, because additional altitudes are swept by the laser. The first effect would reduce the performance, and the latter one would increase it.

In order to find out which effect is dominant, scenarios for different eccentricities have been simulated. The mean altitude, however, always remained fixed at $871km$. Figure 3.21 shows the number of the engageable objects depending on the maximum angular velocity of the laser and the eccentricity. For both selected inclinations, there seems to be a preferable eccentricity of around 0.01 or 0.02.

A noteworthy side aspect is the magnitude of the angular velocity, represented by the x-axis in Figure 3.21. It seems that the mirror must be tracked with at least $2\,°/_s$ to $4\,°/_s$ in order to engage any objects at all, and that the gradient of the curves is steepest at roughly $25\,°/_s$. This means that beyond this point, the ratio of additional objects per improvement of the agility becomes increasingly disadvantageous. These values span a selection range for the mirror agility of the sweeper.

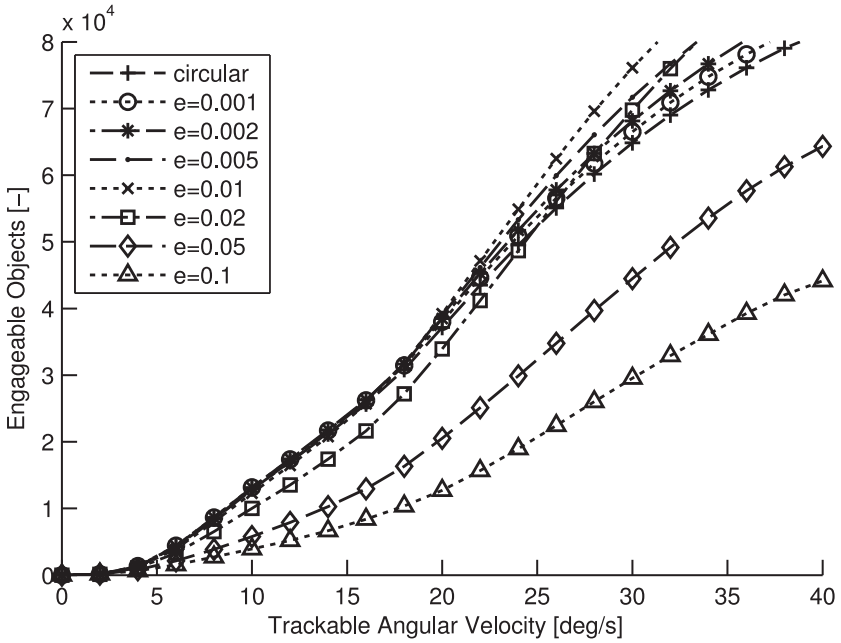

(a) $i = 90°$

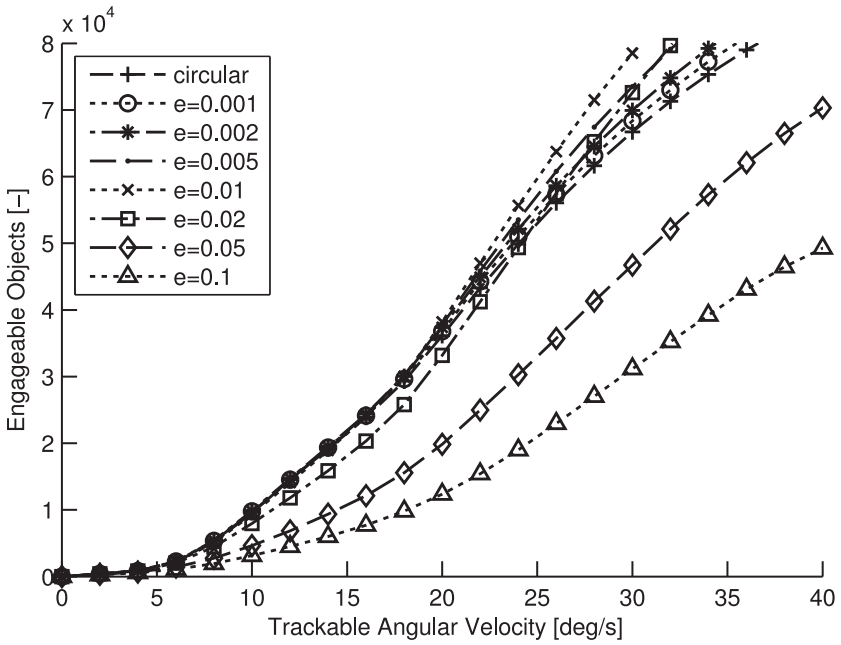

(b) $i = 97.9°$

Figure 3.21: Selection of an orbital eccentricity for the laser (for $1y$-mission)

3.3.4 Impact on the Performance of the Mission

One can substantially extend the mission performance model by using the above considerations. As already explained, debris objects with a perigee altitude below 200 km are considered 'removed'. In the reference population (as well as in the real world one), there are always a small number of those short-lived objects. They can be taken out of further consideration.

Using the geometry analysis tool, all unfavourable objects can be identified. They never acquire a relative position where an engagement would lead to their deorbitation.

Finally, an object must be moving with a tolerable angular velocity while being in a favourable situation. Otherwise, it cannot be engaged by the laser. (Fig. 3.22)

In this section, the influence of the flyby geometries has been analysed and expressed in measurable quantities. The impact on the overall remediation performance of the mission has been determined. The performance estimate from the

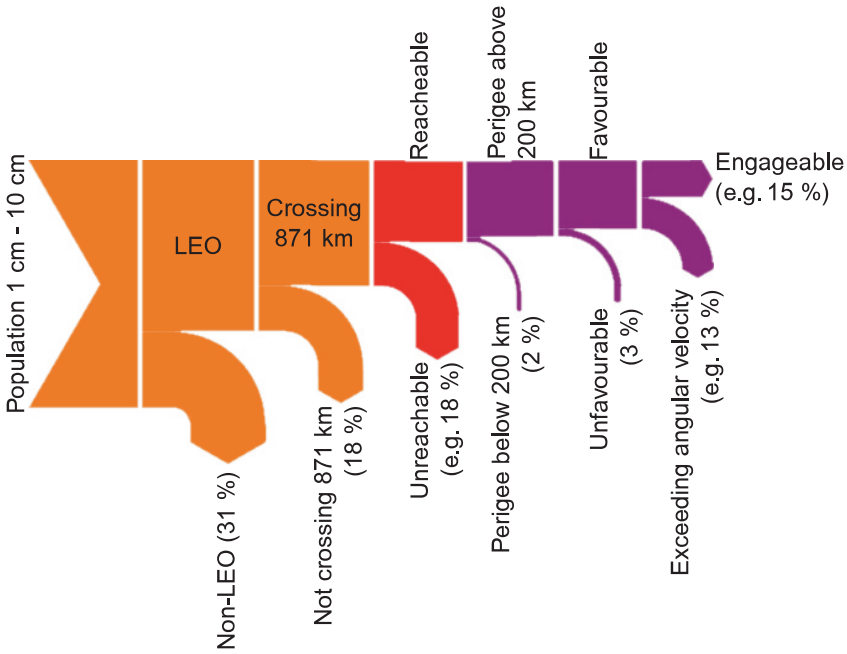

Figure 3.22: Influence of the relative geometry on the performance of the mission

previous section ('Reachability') has been refined.

In addition to that, it has been possible to select an inclination and an orbital eccentricity for the sweeper. Both choices can be justified based on the refined performance model, taking into account both, the reachability and the relative geometry of the crossings.

Up to this point, the model is based entirely on kinematic considerations. The proper motions of the space objects are described by conic sections and the manoeuvres by velocity changes. The next section will add the kinetic aspect and further extend the performance model. The source of the velocity changes, namely a laser and its interaction with the targeted objects, will be introduced.

3.4 Laser-Debris Interaction

So far, the number of engageable objects can be determined. However, just because an object is being engaged by the laser, it does not necessarily mean that it is going to be de-orbited. For example, the interaction time might be too short for the transfer of sufficient velocity change. In that case, the perigee of the object would be lowered, but not below $200\,km$.

This section will fill in the missing piece in the performance model by introducing a model for the interaction between the laser and a debris object.

3.4.1 Modelling Laser-Ablative Propulsion

Generally, laser-ablative propulsion can be described by two figures: A coupling coefficient C_m and a specific impulse I_{sp}. Leaving aside the latter for now, the coupling coefficient is the ratio of the impulse change per incident laser energy. It is the connection between the laser-optical effects and the kinematic state of the object.

To determine the change of the perigee of an individual object, three things need to be done. First, one must calculate the incident laser energy, which can be achieved by using basic geometric relations. Secondly, one must determine the value of C_m. Finally, the laser energy, multiplied with C_m, is the impulse change of the target object.

The determination of C_m is not easy, because the quantity depends on many variables. A laser pulse is usually absorbed in the hulls of the atoms, heating the electrons in the lattice. The electrons, in turn, are then heating the atoms. At the same time, heat conduction will transfer energy away from the site of the ablation, which leads to a loss of energy.

Dissociation and ionization can occur, especially when the intensity at the site of the ablation is high. Then, the generation of a plasma absorbs part of the laser energy.

The ejection process of the ablated material follows the rules of (multiphase) hydrodynamics, and if there is a significant ionization, then additional electrodynamic effects will come into play.

Although the individual effects have been understood, there is no comprehensive model for the prediction of C_m, especially not for large parameter ranges. Therefore, an empirical approach has been chosen. There exists a curve of C_m over $I\lambda\sqrt{\tau}$, which seems to have the same qualitative shape for all ablators (Fig. 3.23a) [36]. This curve seems to be valid for pulse durations from $100\,ps$ to $1\,ms$ and for laser wavelengths from X-ray to infrared. Now, that there is information on the qualitative trend, the remaining question is: What are the scales for the relevant materials in vacuum conditions?

The Institute of Technical Physics (ITP) of the German DLR has conducted a series of experiments on this matter. A Nd:YAG laser has been fired on typical space debris materials, which are mostly metallic, and the resulting recoil has been measured. It turned out, that the resulting coupling coefficients were in the range of $5\,N/MW$ to $20\,N/MW$ [58, 67].

In this light, the C_m curve has been scaled to match these experimental values. The resulting approximation for C_m is shown in Figure 3.23b. This model for C_m will be used for the remainder of this thesis.

The chosen model is limited in its accuracy. First, because the material dependency has been dropped, and an average debris target material is assumed. Because there is insufficient experimental data available, separate C_m curves for different materials could not be justified. Besides, the bulk of the debris objects

are expected to be of metallic nature, and therefore comparable.

Secondly, because the influence of the different shapes of the targets have not been taken into account. This aspect is further discussed in section 6.1 on page 112.

Thirdly, the C_m has been extrapolated for high intensities, because experimental data was not available. Finally, the I_{sp} has not been modelled. From the I_{sp}, one could calculate the ablation rate $\dot{m}$ and deduce an estimate for the shrink rate of the particle. A substantial part of the object must be expected to be ablated. This could lead to smaller incident cross sections and affect subsequent laser interactions (sec. 2.4). However, the experimental data on this aspect is rare, so that it has been decided to omit the simulation of this effect for now. Besides, the object will shrink but become lighter at the same time, so that both effects compensate for each other to a certain degree.

3.4.2 Implementation

Again, the crossing generator tool has been modified. Upon detection of a crossing, the relative trajectory is scanned for engageable situations.

If an engageable situation is found, the laser decides either to engage or not

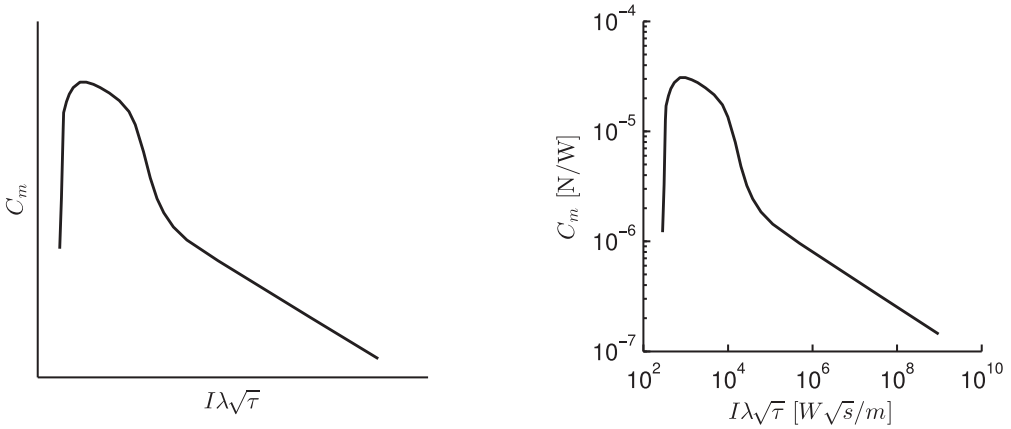

(a) Qualitative trend of C_m over $I\lambda\sqrt{\tau}$ for lasers in the nanosecond range, as published in [36].

(b) Coupling coefficients used for simulation of the laser-debris interaction.

Figure 3.23: Coupling coefficient curves

to engage the object. This decision depends on a logic that has been named *engagement policy*. The engagement policy is modular and can be used to model operational aspects of the mission. For example, the laser could be set to engage only objects of a particular orbit or size, or at a specific time of the day, or when there are certain illumination conditions or when there is ground station coverage.

Within this study, the laser engages on every opportunity, but only once per crossing. This means, it will not engage the object a second time during the same pass. (Sometimes, the objects acquire a very high angular velocity near the point of closest approach.) Much more complex policies are thinkable.

Between the engagement and the disengagement, the propagation along a Kepler ellipse will not work because the laser-ablative thrust is a strong perturbing force. Therefore, the object is propagated using a Runge-Kutta 4/5-algorithm, which takes into account the gravitation of the Earth as well as the laser-ablative thrust. (Fig. 3.24)

For every time step of the propagation, there is an amount of emitted laser energy:

$$W_{\Delta t} = W_p \, f \, \Delta t$$

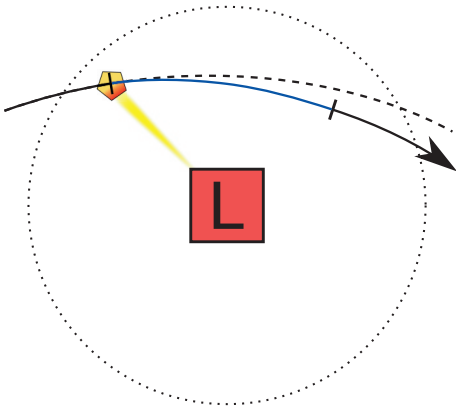

Figure 3.24: Change of the trajectory of the object within an engagement: The blue line indicates the duration of the engagement. This particular section is propagated using a Runge-Kutta solver.

From there, the absorbed energy is calculated

$$W_{\Delta t,absorbed} = W_{\Delta t} \ \min\left(1; \frac{D^2}{d_f^2}\right)$$

using d_f from Equation 2.2 and D as the object's diameter. Then, the coupling value is computed for the current time step. Together with the C_m, the laser-ablative force is determined:

$$\vec{F}(t) = \vec{F}_{Dir}\, C_m(I, \lambda, \tau)\, \frac{W_{\Delta t,absorbed}}{\Delta t}$$

As one can see, many new system parameters have been used. This means that the engagement simulation requires additional input parameters compared to the analysis of the reachability or the analysis of the relative geometry. These are the wavelength λ, the pulse width τ, the diameter of the primary aperture d_L, the quality of the laser beam M^2 and an engagement policy. All these values can be specified by the user, so that the algorithm itself is completely generic.

The technical details of the implementation are documented in a separate report [66].

3.4.3 Impact on Mission Performance

Using the engagement calculating tool, the overall effective impact of the mission on the debris population can be simulated.

In this context, there is a noteworthy effect: In the previous section 3.3, the number of the engageable objects has been determined. There, an algorithm has been developed, which can find the situations that are suitable for engagement. The derivation of this algorithm assumed impulsive manoeuvres and lasers with infinite power. During the simulation of the engagements in this section, however, it turned out that engaging an engageable object will not always lower its perigee. This is because real-world lasers have a finite power, and the transfer of impulse requires a finite interaction time. The underlying assumptions of Eq. 3.11 have been violated.

Mathematically, one can illustrate what happens by deriving the reverse function of Eq. 3.11:

$$ar_{Peri}^2 + br_{Peri} + c = 0$$

$$\begin{aligned} &\text{with} \\ &a = r\Delta v^2 + 2r\Delta v(v_{1R}X + v_{1S}Y) + rv_1^2 - 2\mu \\ &b = 2\mu r \\ &c = -r^3\Delta v^2(Y^2 + Z^2) - 2r^3 v_{1S} Y \Delta v - r^3 v_{1S}^2 \end{aligned} \tag{3.16}$$

Instead of asking for the necessary Δv to achieve r_{Peri}, this equation gives the r_{Peri} resulting from a given Δv. Obviously, the solution is nonlinear.

A typical example is depicted in Figure 3.25. If the laser can only apply a small Δv on the object, its perigee will rise, although the relative situation is favourable! This can happen, for example, if the applied velocity change has a large radial component. Then, the irradiation with the laser causes two competing effects on the perigee of the target: On one hand, the orbital velocity is increased, because orbital energy is added. On the other hand, the eccentricity will increase because the direction of the velocity vector changes. For high Δv, the latter effect predominates. (The orbit would intersect the centre of the Earth, if the engagement was in a radial direction and the Δv went against infinity.)

For this reason some objects will not be engaged, although they are engageable objects. This has a negative effect on the performance of the mission, which can be mitigated by increasing the pulse repetition rate of the laser. Some other objects are not engaged because of operational constraints, which are defined in the engagement policy. (Fig. 3.26)

Some of the engaged objects are removed (perigee below 200 km), while others will left in orbits with a reduced lifetime. Both effects are desirable, although a complete de-orbitation is preferable. Here again, increasing the laser's pulse rate will increase chance of a complete de-orbitation within the available interaction time. The number of the de-orbited objects goes against the number of the engageable objects when the power of the laser goes against infinity.

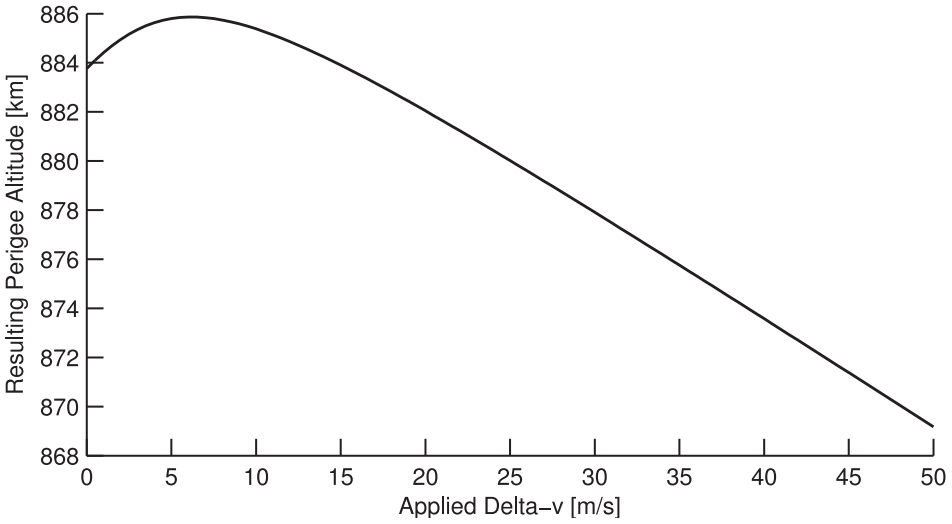

Inclination	81.252°	Eccentricity	0.001
Ω	153.240°	ω	77.694°
Semi-major axis	$7261.318\,km$	True anomaly	169.19°
$\vec{F}_{Dir} = (R = 0.793, S = 0.220, W = -0.568)$			

Figure 3.25: Nonlinearity of the perigee over Δv: The post-engagement perigee can grow, if the applied Δv is too weak. The graph shows an example of a relative situation, and the perigee altitude that would be obtained for different Δv.

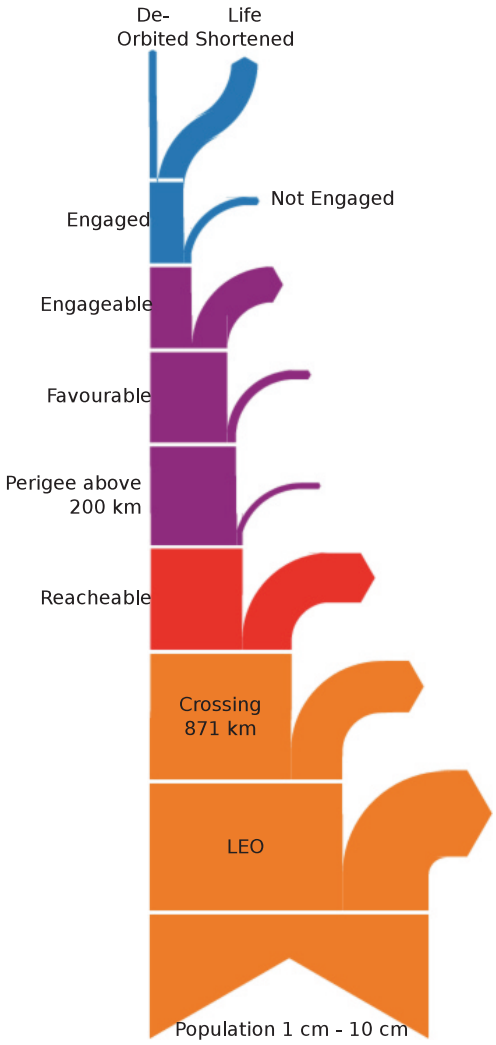

Figure 3.26: Complete model of the mission performance

4 Total System Efficiency

Now that a comprehensive mission performance model has been established, it is time to evaluate the potential of the proposed mission concept. Since the parameter space is fairly large, a curtailing of its boundaries is prudent before the parameters of mission case study are selected.

4.1 Preselection of Mission Parameters

The orbit of the mission has been fixed in the previous chapter. The number of reached particles depends only on the laser range R_{max} and the duration of the mission. In order to quantify this relationship, a larger number of scenarios have been simulated using the crossing generator tool. The result is visualized in Figure 4.1. This graph accounts for the red branching in Figure 3.26. Neither a long mission ($10\,y$) nor a large laser range ($200\,km$) alone seems to be sufficient. Only a combination of both brings a significant fraction of the objects of the population into the influence sphere of the laser.

For a $10\,y$ mission duration, the differential number of the reached particles is shown in Figure 4.2. It gives the additional number of reached objects per additional range of the laser. The total number of the reached objects is measured by the surface under the graph (logarithmic scale!). For an R_{max} up to $10\,km$, large quantities of additional objects can be reached for every kilometre of additional laser range. Beyond $R_{max} = 20\,km$, every additionally reached object comes at the price of a substantially higher range for the laser.

From this curve, one can derive three types of mission: The 'efficient' mission at $R_{max} = 10\,km$, the 'effective' mission at $R_{max} = 50\,km$, and the 'balanced' mission with $R_{max} = 20\,km$. All three variants are characterized by a different

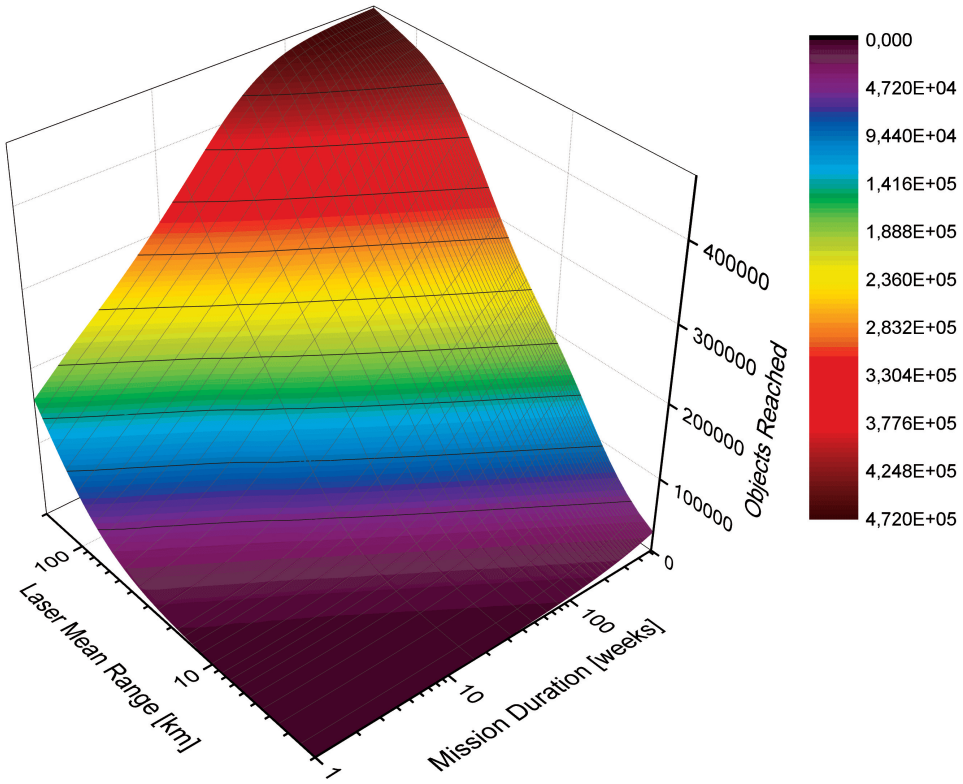

Figure 4.1: The number of the reachable objects depending on R_{max} and the duration of the mission

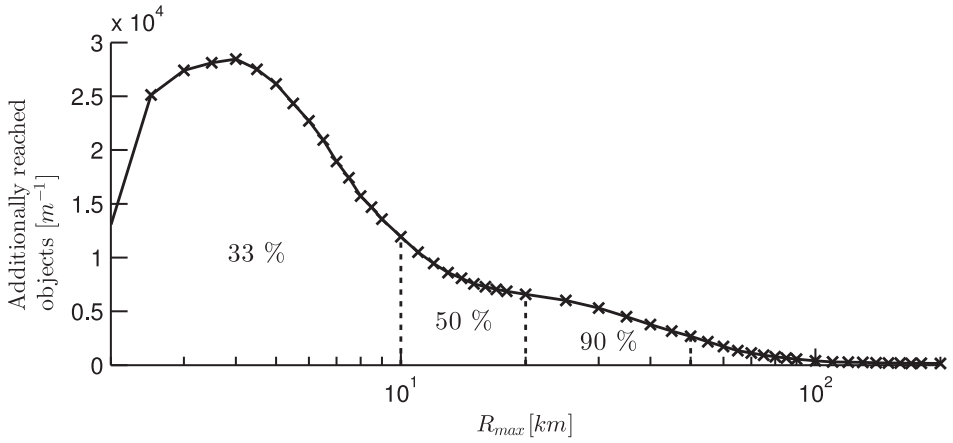

Figure 4.2: Differential reachable objects curve for a 10 y mission: The surface under the curve is a measure for the total number of *reachable objects*.

ratio of reached objects per 'invested' range of the laser.

The next step in the performance model (Fig. 3.26) subtracts all objects, whose perigee already are below an altitude of 200 km. The total number of those objects also depends on R_{max} and the mission duration. Figure 4.3 shows that they never represent more than 1 % of the reachable objects. A figure of 2 % is a safe worst-case presumption for a first-shot study of the remediation performance.

Similarly, one can look at the fraction of unfavourable objects, which also depends only on R_{max} and the duration of the mission. Interestingly, their percentage seems to be nearly invariant of the duration of the mission. (Fig. 4.4)

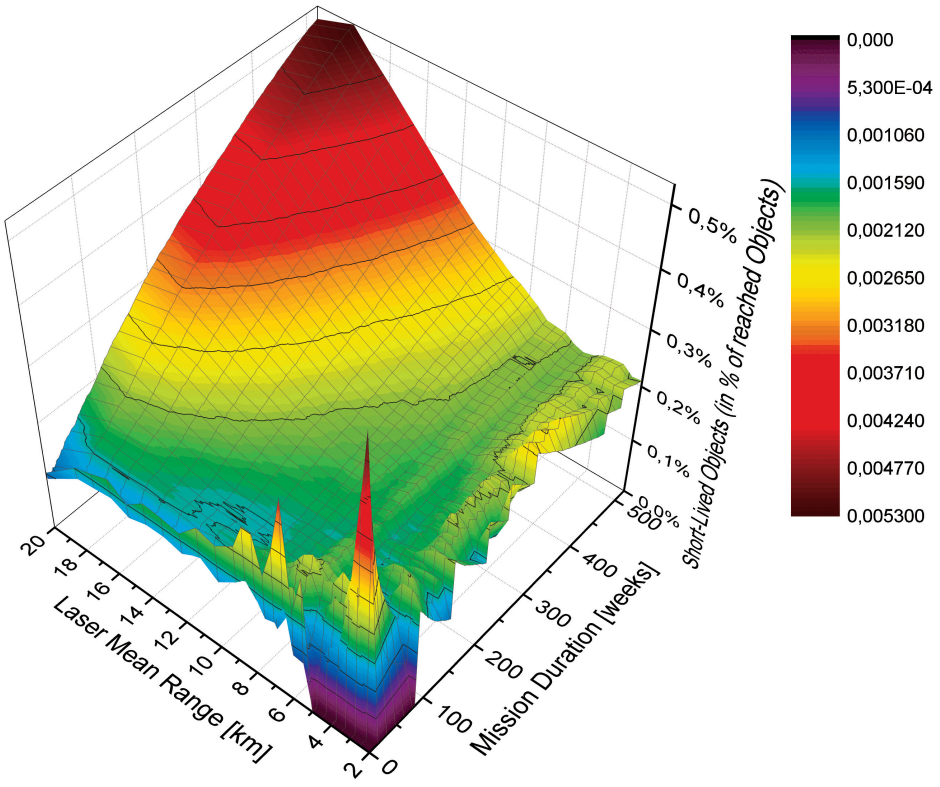

Figure 4.3: Fraction of objects with perigee already below 200 km

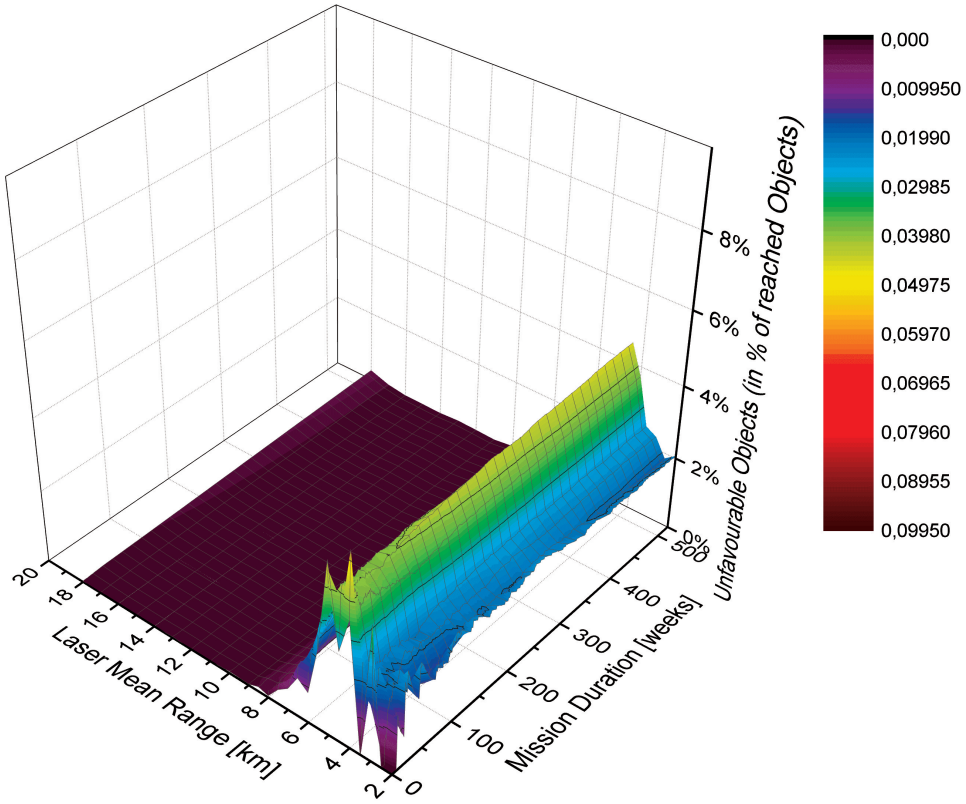

Figure 4.4: Fraction of unfavourable objects

4.1.1 Selection of a Laser

For the simulation of case studies for the sweeper system, a laser system must be specified. A preliminary choice will be made in this subsection. A follow-up study would perform a more thorough selection, which would be based on a systematic trade-off.

The chosen laser system is a Nd:YAG disc laser, which offers short pulses, a fair beam quality and can be scaled to high powers. Its parameters are listed in Table 4.1. The pulse energy W_p is selected individually for every scenario, because it depends on the range of the laser R_{max} in combination with the pulse width τ (eq. 2.5).

It is hard to predict what laser technology will be available in 10 or 20 years from now, because there is a rapid technological development. Generally, using

Parameter	Symbol	Value
Wavelength	λ	$1064\,nm$
Pulse width	τ	$10\,ns$
Beam quality	M^2	12
Shots per second	f	$1\,kHz$
Primary aperture	d_{Aper}	$2.5\,m$

Table 4.1: Parameters of baseline laser system

the laser in space implies additional possibilities, as well as extra constraints. For example, one can use wavelengths that lie in the absorption bands of the atmosphere. This would not be possible for ground-based laser brooms. When choosing such a laser, however, one would abandon the possibility of a synergetic laser development for both removal concepts.

At the same time, the use of laser types with high supply masses would be disadvantageous in space, because all supplies would have to be transported into space. For that purpose, one can rule out the use of chemical lasers, such as military deuterium fluoride lasers. The exchange of wear parts for 'regenerative' laser technologies, such as the exchange of pump diodes, would have to be addressed in a technology trade.

4.2 Removal Efficiency of Reference Scenarios

In this subsection, some exemplary mission cases will be presented. A set of mission parameters for the case studies must be selected as a starting point. Three representative laser ranges, $10\,km$, $20\,km$ and $50\,km$, have been chosen according to Figure 4.2. The laser parameters in Table 4.1 and a default engagement policy (sec. 3.4.2) complement the scenario description. However, one parameter is still undefined: the maximum beam tracking velocity of the laser. According to the observations, which can be made on page 76, at least a few degrees per second are required to engage *any* object at all. On the other side, $25\,°/_s$ seem to be a reasonable maximum value; and $15\,°/_s$ is chosen as a balanced value in between.

Table 4.2 shows a matrix of nine scenarios. Three of them will be discussed in detail: 'demonstrator', 'baseline' and 'high-end'. This should give an impression

	$R_{max} = 10\,km$	$R_{max} = 20\,km$	$R_{max} = 50\,km$
$2.4\,°/_s$	A11 Demonstrator (sec. 4.2.1)	A12	A13
$15\,°/_s$	A21	A22 Baseline (sec. 4.2.2)	A23
$25\,°/_s$	A31	A32	A33 High-End (sec. 4.2.3)

Table 4.2: Simulated Missions A11-A33

of the removal efficiencies that can be reached with space-based laser-ablative debris removal. A comprehensive summary of the three reference scenarios is provided in Table 4.3 on page 100.

Beyond the scope of this thesis, one could also study scenarios with other values for R_{max}, the mission duration or the tracking velocities. Additionally, variations of the operational concept are possible, such as constellations of lasers, other engagement policies or other parameters for the laser.

4.2.1 The Baseline Scenario

The baseline scenario is meant to be an average mission scenario in the centre of the overall parameter space. It balances the technological requirements against the removal effectiveness.

For a laser range of $20\,km$, a laser pulse energy as large as $372\,J$ is necessary (eq. 2.5). Figure 4.5 shows the Sankey chart for the $10\,y$ long mission. Using a $2.5\,m$ mirror, which can be rotated with $15\,°/_s$, roughly half of the favourable objects are still too fast. One can also see that many objects are unreachable.

Both problems could be approached by increasing R_{max}: It reduces the number of the unreachable objects in favour of the reachable objects. Additionally, as a side effect, a larger R_{max} leads to more crossings per object. Consequently,

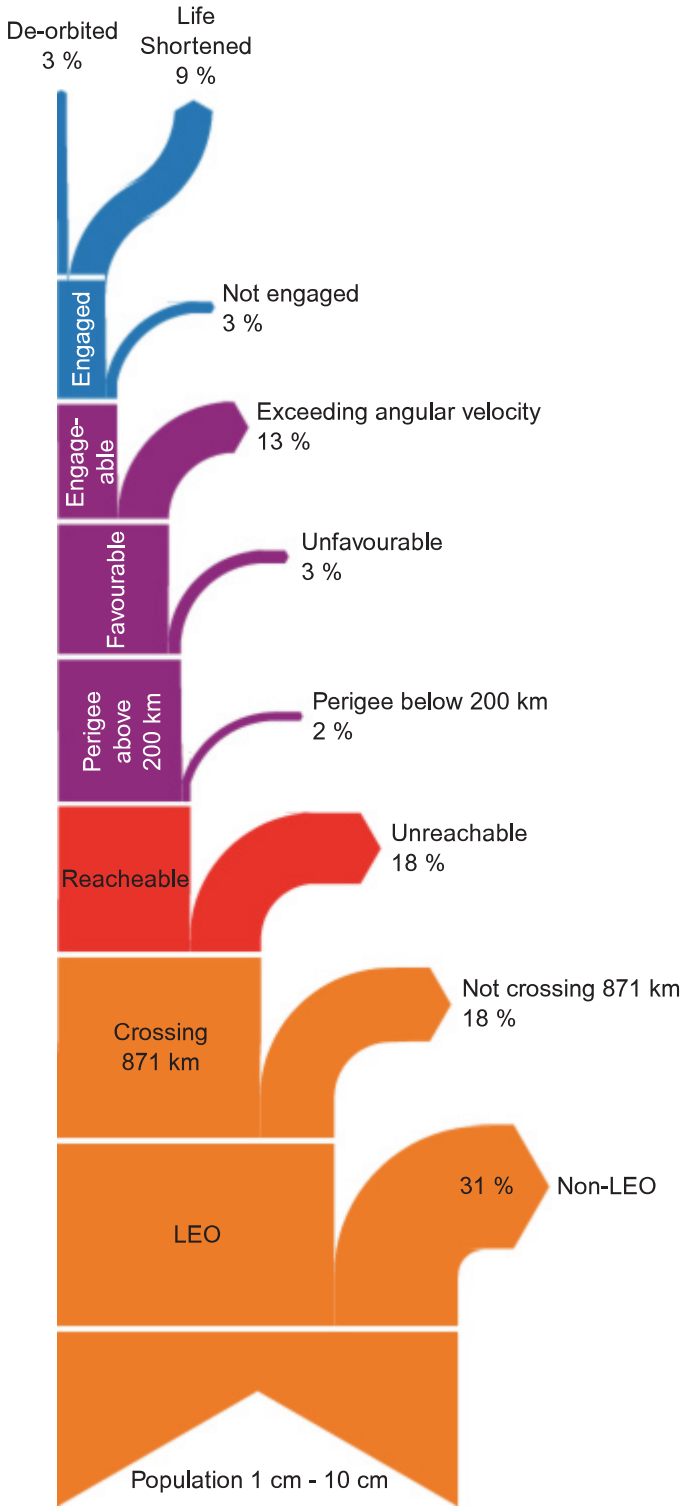

Figure 4.5: Sankey chart of the baseline scenario

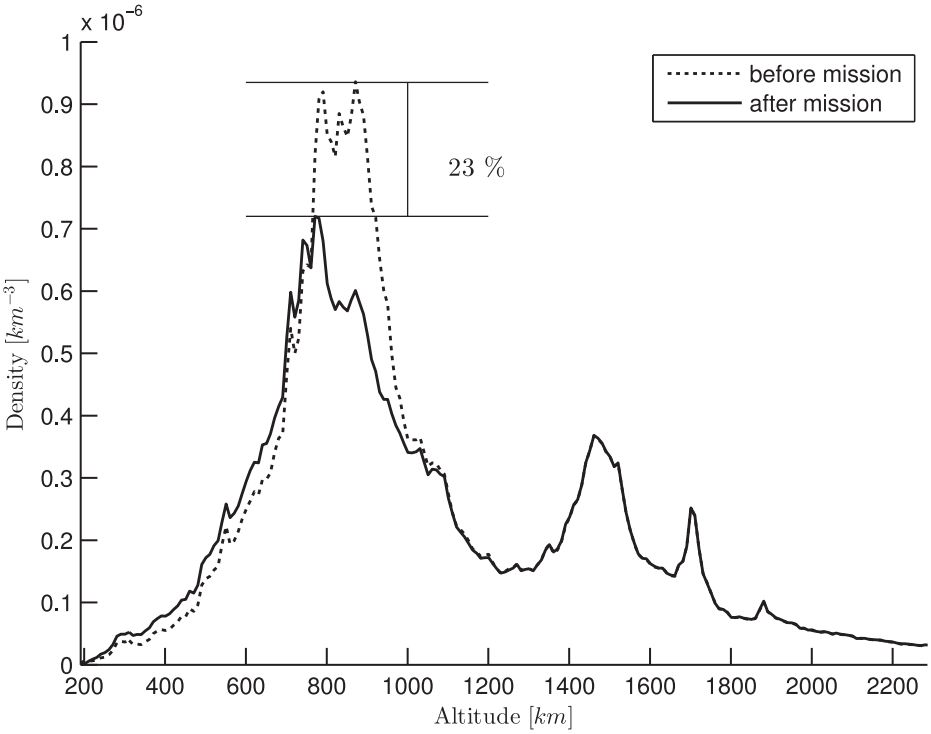

Figure 4.6: Debris density after the baseline scenario

the odds of encountering an object at an acceptable velocity would increase.

Nonetheless, the scenario could contribute to a cleaner orbit, as shown in Figure 4.6: It shows the density of the orbital debris in LEO before and after the mission. Because many objects are not de-orbited, but only moved to lower orbits, the debris density at lower altitudes can increase. The percentage of fully de-orbited objects could be improved by increasing the pulse rate of the laser.

4.2.2 The Demonstrator Scenario

The demonstrator scenario aims at being a mission that could be put into practice within minimum time from now. It is not required to significantly change the debris population. Instead, it shall prove the validity of the overall removal concept, while keeping the need for the development of new technologies low.

The demonstrator mission has practically no impact on the density of the orbital debris, but it requires pulse energies of the laser of 'only' 95 J. Over the 10-year mission time, 420 objects are engaged in 429 engagements. 104 objects are completely removed from orbit. This means that there is an average of 3.5 engagements per month, which would allow a thorough preparation, monitoring and evaluation by ground controllers.

Figure 4.7 shows the Sankey chart of the scenario. The deficiencies are the same as in the baseline scenario, but they are heavier in magnitude: Many objects are not even reached, and most of the remaining objects are too fast for being tracked by the laser beam.

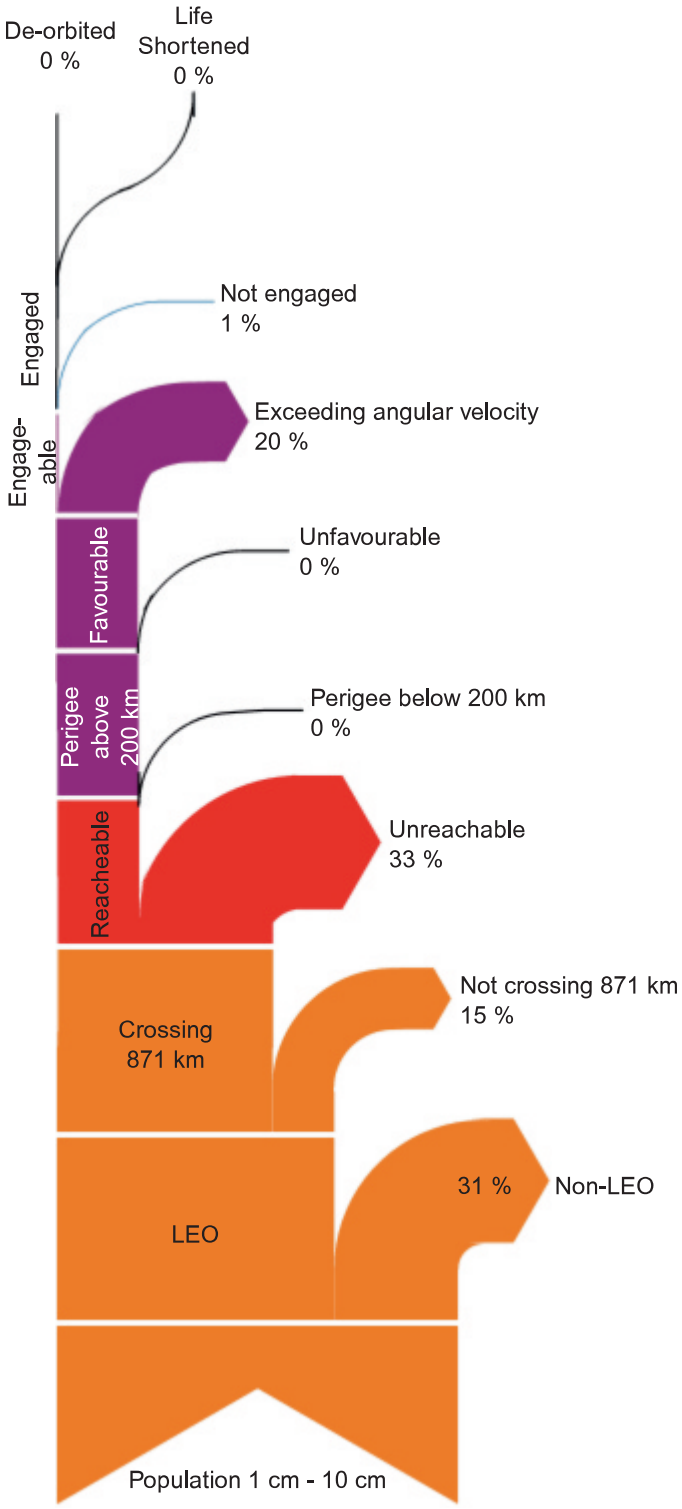

Figure 4.7: Sankey chart of the demonstrator scenario

4.2.3 The High-End Scenario

The high-end scenario assumes the availability and the maturity of all desirable key technologies: Very heavy space-based lasers, agile and precise beam pointing and highly powerful auxiliary systems. The scenario is meant to evaluate the maximum potential of the mission concept in the context of sufficiently advanced technology.

The required laser pulse energy is $2325\,J$, and the resulting peak energy consumption would be in the domain of megawatts. The system has a focussing mirror at the size of the primary mirror of the Hubble Space Telescope, but here it can be rotated with up to $25\,°/_s$. However, on the other side of the balance sheet, the high-end mission shows to be the final solution to the space debris problem (Fig. 4.8). It removes objects at such a high rate that after eight or nine mission years there are practically no targets left. The system is nearly idle for the remaining time of the mission. This shows that the mission scenario is far from being balanced. Nonetheless, it illustrates the full potential of a highly developed laser and attitude control.

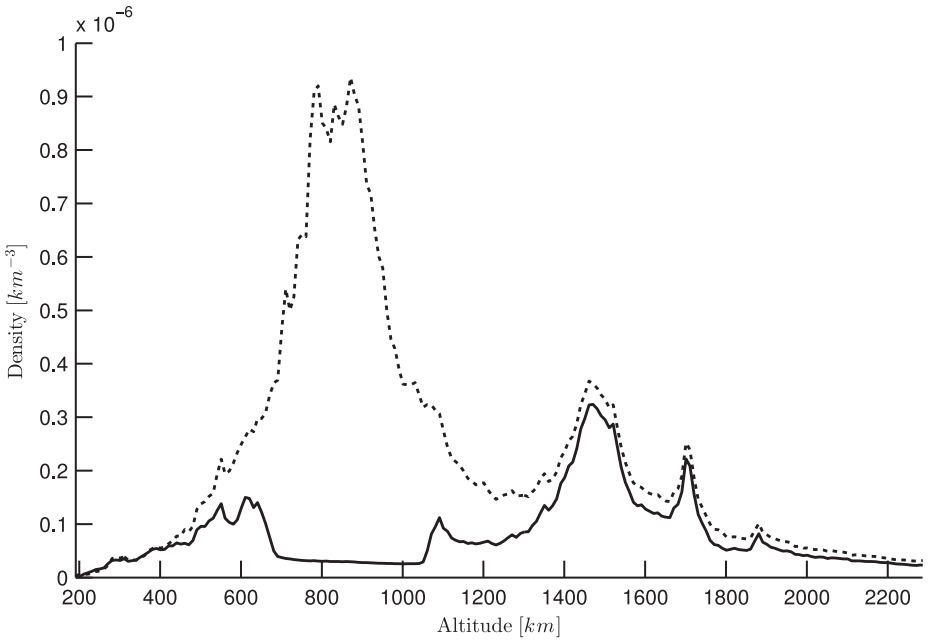

Figure 4.8: Debris density after the high-end scenario

In contrast to the other two reference scenarios, the Sankey chart (Fig. 4.9) shows a small fraction of unreachable objects and a small fraction of objects with excessive angular velocity. At the same time, the high power of the laser shortens the necessary interaction times, which leads to a high number of fully de-orbited objects.

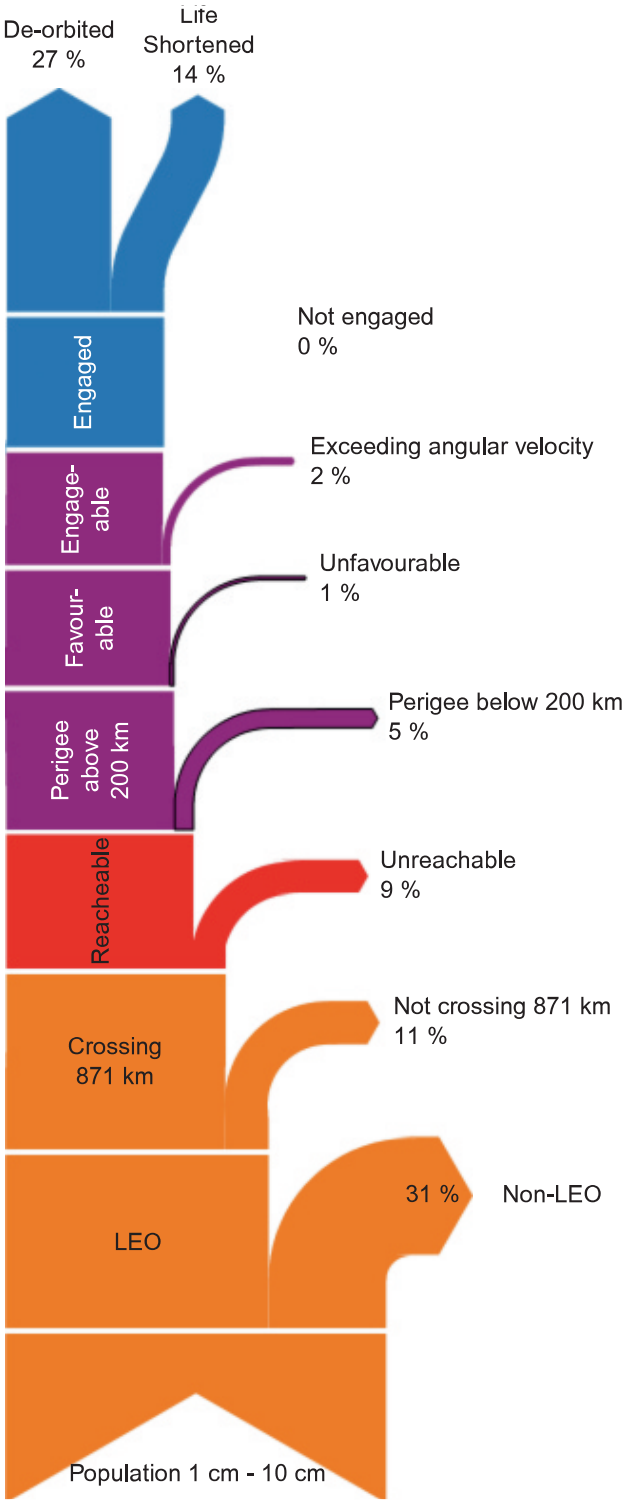

Figure 4.9: Sankey chart of the high-end scenario

	Demonstrator	Baseline	High-End
Assumptions			
R_{max}	$10\,km$	$20\,km$	$50\,km$
Max. tracking vel.	$2.4\,°/_s$	$15\,°/_s$	$25\,°/_s$
Mission duration		$10\,y$	
Target altitude		$200\,km$	
Laser		table 4.1	
Engagement policy		Engage on every opportunity.	
Technical Parameters			
W_p	$93\,J$	$372\,J$	$2325\,J$
Laser output power	$93\,kW$	$372\,kW$	$2.32\,MW$
Mean Φ_{th}		$28\,kJ/m^2$	
Min. pointing acc.	$0.5\,\mu rad$	$0.25\,\mu rad$	$0.17\,\mu rad$
Performance			
Engaged objects	420	99,261	341,448
Removed objects	104	21,930	226,721
Post-mission density	(no significant effect)	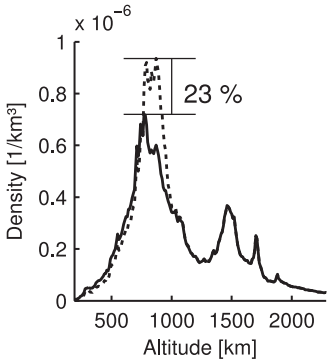	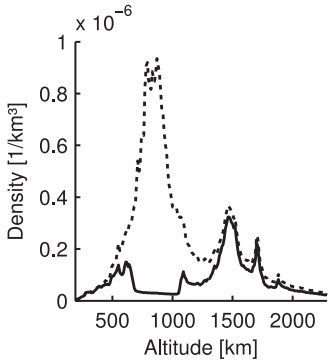

Table 4.3: Summary data of the reference scenarios. (The minimum pointing accuracy is a worst-case value for $6\sigma = d_f$, which means the worst possible cueing system. A better cueing system will result in a reduced requirement for the pointing accuracy, and thus a higher value.)

5 System Aspects

5.1 Scheduling of Engagements

Now it is time to look into the time line of the mission. Of particular interest are scheduling conflicts, workload of the sweeper over time, the idle phases between the firings, the duration of the engagements and the reasons for the disengagements.

Since there is only one laser, only one object can be engaged at a time. It turned out that less than 0.1% of the engagements overlap with other engagements in the baseline scenario. In the demonstrator scenario, there are no overlaps at all, and even in the high-end scenario, less than 3% of the engagements are affected by temporal overlaps. This means that temporal overlaps of engagement opportunities do not play a significant role. In this light, it does not seem sensible to place multiple lasers on the same orbital platform.

Figure 5.1 shows the number of engagements per week for the three main reference scenarios. There are more engagements taking place at the beginning of a mission, because there are still many opportunities. As the mission progresses, more and more objects are removed, and the rate of firing opportunities shrinks. In other words: The fewer objects there are, the fewer engagements will take place. The effect therefore has an exponential quality, and it is complementary to the Kessler syndrome: The higher the density of orbital debris, the higher the rate of removals. It almost seems as if this mission concept was the natural antidote to a Kessler syndrome.

Because the workload for the sweeper is higher at the beginning of the mission, it could be advantageous to dimension the sweeper for the average workload of the mission. This would, to a certain degree, balance the workload over the en-

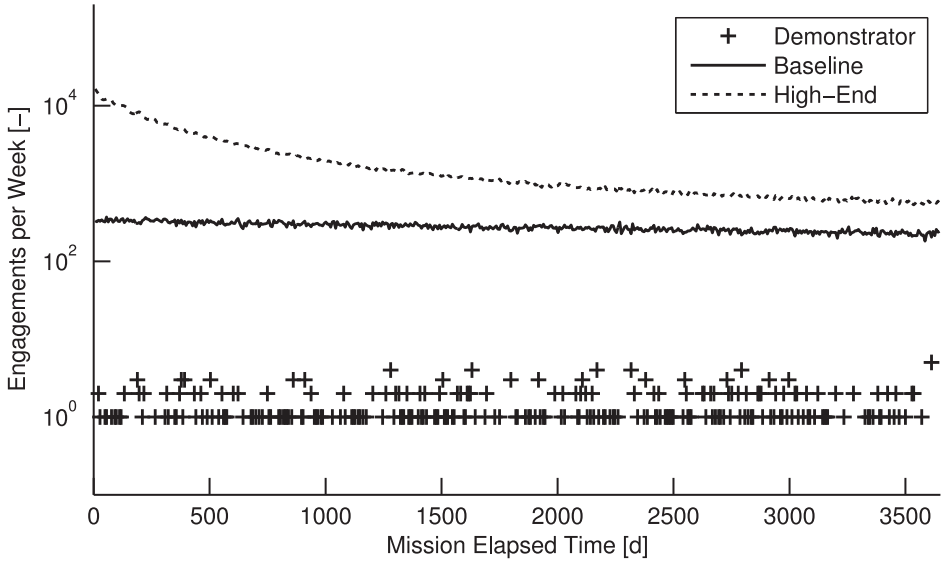

Figure 5.1: Engagements per week for the three reference scenarios

tire duration of the mission. The drawback would be that firing opportunities in the early years of the mission would have to be skipped. One could include this operational alternative in the performance model by implementing a corresponding engagement policy. However, this has not been done within the frame of the present across-the-board-type study.

The next aspect concerns the idle times between the engagements. These times are used to replenish the energy storage (e.g. batteries), to re-align the laser or platform, and to perform other preparatory work for the next engagement. Naturally, the shorter the average time between two engagements is, the more engagements there are within a fixed duration of the mission. The main impact factor on the rate of engagements is therefore the mission scenario. A secondary influence factor is the mission elapsed time (Fig. 5.1).

Figure 5.2 shows the cumulative distribution of these durations of the idle phases for the three reference scenarios. The average time between two firings is around 36 minutes in the baseline scenario, and 5 minutes or 8.5 days for the high-end or the demonstrator mission. If a future study of the system design reveals that the laser will need a minimum time to prepare for the next firing,

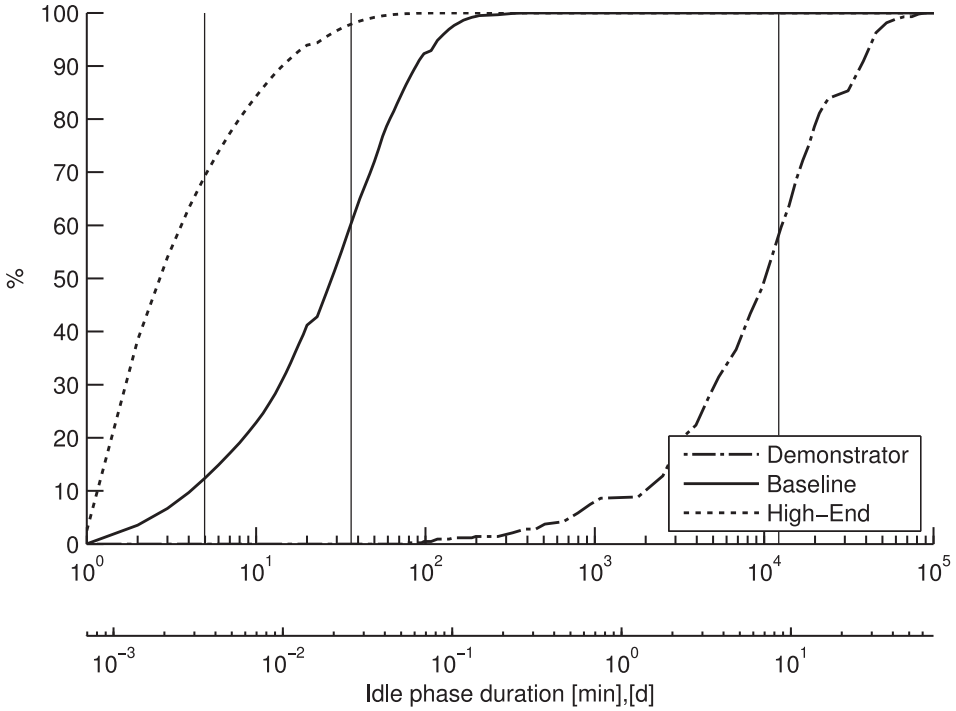

Figure 5.2: Distributions of durations of the idle phases. The upper x-axis shows time in minutes, the lower one shows the time in days. The vertical lines indicate the expectancy values for the time between two engagements.

then one could use these curves to estimate the resulting penalty to the removal performance. In that case, the applicable curve would give the percentage of the engagements that cannot be carried out.

One last aspect to mention is the duration of the engagements. The main driver is the angular tracking velocity of the laser: For small maximum tracking velocities (e.g. in the demonstrator scenario), only objects with a small relative velocity can be engaged. These are usually objects on nearly coplanar orbits. Due to the small relative velocities, they linger within firing range for a relatively long time. The main reason for disengaging the laser is the successful de-orbitation of the object. Moreover, the interaction time is sensitive to the orbit of the laser. (Fig. 5.3, 5.4)

The baseline scenario has a higher tracking velocity of the laser beam, so that it can engage additional objects on non-coplanar orbits. These have a higher relative velocity, and the average time for the interaction is much smaller. The dominant disengagement reason is that target objects acquire excessive angular velocity.

Finally, the high-end scenario has a much higher tracking agility, so that it can

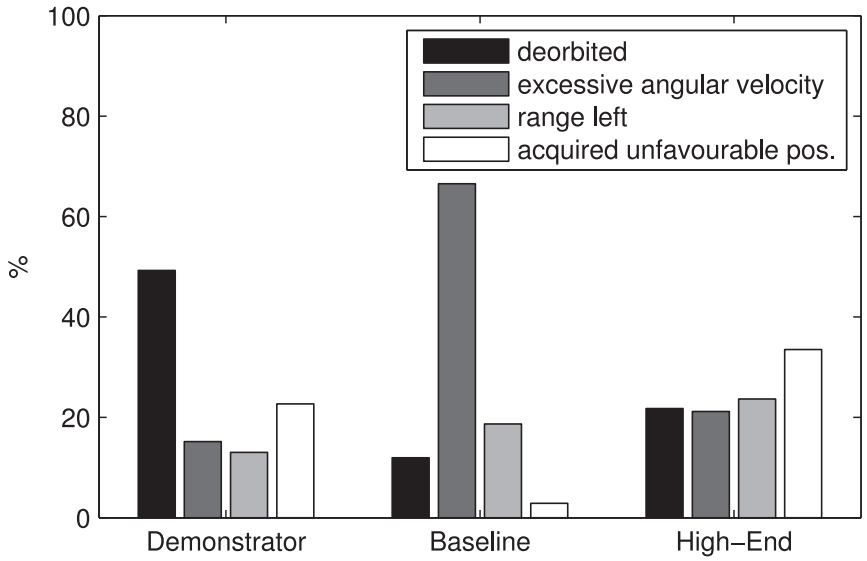

Figure 5.3: Reasons for the disengagements in the reference scenarios

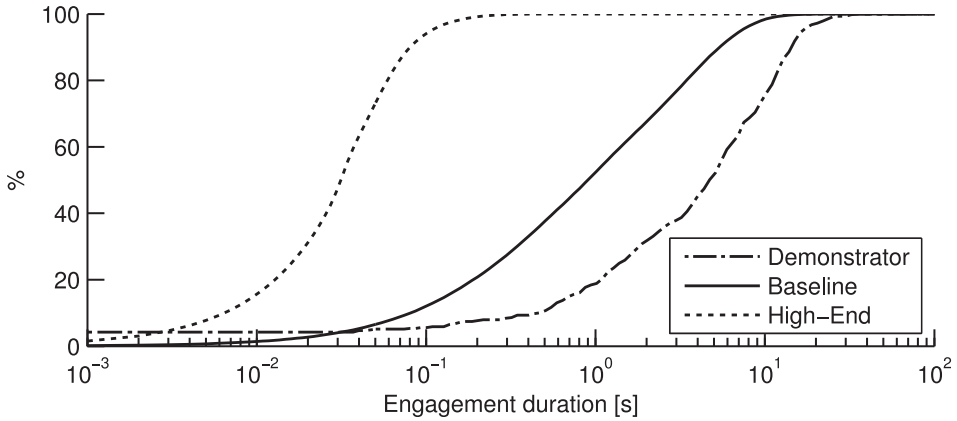

Figure 5.4: Distribution of the durations of the engagements

engage and track nearly every object. In that scenario, the average interaction time depends on the range of the laser. The larger its influence sphere, the longer is the dwell time of the object.

Overall, it has been possible to extract significant information and general relationships on the operational flow of a debris sweeper mission.

5.2 Required Power Supply and Waste Heat Removal

Figure 5.1 shows that there are more engagements at the beginning of the mission than at its end. This effect is stronger for scenarios with a high removal performance. A power generator, which has been dimensioned for the higher-load phase at the mission beginning, is oversized for the remainder of the mission. Alternatively, one can omit firing opportunities in the early phase of the mission.

Cornerstone values for the three baseline scenarios are provided in Table 5.1. The specified excess generation accounts for the fact that the beginning of the mission is busier than its end. The values have been determined numerically by analysing the raw data from the engagement analysis. A detailed description of the algorithm can be found in [66].

The average generator power describes the necessary power supply, which must be provided permanently. It replenishes the storage (e.g. batteries) day and night. Depending on the method of the generation of power, eclipse phases must be considered, leading to larger mean powers for the generator and additional buffering capacities.

The necessary storage capacity has also been calculated by analysing the engagements. It can be considerably reduced when omitting a few, individual engagements. This is because some engagements coincidentally occur in short sequence, leading to a massive demand for energy in a very short time. This happens only a few times per mission, but poses the dimensioning case for the energy storage. An alternate, smaller capacity is therefore specified in the table.

Using the smaller capacity will force the laser to skip some firing opportunities, but the impact on the overall removal performance is negligible.

The discharge power of the storage is given by the electrical power consumption of the operating laser. It is in the range of megawatts.

Now that the orders of magnitudes are known, one can narrow down the potential technologies. Figure 5.5 shows a popular selection chart for energy sources for spacecraft. The demonstrator and the baseline scenario can easily be equipped with photovoltaic generators, while the high-end type system would need a solar dynamic power plant. A nuclear reactor would be feasible, but is relatively risky in environmental, political and ethical regards.

Overall, the energy required for a demonstrator or baseline mission can be generated by conventional means. The energy storage, however, is more challenging. The storage of the demonstrator mission must be able to accumulate 30kWh over hours or days, and then release up to 12 kWh with 1.4 MW in 34 seconds. The storage of the baseline mission must be able to accumulate at least 150 kWh

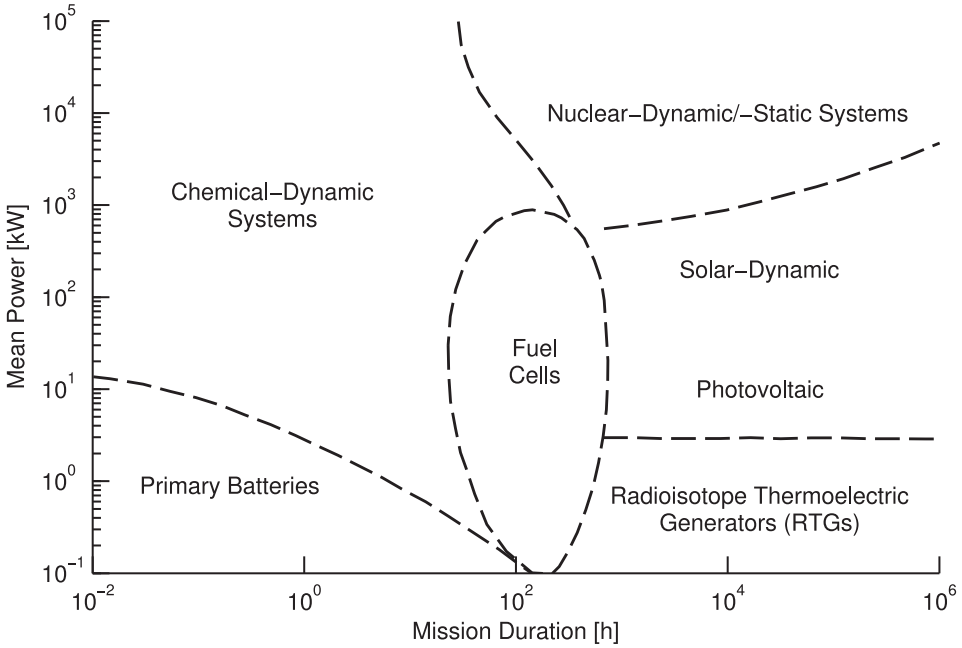

Figure 5.5: P-t-diagram of spacecraft energy sources[68]

within hours, and release up to 40 kWh within 40 seconds. Additional energy must be generated and stored for the platform and the auxiliary systems.

	Demonstrator	**Baseline**	**High-End**
Laser when operating			
Optical output power	93 kW	372 kW	2.32 MW
Overall efficiency	7%	7%	7%
Electrical power input	1.33 MW	5.31 MW	33.21 MW
Waste heat power	1.24 MW	4.94 MW	30.89 MW
Mission averages and energy storage			
Required power	11.4 W	4.8 kW	276.0 kW
Excess generation	5%	30%	900%
Generator mean power	11.9 W	6.2 kW	2.76 MW
Storage capacity	46.9 (30.0) kWh	255 (150) kWh	1674 (1200) kWh
Storage discharge	empty Electrical power input		
Waste Heat			
Avg. laser waste heat	10.6 W	4.46 kW	256.7 kW
Avg. shunt waste heat	0.5 W	1.4 kW	2.5 MW
Mean waste heat	11.1 W	5.86 kW	2.7 MW
Peak waste heat	empty Waste heat power		
Engagement total electrical energy			
Average engagement	2.31 kWh	2.92 kWh	22.24 kWh
Worst-case engagement	12.70 kWh	29.1 kWh	598.49 kWh

Table 5.1: Cornerstone values for the power supply. All data is under the assumption of a 7% overall efficiency of the laser. (The number and values of the decimal places are determined by the calculation, and do not necessarily represent an actual accuracy of the result.)

6 Discussion of the Results

In the introduction, it has been explained why space debris must be actively remediated in the long term: Even if all space-bound traffic stopped tomorrow, the number of hazardous debris objects would keep on growing and eventually make important orbital regions unacceptably hazardous for satellites. The driving mechanism for this dire prognosis is the Kessler Syndrome, which predicts an exponential growth of the debris objects caused by mutual collisions (Fig. 6.1).

Most space agencies have developed their own predictive models of the orbital debris. They appear to be highly sensitive to some key presumptions, such as future launch traffic or the activity of the Sun [69, 70, 71]. However, they do not

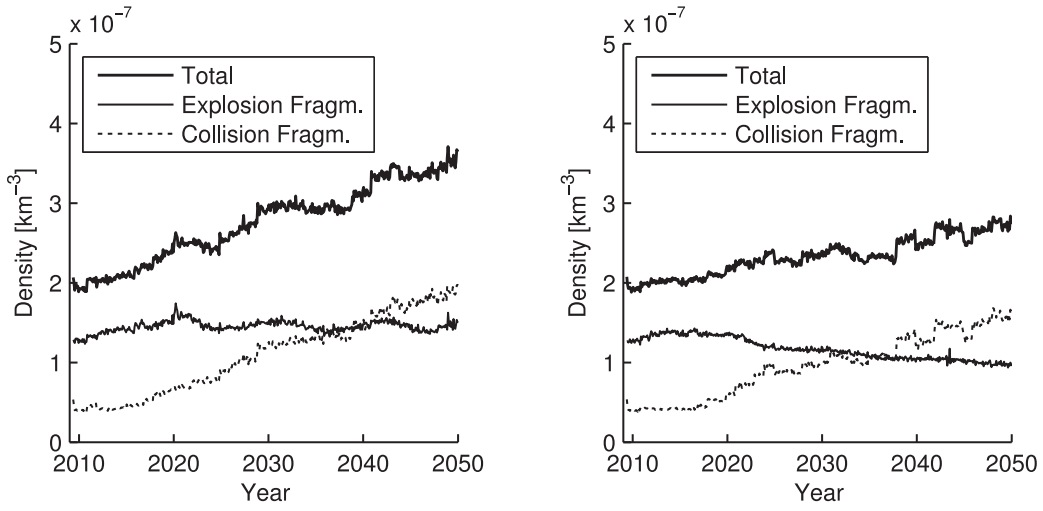

(a) 'Business as usual' (b) 'Full debris mitigation'

Figure 6.1: Prognosis on the density of the orbital debris in the LEO in the 1 *cm* to 10 *cm* regime: Even in a full mitigation scenario, the number of the objects will keep on growing, driven by collisions. (Data calculated by the ESA MASTER model [35].)

contradict one another and they predict a Kessler syndrome for the most likely future scenarios.

Arguing that an effective approach to active removal would not ignore the highly hazardous medium-sized objects, a laser-based debris sweeper has been suggested. In contrast to most of the other proposals for the active removal of the debris, it is directed against the medium-sized objects. These are hard to avoid, numerous, and they yield a high damage potential. Having an effective means to neutralize this threat would substantially ease the overall debris problem.

Such a laser-based debris sweeper has been proposed in the past by Wolfgang Schall [52, 53] and others. However, neither did his investigations show the sensitivity to key parameters, such as the orbit of the laser, nor did they provide a set of boundaries for the mission to work.

Within the previous chapters, it has been demonstrated that the concept can be an effective measure against the space debris. There is not only one optimal design point in which the laser can be successful. Instead, there is a whole spectrum of missions. One mission may, for example, employ a very powerful laser, while another mission draws its strength from a high agility. As long as they meet certain boundary conditions, all of them can be effective against the debris. The overall concept is somewhat insensitive to minor deviations in the key parameters.

There is a commonality that is shared by all laser debris sweepers: The higher the density of the debris in orbit, the higher is their efficiency (sec. 5.1). This means that the concept becomes increasingly interesting as the Kessler Syndrome develops.

Before concluding on the prospects of a space-based laser debris sweeper, the prerequisites and the boundary conditions of the analysis will be summed up.

6.1 Assumptions and Boundary Conditions

In subsection 2.6.2 ('Detection'), it has been deduced that the sweeper will require an object catalogue that contains all targeted debris objects. It might be argued that once the catalogue is established, satellites can evade the medium-size debris

just as they avoid collisions with large objects today. An active removal would therefore not be necessary once the catalogue has been set up.

However, this is not necessarily true. The catalogue that supports the debris sweeper must merely keep an inventory of the targeted objects. Debris on other altitudes, which are unreachable to the laser, can be ignored. Moreover, the accuracy of the sweeper catalogue must only be good enough to keep objects on reachable altitudes in the catalogue. (Only objects that are scheduled for immediate engagement should be determined with a higher accuracy.) This means that the required accuracy could possibly be lower than in the collision avoidance scenario.

Besides, relying only on collision avoidance would not stop the density of the debris from growing. This would make the planning of evasive manoeuvres increasingly difficult over time. Collision avoidance does not appear to be a viable long-term strategy for dealing with the medium-size space debris.

Another prerequisite for a laser sweeper mission is the establishment of legal and political frameworks. This type of mission has apparently not been considered by the authors of the Outer Space Treaty in the 1960s.

A fundamental problem is the present lack of a legal definition for the term 'space debris'. This expression is not being used in any of the international law treaties. This creates a potential for disagreement between states [25].

Larger objects in space are usually registered in accordance with the Registration Convention [61]. However, for smaller debris it is nearly impossible to determine the launching state [25]. It is equally difficult to determine the rightful owner with regard to the Outer Space Treaty. The ownership status, the launching state and the state of registry are usually unclear for medium-size debris. Therefore, the sweeper mission will require a legal regime, which must at least exempt the operator from ownership claims by third parties.

Furthermore, the sweeper alters the trajectory of (presumably) ownerless objects. What if one of these objects damages an active satellite? The Space Liability Convention applies only to objects that have been made space objects by launch. Since the launching state cannot be determined for the debris object, there appears to be a legal vacuum. In order to prevent international disputes well in advance, a regulation will be necessary that determines when, how and

by whom a claimant is to be compensated.

In addition, the sweeper mission may touch national laws or intergovernmental treaties, such as export regulations [26].

Apart from the legal uncertainties, any active removal mission could be misperceived as a space weapon. Weeden has already pointed out that no weapons-grade lasers are being used [25]. Other satellites can, nonetheless, sustain damage if they are illuminated accidentally.

Because the debris sweeper performs best at altitudes with high debris densities, it might be useful for clearing the rubble that has been left by the deliberate destruction of satellites (e.g. by an ASAT).

All political and legal aspects should be comprehensively identified upfront and resolved well before the mission takes place [26]. It has been proposed to conduct this work in parallel to the technical development [25].

Another assumption on which the study has been based is the population of the debris. As it has been described in section 3.1, it is derived from and validated against the ESA MASTER model. However, this model, in turn, is partly based on extrapolations and assumptions, such as fragmentation models [35]. Most information on the medium and the small sized debris has been obtained indirectly, by counting and examining the defects on returned spacecraft.

Moreover, the debris situation as per May 2009 has been taken into account. However, the orbital population is changing constantly. The long-term development is sensitive to some key parameters such as future launch traffic, the adherence to PMD guidelines, or the solar activity [69, 70, 71]. In addition, other active remediation activities may influence the debris population of the future.

The software tools that have been developed in the frame of this study facilitate the use of other reference populations. This way, one can assess the performance of a laser debris sweeper in the context of other debris models or for other reference epochs.

An important part of the prediction of the sweeping performance is the model of the interaction between the laser and the debris. It has been presented in section

2.4. It is also the source of the most dominant uncertainty in the entire performance model. The best available reference data for the coupling coefficients under real-world conditions has been used: The DLR has measured laser-ablative thrust, on debris-like ablator materials, under vacuum conditions [58]. It is believed that the bulk of the debris is metallic, being mostly fragments of explosions or collisions (Fig. 6.2).

Unfortunately, there are relatively few measured data points compared to the vast parameter space (λ, τ, ...). The reference data that has been used is in line with the more general theory of laser-ablation propulsion. However, it lacks an experimental reproduction by an independent party.

It is desirable to increase the credibility of the model and minimize its error. This can only be achieved by the systematic, experimental measurement of additional reference points [72]. This applies particularly to laser intensities that are far beyond the point of the optimum coupling, where additional levels of ionization come into play.

Another aspect, of which the effects have only been taken into account by an estimated factor, is the geometry and the spin of the target objects. The following effects could be relevant in this context:

First, the laser beam hits the surface of the target not perpendicularly (Fig. 6.3a). Due to a cosine factor, the intensity will be lower. This not only changes the

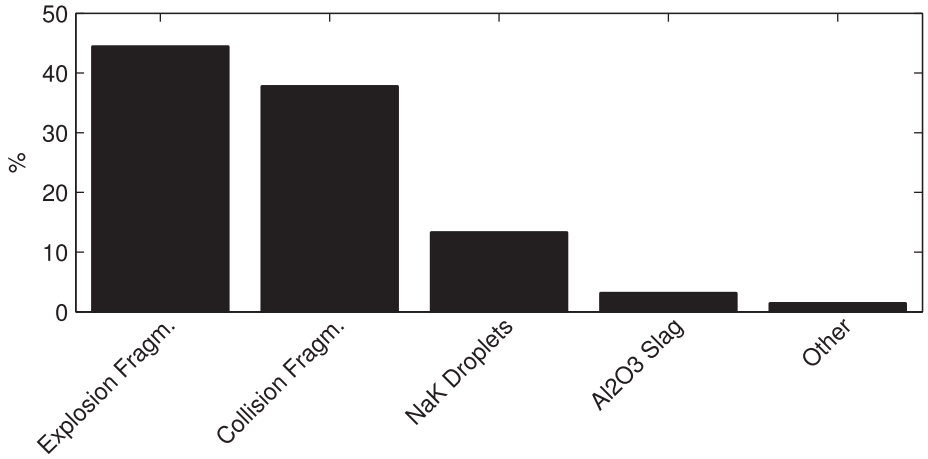

Figure 6.2: Engaged objects of the baseline mission scenario by source type

value of the coupling coefficient [72, 73] and the specific impulse, but it can also prevent any propulsive effect when the intensity ends up below the ablation threshold.

Secondly, when the laser hits a surface non-perpendicularly, the resulting thrust vector does not point into the direction of the laser beam (Fig. 6.3b). The thrust vector will instead be perpendicular to the illuminated face of the target [72, 73].

Thirdly, if the laser hits the object eccentrically, the resulting thrust vector will not intersect its centre of mass. The spin of the object will change in this case [72, 73].

Fourthly, the spin of the target can, in turn, be the source of a 'kinematic torque'. This torque can counteract the existing angular velocity [72].

Fifthly, if an edge is illuminated, the resulting thrust components of the two illuminated surfaces can cancel each other out (Fig. 6.3c). The same applies for the illumination of objects with a continuously changing surface normal, such as spheres or cylinders [72, 73].

Sixthly, there is at least one reason (non-normal target surface orientation) why the thrust vector could have a component that is traverse to the laser beam. As a result, the object may 'jump' erratically between the laser pulses, and potentially leave the beam of the laser. The tracking of the object would be more challenging.

Seventh, the object may feature extreme geometries, such as cavities or drills. This affects the expansion of the ablated vapour or plasma. The current model of the interaction may not be even remotely applicable in these cases. Additionally, there can be self-shadowing when the object has a non-convex surface [72].

In order to compensate for these uncertainties, an efficiency factor of 70% has been assumed. This figure corresponds to the ratio of typical 'effective surface areas' to a circular reference cross section (Table 6.1). The tangential thrust components have been assumed to cancel out for a high number of pulses and that the mean thrust vector points into the direction of the laser beam. This is in line with a hypothesis established in the literature [73], although there may be degenerated cases when the object rotates with the same frequency as the laser emits pulses [72]. Another presumption is that cavities are a rare geometrical feature among the medium-size space debris objects.

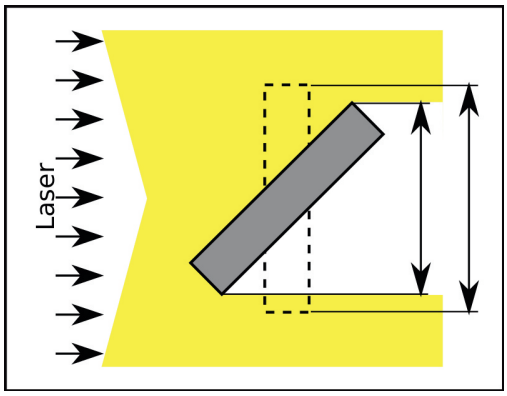

(a) The illuminated surface area is the same, but less laser energy is absorbed. Therefore, the intensity is lower, and the coupling is different.

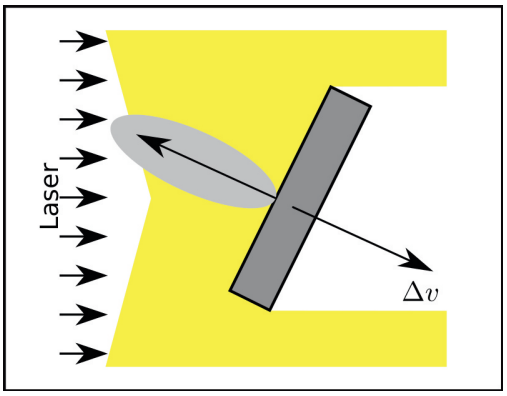

(b) The thrust is perpendicular to the tilted surface. The target will acquire a traverse velocity component.

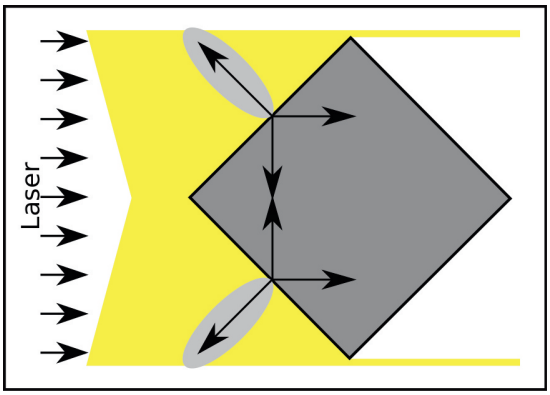

(c) Two faces are illuminated; the vertical thrust components counteract one another.

Figure 6.3: Selected effects of the target shape

Shape	**Eff. Surface**	**% of A_{ref}**
Reference Cross Section	$A_{ref} = \pi R^2$	
Sphere	$A = \frac{2}{3}\pi R^2$ [73]	66.67 %
Cylinder $h = 2R$	$A = \pi R^2$ [73]	100.00 %
Cube	$A = 2R^2$ [72]	63.66 %

Table 6.1: Effective surfaces of selected geometrical primitives

The implemented interaction model is capable of simulating the shrinking of objects due to the ablation. However, this feature has been disabled, because the available experimental data on the ablation rates and the specific impulses in the relevant parameter ranges was judged too sparse. It has already been mentioned that the ablation may not only shrink objects, but it may also alter their shape [73].

6.1.1 The Laser

Choosing a Nd:YAG disc laser has been an 'informed guess'. In a future, higher-definition analysis of the mission, one would certainly compile an exhaustive list of the available types of lasers and perform a thorough trade-off. By selecting a more optimized laser, one should be able to reduce the technical requirements for the other systems of the sweeper. For example, the brand new International Coherent Amplification Network (ICAN) technology may be exceptionally well suited because of its high efficiency, its excellent beam quality and its beam-shaping option [74].

Table 6.2 compares the laser of the baseline scenario to the current projections for a ground-based debris remediation laser system. The comparison is not exact, because the ground-based systems target slightly different size ranges and debris on different altitudes. Nonetheless, a comparison of the orders of magnitudes should yield valid results.

Interestingly, all teams have chosen more or less the same wavelength for the laser. The pulse width that has been chosen for the space-based sweeper is comparable to the ground-based lasers and appears to be a bit conservative.

The major differences between the ground-based lasers and the space-based laser are the pulse energy and the repetition rate. The laser in space requires a higher pulse rate because of the shorter interaction times. However, the energy of the pulses can be lower because the targets are much closer. The output power of the space-based laser and the ground-based lasers are in the same order of magnitude (a few $100\,kW$), but the space-based laser has to maintain that power level for only a few seconds. The choice of the primary aperture and the choice of the beam quality have been rather defensive for the baseline scenario. This design margin could be used for a smaller mirror or a smaller pulse energy (and therefore a smaller power) of the laser.

All in all, the chosen laser fits well into the landscape of the laser brooms. The choice of the laser for the baseline scenario has a conservative tendency.

Another assumption worth noting is the rectangular beam profile of the laser. Although most laser sources exhibit other (e.g. Gaussian) beam profiles, this simplification is commonly used [72].

Moreover, there can be a minimum firing range, depending on the mechanism of the beam focusing [74]. This effect has not yet been taken into account, but could be easily incorporated in the model by adding a rule to the engagement policy. In the same manner, one can model restrictions on the kinematic freedom of the laser. For example, there could be directions into which the laser is not allowed to fire.

6.2 Conclusion

Within the present thesis, the boundaries of a potential laser debris sweeper mission have been outlined. The interplay between the removal strategy, the mission profile, the key system parameters and the remediation performance has been investigated. Using these relationships, a new model of the mission performance has been established. This model employs a numerical simulation of mission scenarios. The model delivers consistent, reliable and understandable results. Additionally, the ‘design space’ for possible sweeper missions has been outlined.

	Phipps et al. ([45])	**Rubenchik et al.** ([46])	**CLEANSPACE** ([75])	**Baseline Scenario** (p. 92)
Year of publication	2012	2012	2014	2015
Laser wavelength	$1.06\,\mu m$	$1054\,nm$	$\approx 1\,\mu m$	$1064\,nm$
Pulse energy	$7.3\,kJ$	$\approx 8\,kJ$	$10\,kJ$ - $20\,kJ$	$372\,J$
Pulse width	$5\,ns$	$\approx 4\,ns$	$5\,ns$ - $50\,ns$	$10\,ns$
Beam quality M^2	2			12
Shots per second	11.2		10 - 50	1000
Primary aperture	$13\,m$	$3\,m$	$5\,m$	$2.5\,m$

Table 6.2: Comparison of projected laser systems

Parameter	**Value**
Mission duration	$10\,y$
Mean altitude / inclination	$871\,km$ / near-polar
Orbital eccentricity	≈ 0.01
Operational range	$20\,km$
Avg. time between engagements	$36\,min$
Laser	Nd:YAG, $1064\,nm$, $10\,ns$, $M^2 = 12$
Laser overall eff.	$7\,\%$
Laser pulse rate	$1\,kHz$
Primary aperture	$2.5\,m$
Avg. power to generate	$6 - 10\,kW$
El. energy storage capacity	$150\,kWh$
Beam tracking velocity	$15\,°/_s$
Effectivity	**reduces** $23\,\%$ **debris density at the most important orbital altitudes within** 10 **years**

Table 6.3: Key figures of the baseline mission

Three mission case studies have been performed to demonstrate the application and the potentials of the model. The most important one is the 'baseline scenario': It represents a fairly balanced, but not yet optimized mission scenario. The characteristic figures of this baseline scenario are summarized in Table 6.3. The simulations have shown that this sweeper configuration can reduce the density of the medium-sized debris by 23 % in ten years (Fig. 6.4a).

By using the performance model, one can also *optimize* the mission to different criteria. For example, one could increase the remediation performance by using constellations of lasers, or by the addition of ground-based laser stations. Or, one could tune the parameters of the mission to a particular laser technology. Moreover, the requirements regarding the power supply and the waste heat removal subsystems could be minimized by implementing alternate engagement policies.

So far, the mission performance model can be used to conduct case studies. Beyond that, it can be used to analyse the dominant traits and relationships of the mission design space, such as the sensitivities to key parameters.

The most important parameter of an orbital sweeper laser is its maximum operating range, which has been introduced in section 2.2. Generally, the wider the range, the more debris objects can be reached. Simulations have shown that a laser range lower than $10\,km$ is equally pointless as a value larger than $50\,km$ (Fig. 4.2). These boundaries apply to scenarios with a single laser as well as to scenarios with constellations of multiple lasers. The range of the laser determines its pulse energy, which is a driver for the design of the laser.

The second driving parameter of the mission concept is the beam tracking velocity, or mirror agility. A higher value will enable the laser to engage more of the passing objects. For the minimum value, which is around $2\,°/_s$ to $3\,°/_s$, the laser can engage only near coplanar objects. The higher the agility, the more off-plane velocity of the object can be tolerated. There will be suitable encounters with nearly every reachable object if the beam can be tracked with up to $25\,°/_s$.

When there is only one laser platform that is adrift, then the orbital altitude of the highest density of the debris should be selected for the laser platform. In the current population model, this altitude is $871\,km$. If the laser could perform orbital manoeuvres, it might be plausible to begin the mission at a higher altitude

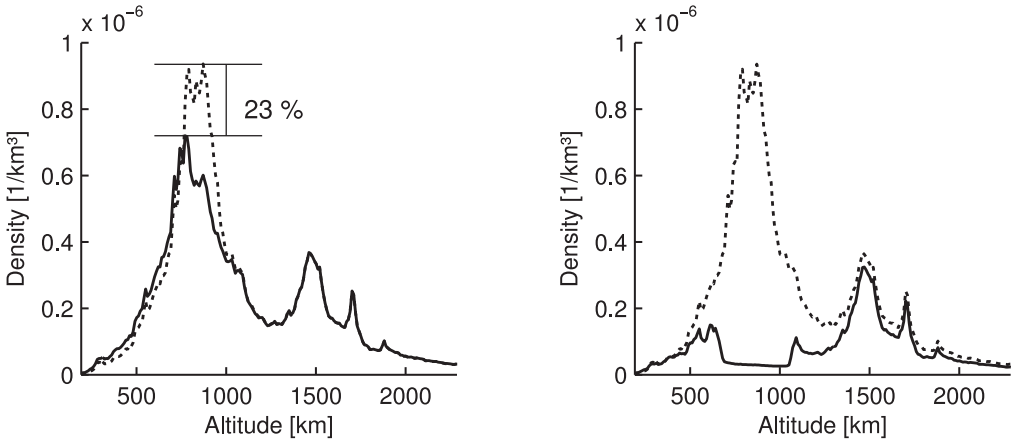

(a) 'Baseline' (b) 'High-End'

Figure 6.4: Projected density of the debris after two mission scenarios

and gradually lower the orbit of the sweeper over the course of the mission. This way, additional objects can be reached when R_{max} is between $20\,km$ and $50\,km$.

To maximize the number of firing opportunities, a near-polar inclination should be selected for the sweeper. Most of the target objects will be on near Sun-synchronous orbits, and the inclination difference is driving the relative velocity between the laser and its targets. Therefore, in order to minimize the relative velocity, one would try to minimize the standard deviation of the inclination difference between the laser and the reachable sub-population. Once a statistically representative sample of the real-world, medium-sized debris population has been catalogued, one can state the optimum inclination more precisely than 'near-polar'.

Moreover, it has been shown that a small orbital eccentricity of about 0.01 enhances the removal performance. For eccentricities beyond ≈ 0.05, the laser will spend much time at altitudes where there are few possible targets. For smaller eccentricities, heavily populated altitudes will remain untouched.

The third parameter, which drives the removal performance, is the pulse repetition rate of the laser. It is closely linked to the power output of the laser and its requirement for electrical power. The more power the platform can deliver, the higher the repetition rate can be.

The available interaction time is limited by the orbital dynamics of the laser and the target. If the pulse rate is too low, then the laser will fail to deliver the momentum that is necessary for de-orbitation within the available interaction time. Thus, the object will have to be engaged multiple times. Even worse, a non-linearity effect has been discovered. Its discussion shows that an increasing percentage of the engageable objects would not be engageable at all if the repetition rate became too low. (sec. 3.4.3)

Another, tabular representation of the performance-driving relationships can be found in appendix B.

Summing up, there now is a mission performance model that delivers consistent, reliable and understandable results. It can be used to analyse the general characteristics of the design space, as well as to simulate individual missions. When

used to simulate individual missions, it reveals the strengths and the weaknesses of the particular scenario, and it tells the user how the mission could be improved.

The model covers the entire design space in a generic way. This enables systematic parameter studies. It is generic, modular and easy to extend. It has been thoroughly tested and validated. Given the availability of this powerful tool, its full exploitation is to be addressed in an outlook for the future.

6.3 Outlook

The 'high-end' scenario, representing the hypothetical pinnacle of laser debris sweepers, shows how far the concept can be taken to the extreme. It demonstrates that, given the proper maturity of some key technologies, a single orbital laser can clean up the complete LEO region within a few years (Fig. 6.4b).

The mission concept benefits highly from technological advancements in laser technology or satellite attitude control. Once these key technologies have reached the maturity level of a demonstrator mission, a large number of mission variants can be put into practice.

According to Liou, debris in the range of $5\,mm$ to $1\,cm$ is particularly dangerous [69]. The mission concept of the laser debris sweeper can be extended to sweep away those objects as well. The removal efficiency will be even higher, because the density of the smaller objects is higher. However, the detection, the tracking and the cueing of the smaller objects are more difficult.

The performance model can accommodate to that extension simply by feeding it a population that contains smaller objects as an input parameter. When doing so, the required calculation time will be higher, because there are more target objects to process. Therefore, it is advisable to use a computer with as many computing cores as possible. Conceptually, the algorithms should be able to handle object diameters down to at least $1\,mm$ correctly. The small debris population has been described as highly dynamic [69], so that the introduction of a source/drain model for the debris could be justified. Changing the propagation scheme could be an easy-to-implement provisional alternative, which requires fewer assumptions to be taken along the way.

Both, the mission concept and the performance model, can deal with objects larger than 10 cm. Due to their lower density in space, the quasi-statistical approach of establishing an object balance may not be applicable any more. It seems prudent to adapt the propagation scheme for higher accuracy, especially when feeding real-world, catalogued objects into the algorithms. The object balance could be replaced by another measure of the performance such as ranking criteria. These criteria are being discussed for the selection of targets for the removal of larger debris objects (e.g. collision probability times mass [22]).

The present work has answered many questions in the field of debris-sweeping lasers in space. It also raised new questions, which are waiting to be addressed in follow-up research.

Some questions are linked to the assumptions in section 6.1. Those are to be verified and assured. There are substantial overlaps with other research activities. It appears plausible to team up in interdisciplinary groups. For example, the cataloguing and the cueing are typical problems of the space situational awareness (SSA) community. Concerning the model for the laser-ablative interaction, one could team up with the investigators of ground-based laser brooms. Most of the legal and the political questions are shared with other active debris removal concepts. Nonetheless, there is at least one topic that is very specific to laser debris sweepers.

Within the course of this study, the technological requirements for a debris sweeper mission have been outlined. The software tool chain can quickly estimate the requirements for a specific mission scenario. This allows performing a technology trade-off within the frame of a follow-up research project. Its task would be the identification of possible technologies for the laser, the beam focusing, the cueing, the attitude control, the power generation and storage, and the removal of waste heat. Then, combining different technical solutions, practical system alternatives can be drafted, using first-order subsystem models.

This thesis has determined how efficiently a sweeper could clean up near-Earth space. It has also revealed the generic boundary conditions of the concept. This includes the estimation of requirements for the subsystems, such as the laser, the

power supply and storage, and the cueing. At first glance, the technological requirements may seem unusually challenging. However, the unusual mission could serve as a proving ground for new technologies, or novel types of synergies. For example, one could employ solar-dynamic generation of electricity, or flywheels for the storage of energy.

7 Summary

The present thesis has summarized the important facts about the space debris. Active debris removal can be an effective measure to reduce the risk of future space missions. It can become even more relevant in a future scenario where the density of the debris is higher than today. Such a scenario is not unlikely, particularly with the Kessler syndrome theory in mind.

There are two types of active removal missions. The first type aims at the removal of few, large objects. This would stabilize the debris population in the long term, because the disintegration of a single larger body can produce a high number of small, shrapnel-like fragments. Missions that aim at the de-orbitation of large junk require rendezvous operations with every individual target.

The second type of active removal mission takes out medium-sized and small objects. This is a more direct approach to reducing the risk of collision for the active satellites. There are so many objects in this size range that one cannot rendezvous with every one of them. This type of mission must therefore be able to engage objects at greater distance or at higher relative velocities. One promising approach is the use of a space-based laser, which effects laser-ablative propulsion on the debris objects.

The current state of progress in the field of space-based laser debris sweepers has been assessed. All key publications on the topic have been reviewed and discussed. It turned out that the development has been proceeding at a slow pace and that important aspects remained to be investigated further. Among these aspects were the number of reachable objects, the influence of the relative motion of the debris objects with respect to the laser, and the relationship between the laser system and the remediation performance.

A model of the mission has been established. It computes the effects of a laser

sweeper on a debris population. The key figures of the mission and the system are an input to the model. One of its outputs is the change of the debris density over the course of the mission.

Technically, this new model is based on a particle simulation approach. The equations of motion are the laws of orbital mechanics. The relative motion of the laser and the targets is reproduced more accurately than in previous studies.

A representative debris population has been generated as starting condition for the simulation. The population has been compared and validated against the ESA MASTER 2009 model. The mission performance model is not limited to this population, and it is possible to exchange it without a modification of the source code.

The mission model is completely generic. It has been designed to cover all thinkable variants of a laser debris sweeper mission. All relevant aspects are parametric.

The space of syntactically valid input parameter combinations has been systematically screened for meaningful mission designs. The applied filtering conditions have been justified by fundamental considerations. For the first time, it is possible to specify hard limits for key mission parameters.

If the laser range (R_{max}) is smaller than $10\,km$, the sweeper will reach very few objects during a multi-year mission. If the laser range is larger than $50\,km$, nearly all objects on the sweeper's orbital altitude can be reached. The sweeper must be able to track an object with at least $2\,°/_s$ to $3\,°/_s$. With a tracking agility of about $25\,°/_s$, the sweeper can engage nearly every reachable object at least once in a 10 year mission. A preferred altitude for the sweeper is where the debris density is highest, which is $871\,km$ for the assumed population. The orbital inclination of the sweeper should be near-polar, and an orbital eccentricity in the range of 0.001 to 0.02 enhances the remediation performance.

The parameters that are driving the remediation performance are (in that order): The maximum laser operating range, the beam tracking agility and the laser pulse repetition rate.

The engagements are short, in the range of milliseconds to a few seconds. Although the required electrical power is high when the laser is firing, the required average electrical power is in the order of kilowatts. The time between two

engagements ranges from a few minutes in the high-end scenario to a few days in the demonstrator scenario.

Putting multiple lasers onto the same platform does not make sense from an operational point of view. Temporal overlaps of the engagement phases are rare. Three mission scenarios have been selected to exemplify the use of the model: The demonstrator scenario, the baseline scenario and the high-end scenario. Their remediation performance has been assessed along with various secondary figures of interest.

The demonstrator scenario has a Nd:YAG disc laser with a pulse energy of $93\,J$, and objects can be engaged at an angular velocity of up to $2.4°/_s$. There are a few engagement opportunities per week. This would be enough to test the principle of removing small objects with a laser, but a noticeable effect on the overall population cannot be achieved.

The baseline scenario has a laser with $372\,kW$ optical output power. The tracking agility is $15°/_s$. The sweeper can reduce the debris density in its altitude range by up to $23\,\%$ in 10 years mission duration.

The high-end scenario assumes a multi-megawatt laser, which can track objects at a distance of $50\,km$ with up to $25°/_s$. The result is a very effective cleaning of its orbital band. After few years, the sweeper's workload drops in this scenario, because the number of remaining objects has become small. This design would be oversized.

The present thesis makes it clear that the development of laser debris sweepers should be continued. At least two types of studies can be done as an immediate follow-up.

The first type of follow-up work is the refinement of the model that is the centrepiece of this work. Allowing the laser to perform orbital manoeuvres would introduce an additional degree of freedom into the mission design. It could be possible to increase the removal performance by some per cent, just by altering the sweeper's altitude from time to time. Maybe, there are different manoeuvring strategies with different advantages and disadvantages. Another refinement of the model would be the simulation of constellations of multiple laser sweepers. It could be possible to achieve the same remediative effect of a sophisticated sweeper system with a number of laser satellites that are less technologically

challenging. A series production can also help to reduce costs.

The second type of follow-up work would be the examination of other key aspects of the mission. For example, it is necessary to define the accuracies of cueing and beam tracking subsystems more accurately. One would take a closer look at the available technologies for the tracking of the objects, the prediction of these trajectories and the attitude control of the sweeper. From there, it should be possible to narrow down the possible pointing accuracies of the laser. Finally, this information can be used to create a refined set of mission scenarios. The stepwise introduction of new aspects into the consideration will eventually boil the parameter space down to few, very specific designs.

A Background Information: The Population Generator

This appendix provides a more detailed insight into the algorithms that are used by the population generator. The population generator tool, named `DebrisCloudGen2`, can create a discrete space debris population from a source of statistical data. Such statistical data can be provided by the ESA MASTER model or by other debris models.

This appendix provides an overview of the working principles of the population generator. The actual implementation must take into account additional technical details, special cases and performance considerations.

A.1 Main Program

Debris populations are generated separately for the different source types. This allows a parallelization of the process. The sub-populations for all source types are merged afterwards into the complete reference population. A pseudocode version of the main program is depicted in Fig. A.1.

```
function MainProgram
    User selects an epoch and a future scenario
    for each sourcetype do
        GenerateElementsPop(epoch, future scn., sourcetype)      ▷ (sec. A.2)
    end for
    Merge sub-populations for all sourcetypes
    Store population in an SQL database
end function
```

Figure A.1: The main programme routine as pseudocode

A.2 Main generator routine: GenerateElementsPop()

The main generator routine generates the sub-population for one source type at a time. It starts with generating the LEO population. Then, the MEO and the GEO populations are generated (Fig. A.3). Every one of these three altitude regions is processed in two basic steps:

1. Generate objects regarding their diameters, their eccentricities and their perigee altitudes. (The arguments of node and the arguments of the perigee are uniformly distributed, as well as the anomaly.) The orbital inclinations of the objects are left blank.

2. Add the inclination values in a post-processing step. (sec. A.3)

The altitudes within an altitude region (e.g. $186\,km$ - $2286\,km$ for LEO) are discretized into smaller altitude slices. These altitude slices have a width of a few kilometers.

For each altitude regime, the algorithm prepares a so-called triplet vector. A single triplet consists of a diameter value, an eccentricity value and a perigee altitude value. It can be seen as a type, a 'blueprint' or a 'template' for a new object. Furthermore, the algorithm prepares a so-called density table, which holds a number density value for every triplet and every altitude step. (Fig. A.2)

The combination of the triplet vector and the associated density table represents the targeted statistical properties of the new sub-population. It says, how many objects there are on a particular altitude with a given diameter and orbital shape. The values can be queried from the ESA MASTER model automatically, by using a wrapper routine. The wrapper routine is documented in [66].

Some of the debris elements in the LEO region can have highly eccentric orbits. They spend some time of their orbital period in higher altitude regions. Thus, when generating the sub-population for the MEO region or the GEO region, then the density table is reduced by the density contributions, which are caused by the already generated debris elements. The same applies to the objects of the MEO region when generating the GEO sub-population.

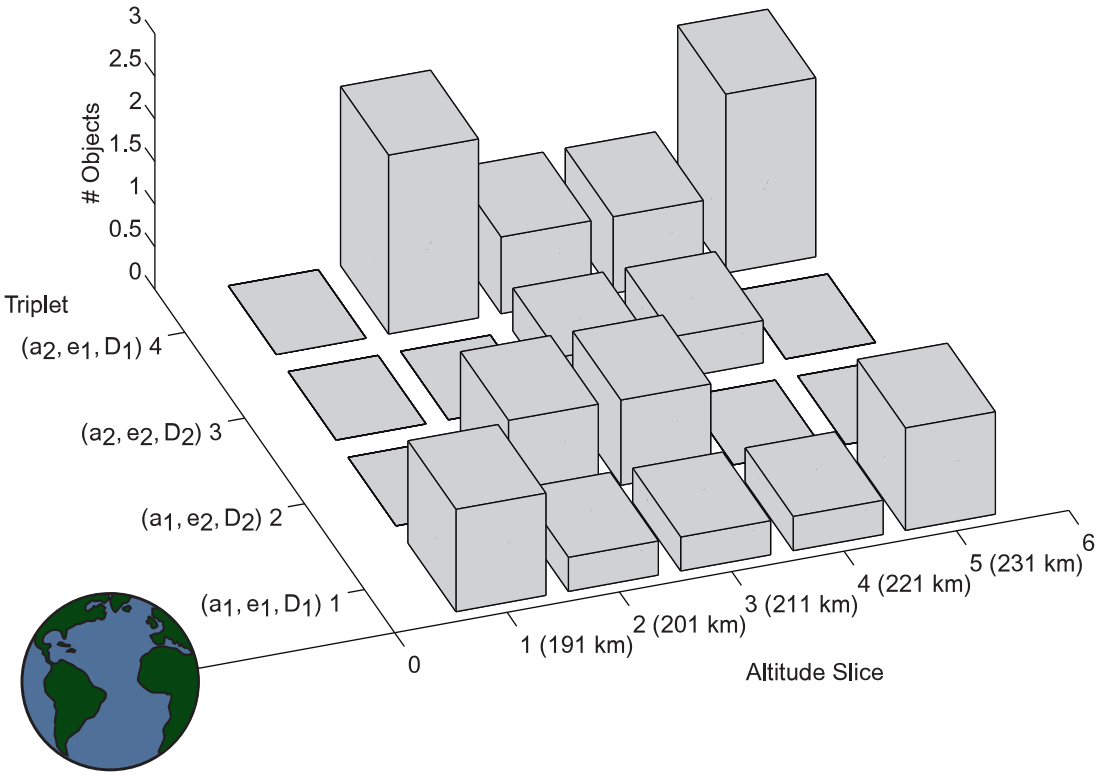

Figure A.2: Density table and triplet vector. (The triplet vector is the Y-axis.)

At this point, the density table starts being the delta between the objects, which have been already generated, and the targeted population. Or, in other words, it describes the statistical properties of the to-be-generated debris objects.

After these preparations, the actual generation of the debris objects takes place. The algorithm starts at the lowest altitude slice, and proceeds to the uppermost altitude slice of the altitude region. Within an altitude slice, all triplets are processed independently in the following way:

First, the algorithm determines the fraction of the orbital period which an object of this (triplet-)type would spend within the altitude slice. Then, it divides the entry in the density table for this altitude slice and triplet by this fraction. The result is the number of objects to be generated for this particular triplet type. These objects are generated and added to the sub-population. All of them have the same perigee altitude, eccentricity and diameter of the triplet. The anomaly argument, the perigee argument and the node argument are generated

```
function GenerateElementsPop
    T ←prepare triplet vector for LEO
    ρ ←prepare density table for LEO
    for each altitude slice as A do
        for each T as t do
            GenerateObjects(ρ,A,t)
        end for
    end for
    PostProcessInclinations()

    T ←prepare triplet vector for MEO
    ρ ←prepare density table for MEO
    Reduce ρ by effect of eccentric LEO objects on MEO density
    for each altitude slice as A do
        for each T as t do
            GenerateObjects(ρ,A,t)
        end for
    end for
    PostProcessInclinations()

    T ←prepare triplet vector for GEO
    ρ ←prepare density table for GEO
    Reduce ρ by effect of eccentric LEO objects on GEO density
    Reduce ρ by effect of eccentric MEO objects on GEO density
    for each altitude slice as A do
        for each T as t do
            GenerateObjects(ρ,A,t)
        end for
    end for
    PostProcessInclinations()
end function
```

Figure A.3: Main generator routine as pseudocode

randomly, and they can differ among the generated objects.

Finally, the contribution of the generated objects to the density on the current altitude and to the density on the other altitudes is calculated and subtracted from the density table. The row in the density table that corresponds to the current triplet, should contain only zeros now. This way, the density table always represents the statistical properties of all to-be-generated objects. (Note: The contributions of one object to the orbital densities are calculated in advance for every triplet. This look-up table, which is named ψ-table, increases the performance considerably.)

When determining the number of objects to be generated for one triplet and altitude, the division may not necessarily yield an integer value. A rounding scheme ensures that the overall debris density of the generated population will be consistent with the statistical density of the MASTER model. Additionally, the rounding scheme filters possible inconsistencies in the statistical source data to a certain degree.

After generating the debris objects for all triplets and all altitudes in one altitude region, the orbital inclination of all objects is set in a post-processing step (sec. A.3). Then, the algorithm proceeds to the next altitude region. Finally, the sub-populations for all source types are merged into the overall population.

A.3 Post-Processing the Inclinations

At this point, the newly generated objects are left without a value for their orbital inclination. This parameter is filled in as a post-processing step after generating the objects for an altitude region. The inclination processing is performed independently for different object diameter ranges.

The inclinations are processed incrementally, from the lowest altitude slice to the highest. The algorithm determines the discrete, relative inclination distribution from MASTER using the wrapper routine from [66]. The distribution is valid for a particular epoch, source type, altitude slice and object diameter range. Then,

the distribution is multiplied with the absolute number of objects within that altitude slice, so that the absolute distribution of inclination values among the objects at that altitude slice is known.

Secondly, the algorithm prepares a list of all objects crossing the current altitude slice. (Fig. A.4)

Some objects spend orbital time in multiple altitude slices due to their orbital eccentricity. Because the algorithm processes the altitude steps sequentially, some objects may already have been assigned an inclination value. These objects are removed from the list, and their contribution to the inclination distribution is subtracted from the distribution. Naturally, this step can be skipped when processing the first altitude slice.

Now, the actual assignment of inclination values to the remaining objects in the list takes place. Assuming that the distribution of the inclinations has n classes, and there are m objects, then there are n^m possibilities of assigning inclination values to the objects. Some of them will lead to an inclination distribution that matches the MASTER data very closely, whereas other combinations will be completely unrealistic.

Testing all of the n^m solutions and determining the best one can be a very resource-consuming task. For this reason, an arbitrary tuple of k objects is taken from the list, and the problem is solved only for these k objects. The process is repeated until all objects of the altitude slice have been assigned an inclination value.

Introducing this granularity yields an extra error for the inclination distribution of the generated population. However, an empirical analysis showed that the error will be small. Setting $k = 3$ or $k = 4$ has proven to be a practical choice.

After all population objects have been assigned an inclination value, the algorithm proceeds with generating objects for the next altitude region.

```
function PostProcessInclinations
    for each object diameter class do
        for each altitude slice as A do
            I ←Prepare inclination distribution for A
            L ←List of all all objects crossing A
            Remove all objects outside the current diameter range from L
            for each L as l do
                if l already has an inclination value then
                    Remove l from L
                    Reduce I by effect of l
                end if
            end for

            while L contains objects do
                M ←arbitrary k-tuple out of L
                Test all possible combinations of values within I on m ∈ M
                Find the combination which matches I best.
                Assign inclination values to the objects in M.
                Reduce I be effect of all m.
                Remove all m from L.
            end while
        end for
    end for
end function
```

Figure A.4: Inclination post-processing as pseudocode

A.4 Obtaining Statistical Data from MASTER

The population generator relies on a statistical description of the population as source data. This data is queried from the MASTER model using a set of wrapper routines, which are implemented within the `DebrisPopValidation.cpp` file in the `DebrisLib` assembly.

The population generator is in no way limited to using MASTER data; any other source of statistical information can be used used as well. In that case, one would replace the wrapper routines by other, user-defined data-providing routines. These can either contain statistical relationship themselves, or procure statistical data from files, pipes, sockets or other sources.

The wrapper routines used here all share the same working principle: First they create a local working directory and populate it with input files for MASTER, most notably a `Master.inp` and a `Default.def` file. Then, the operating system is instructed to launch the MASTER executable file. After the executable has finished operations, the corresponding output files are parsed and the obtained data is returned to the caller (e.g. the population generator). A more detailed explanation of this process can be found in a separate technical report [66].

In all cases, the analysis dates are set to the epoch for which the population is to be generated, and so is the future scenario parameter. In the impactors section, only the one source type that is currently being processed is switched on. All other impactors are switched off, such as meteoroids, clouds or the other source types. The other input parameters for MASTER differ, depending on which kind of information is requested.

The debris density for the altitude slices within one altitude region is queried by running MASTER in the 'spatial density' mode. The corresponding output file will contain the density over altitude distribution (for the selected source type, future scenario and epoch).

The density table (sec. A.2) is generated in two steps, making use of the 'target orbit' mode of MASTER. First, the MASTER is executed for every altitude step to determine the diameter distribution of debris at every altitude step. Secondly, MASTER is executed for every altitude step and diameter class to obtain the two-dimensional relative distribution over perigee altitude and orbital eccentricity. In both cases, multiple orbital arcs within the respective altitude slice are processed by MASTER, so that a representative amount of data is sampled. If there are n altitude steps and m diameter classes, then a total number of $n(m+1)$ runs of the MASTER program are necessary.

Then, all distributions are normalized. The two-dimensional distributions of the orbital shapes are multiplied with the relative probability of the respective diameter. Finally, the now three-dimensional relative probability table is scaled with the absolute number of objects on the altitude slice, forming the density table.

Similarly, the inclination distribution is obtained. But instead of a two-dimensional distribution, the one-dimensional inclination distribution is queried from MASTER. The distribution is valid for the given diameter range and altitude slice. Once again, the distribution is normalized and scaled with the absolute number of objects on the altitude slice.

B Impact of Mission Parameters on the Performance

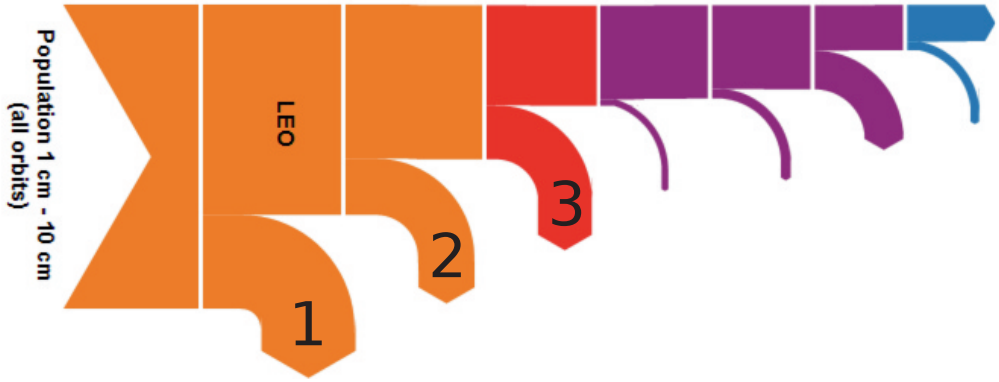

	Filter	Driver Qty.	Limits	Improve by	See
1	LEO/non-LEO	mission concept	near-Earth space	Add GEO sweeper. (Requires additional study.)	pp. 11,54f
2	crossing laser altitude	a_L, e_L	extreme e_L cuts reachability (3)	• Tune H_L to altitude of the maximum debris density. • Increase e_L. • Perform altitude-changing manoeuvres. • Deploy multiple lasers on different altitudes.	sec. 3.2.3
3	reachability	R_{max}, mission duration	$10\,km \leq R_{max}$ $R_{max} \leq 50\,km$	• Increase R_{max}. • Increase mission duration. • Deploy multiple lasers.	sec. 3.2.3 sec. 4.1

	Filter	Driver Qty.	Limits	Improve by	See
4	low perigee already	r_{Peri}	r_{Peri} $< a_L(1+e_L)$	Increase r_{Peri}. (Objects will be left with a higher residual lifetime.)	sec. 3.3.4 p. 48 Fig. 4.3
5	unfavourable	R_{max}, mission duration		• Increase R_{max}. • Increase mission duration. • Deploy multiple lasers (on the same altitude).	sec. 3.3.4 Fig. 4.4
6	too fast	max. beam tracking velocity (mission duration, i_L, R_{max})	2.4 °/$_s$ to 25 °/$_s$	• Increase maximum beam tracking velocity. • (Tune orbital inclination of laser.) • (Increase mission duration.) • (Increase R_{max}.) • (Deploy multiple lasers.)	sec. 3.3.4 sec. 4.1 sec. 3.3.3
7	not engaged	engagement policy, f		• Optimize engagement policy. • Increase laser power.	sec. 3.4.2 sec. 3.4.3
8	life shortened	f		• Increase laser power.	sec. 3.4.3

Bibliography

[1] H. R. Hertzfeld, A guide to space law terms, George Washington University, Space Policy Institute, Washington, 2012.

[2] European Space Agency, SST System Requirements (Mar 13,2013).

[3] IADC, Report of the IADC activities on space debris mitigation measures. URL http://www.iadc-online.org/Documents/IADC-UNCOPUOS-final.pdf

[4] D. A. Vallado, Fundamentals of astrodynamcis and applications, Space technology series, McGraw-Hill, New York [u.a.], 1996.

[5] E. Messerschmid, S. Fasoulas, Raumfahrtsysteme: Eine Einführung mit Übungen und Lösungen, 4th Edition, Springer, Heidelberg [u.a.], 2011.

[6] Debi Shoots, Orbital Debris Quaterly News (October 2014).

[7] Union of Concerned Scientists, UCS Satellite Database: includes launches through 7/31/14 (2014).
URL https://s3.amazonaws.com/ucs-documents/nuclear-weapons/sat-database/7-31-14+update/UCS_Satellite_Database_8-1-14.xls

[8] D. J. Kessler, B. G. Cour-Palais, Collision frequency of artificial satellites: The creation of a debris belt, Journal of Geophysical Research 83 (A6) (1978) 2637. doi:10.1029/JA083iA06p02637.

[9] J.-C. Liou, N. L. Johnson, N. M. Hill, Controlling the growth of future LEO debris populations with active debris removal, Acta Astronautica 66 (5-6) (2010) 648–653. doi:10.1016/j.actaastro.2009.08.005.

[10] L. Innocenti, Clean Space - Guaranteeing the future of space activities by protecting the environment, in: European conference on on-orbit satellite servicing and active debris removal, 2012.

[11] C. R. Phipps, L' ADROIT - A spaceborne ultraviolet laser system for space debris clearing, Acta Astronautica 104 (1) (2014) 243–255. doi:10.1016/j.actaastro.2014.08.007.

[12] Dantor, Satellite lifetime dependent on orbit high (2007).
URL http://commons.wikimedia.org/wiki/File:Satlifetimerp.png

[13] European Space Agency, Hypervelocity impact (2013).
URL http://www.esa.int/var/esa/storage/images/esa_multimedia/images/2013/hypervelocity_impact/12635239-1-eng-GB/Hypervelocity_Impact.png

[14] E. Messerschmid, R. Bertrand, Space stations: Systems and utilization, Springer, Berlin and New York, 1999.

[15] J.-C. Liou, A. Rossi, H. Krag, Raj, M. X. James, A. K. Anilkumar, T. Hanada, H. G. Lewis, Stability of the future LEO environment: IADC-12-08 (January 2013).
URL http://www.iadc-online.org/Documents/

[16] NASA, Guidelines and assessment procedures for limiting orbital debris (August 1995).

[17] International Academy of Astronautics, Position paper on space debris mitigation: Implementing zero debris creation zones (October 15, 2005).

[18] IADC, IADC space debris mitigation guidelines (September 2007).

[19] L. Anselmo, C. Portelli, R. Crowther, R. Tremayne-Smith, F. Alby, H. Baccini, C. Bonnal, D. Alwes, W. Flury, R. Jehn, H. Klinkrad, European code of conduct for space debris mitigation, Henry L. Stimson Center, Washington, D.C, 2004.

[20] T. S. Kelso, Analysis of the 2007 Chinese ASAT test and the impact of its debris on the space environment, in: Advanced Maui optical and space

surveillance technologies (AMOS) conference, 2007.
URL http://celestrak.com/publications/AMOS/2007/AMOS-2007.pdf

[21] J. Utzmann, Security in space at Airbus DS: E-Mail (October 6, 2014).

[22] J.-C. Liou, An active debris removal parametric study for LEO environment remediation, Advances in Space Research 47 (11) (2011) 1865–1876. doi:10.1016/j.asr.2011.02.003.

[23] C. Bonnal, J.-M. Ruault, M.-C. Desjean, Active debris removal: recent progress and current trends, Acta Astronautica 85 (2013) 51–60. doi:10.1016/j.actaastro.2012.11.009.

[24] J.-C. Liou, The top 10 questionsfor active debris removal, in: 1st European workshop on active debris removal, 2010.
URL http://ntrs.nasa.gov/archive/nasa/casi.ntrs.nasa.gov/20100025507.pdf

[25] B. Weeden, Overview of the legal and policy challenges of orbital debris removal, Space Policy 27 (1) (2011) 38–43. doi:10.1016/j.spacepol.2010.12.019.

[26] A. Soucek, Active space debris removal and export control, in: C. Bonnal (Ed.), 3rd European workshop on space debris modelling and remediation, 2014.

[27] L. J. Smith, Legal challenges of OOS and ADR liability: An overview, in: European conference on on-orbit satellite servicing and active debris removal, 2012.

[28] D. Reintsema, J. Thaeter, A. Rathke, W. Naumann, P. Rank, J. Sommer, DEOS – The german robotics approach to secure and de-orbit malfunctioned satellites from low Earth orbits, in: International symposium on artificial intelligence, robotics and automation in space (i-SAIRAS), 2010.

[29] B. Chamot, M. Richard, A. Ivanov, V. Gass, C. Nicollier, CleanSpace One project, in: European conference on on-orbit satellite servicing and active debris removal, 2012.

[30] C. Pardini, T. Hanada, P. H. Krisko, Benefits and risks of using electrodynamic tethers to de-orbit spacecraft, Acta Astronautica 64 (5-6) (2009) 571–588. doi:10.1016/j.actaastro.2008.10.007.

[31] S.-I. Nishida, S. Kawamoto, Y. Okawa, F. Terui, S. Kitamura, Space debris removal system using a small satellite, Acta Astronautica 65 (1-2) (2009) 95–102. doi:10.1016/j.actaastro.2009.01.041.

[32] M. M. Castronuovo, Active space debris removal - a preliminary mission analysis and design, Acta Astronautica 69 (9-10) (2011) 848–859. doi:10.1016/j.actaastro.2011.04.017.

[33] M. Andrenucci, P. Pergola, A. Ruggiero, Active removal of space debris - expanding foam application for active debris removal (2011).
URL http://www.esa.int/gsp/ACT/doc/ARI/ARI%20Study%20Report/ACT-RPT-MAD-ARI-10-6411-Pisa-Active_Removal_of_Space_Debris-Foam.pdf

[34] C. Bombardelli, J. Pelaez, Ion beam shepherd for contactless space debris removal, Journal of Guidance, Control, and Dynamics 34 (3) (2011) 916–920. doi:10.2514/1.51832.

[35] S. K. Flegel, J. Gelhaus, M. Möckel, C. Wiedemann, D. Kempf, Maintenance of the ESA MASTER model: Final report (2011).

[36] C. R. Phipps, M. Birkan, W. L. Bohn, H.-A. Eckel, H. Horisawa, T. Lippert, M. Michaelis, Y. Rezunkov, A. Sasoh, W. O. Schall, S. Scharring, J. Sinko, Laser-ablation propulsion: Review, Journal of Propulsion and Power 26 (4) (2010) 609–637. doi:10.2514/1.43733.

[37] C. R. Phipps, J. R. Luke, D. Funk, D. Moore, J. Glownia, T. Lippert, Laser impulse coupling at 130fs, Applied Surface Science 252 (13) (2006) 4838–4844. doi:10.1016/j.apsusc.2005.07.079.

[38] C. R. Phipps (Ed.), Laser ablation and its applications, Springer Series in Optical Sciences, Springer US, 2007.

[39] H. Hügel, T. Graf, Laser in der Fertigung: Strahlquellen, Systeme, Fertigungsverfahren: mit 400 Abbildungen, 2nd Edition, Studium, Vieweg + Teubner, Wiesbaden, 2009.

[40] C. R. Phipps, J. R. Luke, G. G. McDuff, T. Lippert, Laser-ablation-powered mini-thruster, in: International symposium on high-power laser ablation 2002, SPIE Proceedings, SPIE, 2002, pp. 833–842. doi:10.1117/12.482038.

[41] C. R. Phipps, Description of the Photonic Associates "LPT" thruster (2009). URL http://photonicassociates.com/LPT.pdf

[42] C. R. Phipps, M. M. Michaelis, NEO-LISP: Deflecting near-Earth objects using high average power, repetitively pulsed lasers, in: 23rd European conference on laser interaction with matter, 1994.

[43] A. M. Rubenchik, C. P. J. Barty, R. J. Beach, A. C. Erlandson, J. A. Caird, C. R. Phipps, Laser systems for orbital debris removal, in: International symposium on high power laser ablation 2010, AIP Conference Proceedings, AIP, 2010, pp. 347–353. doi:10.1063/1.3507120.

[44] C. R. Phipps, K. L. Baker, S. B. Libby, D. A. Liedahl, S. S. Olivier, L. D. Pleasance, A. M. Rubenchik, J. E. Trebes, E. V. George, B. Marcovici, J. P. Reilly, M. T. Valley, Removing orbital debris with pulsed lasers, in: International symposium on high power laser ablation 2012, AIP Conference Proceedings, American Institute of Physics, 2012, pp. 468–480. doi:10.1063/1.4739901.

[45] C. R. Phipps, K. L. Baker, S. B. Libby, D. A. Liedahl, S. S. Olivier, L. D. Pleasance, A. M. Rubenchik, J. E. Trebes, E. Victor George, B. Marcovici, J. P. Reilly, M. T. Valley, Removing orbital debris with lasers, Advances in Space Research 49 (9) (2012) 1283–1300. doi:10.1016/j.asr.2012.02.003.

[46] A. M. Rubenchik, A. C. Erlandson, D. A. Liedahl, Laser system for space debris cleaning, in: International symposium on high power laser ablation 2012, AIP Conference Proceedings, American Institute of Physics, 2012, pp. 448–455. doi:10.1063/1.4739899.

[47] C. R. Phipps, J. P. Reilly, ORION: clearing near-Earth space debris in two years using a 30-kW repetitively-pulsed laser, in: XI International symposium on gas flow and chemical lasers and high power laser conference, SPIE Proceedings, SPIE, 1997, pp. 728–731. doi:10.1117/12.270174.

[48] C. R. Phipps, J. Sinko, Applying new laser interaction models to the ORION problem, in: International symposium on high power laser ablation 2010, AIP Conference Proceedings, AIP, 2010, pp. 492–501. doi:10.1063/1.3507138.

[49] S. Bartosz, C. Jacquelard, Cleanspace: Time for laser debris removal strategy.
URL http://www.clean-space.eu/

[50] Clean-Space, Cleanspace - Small debris removal by laser illumination and complementary technologies: Leaflet.
URL http://www.clean-space.eu/uploads/63_bd1e7e6f7.jpg

[51] J. D. Metzger, R. J. Leclaire, S. D. Howe, K. C. Burgin, Nuclear-powered space debris sweeper, Journal of Propulsion and Power 5 (5) (1989) 582–590. doi:10.2514/3.23193.

[52] W. O. Schall, Removal of small space debris with orbiting lasers, in: High-power laser ablation, SPIE Proceedings, SPIE, 1998, pp. 564–574. doi:10.1117/12.321602.

[53] W. O. Schall, Laser radiation for cleaning space debris from lower Earth orbits, Journal of Spacecraft and Rockets 39 (1) (2002) 81–91. doi:10.2514/2.3785.

[54] I. Bekey, Project ORION: orbital debris removal using ground-based sensors and lasers, in: 2n European conference on space debris, ESA Publications Division, Noordwijk, 1997.

[55] C. R. Phipps, J. R. Luke, Laser space propulsion: Applications at two extremes of laser power, in: C. R. Phipps (Ed.), Laser ablation and its applications, Springer Series in Optical Sciences, Springer US, 2007, pp. 407–433.

[56] C. R. Phipps, G. Albrecht, H. Friedman, D. Gavel, E. V. George, J. Murray, C. Ho, W. Priedhorsky, M. M. Michaelis, J. P. Reilly, ORION: Clearing near-Earth space debris using a 20-kW, 530-nm, Earth-based, repetitively pulsed laser, Laser and Particle Beams 14 (01) (1996) 1. doi:10.1017/S0263034600009733.

[57] Naval Research Laboratory, KrF laser development (January 2011).
URL http://fire.pppl.gov/IFE_NAS2_KrF3_Technology.pdf

[58] H.-A. Eckel, Discussion on feasability and key parameters of active debris removal with space-based lasers (July 11, 2013).

[59] M. Schmitz, S. Fasoulas, J. Utzmann, Performance model for space-based laser debris sweepers, Acta Astronautica 115 (2015) 376–383. doi:10.1016/j.actaastro.2015.05.032.

[60] M. N. Quinn, R. Soulard, Space-based laser debris sweepers and the ICAN laser: Conversation (June 17, 2014).

[61] Genreal Assembly of the United Nations, Convention on registration of objects launched into outer space: General assembly resolution 3235 (XXIX) (11/12/1974).

[62] C. Levit, W. Marshall, Improved orbit predictions using two-line elements, Advances in Space Research 47 (7) (2011) 1107–1115. doi:10.1016/j.asr.2010.10.017.

[63] J. Utzmann, Gespräch über Genauigkeit zukünftiger Kataloge (SSA) (09/22/2014).

[64] J. Gelhaus, S. K. Flegel, C. Wiedemann, Program for radar and optical observation forecasting: Final report (May 12, 2011).

[65] Martyn Corden, Consistency of floating point results: or Why doesn't my application always give the same answer? (March 2008).
URL http://www.nccs.nasa.gov/images/FloatingPoint_consistency.pdf

[66] M. Schmitz, Tools and Numerical Codes for the Simulation of Space-Based Laser Debris Removal: Comprehensive Software Documentation (2016).

[67] S. Scharring, J. M. Peter, D. J. Förster, H.-A. Eckel, Modellierungskonzepte zur laser-induzierten Ablation für den MICROLAS-Antrieb, in: H.-A. Eckel (Ed.), Workshop Mikroantriebe, Stuttgart, 2013.

[68] S. Fasoulas, Energiesysteme für die Raumfahrt: Manuskript zur gleichnamigen Vorlesung (April 2012).

[69] J.-C. Liou, Modelling the large and small orbital debris populations for environment remediation, in: C. Bonnal (Ed.), 3rd European workshop on space debris modelling and remediation, 2014.

[70] P. J. Dolado, B. Revelin, MEDEE - Modeling the evolution of space debris in Earth environment: How to consolidate statistically the predictions?, in: C. Bonnal (Ed.), 3rd European workshop on space debris modelling and remediation, 2014.

[71] C. Pardini, L. Anselmo, Review of the uncertainty sources affecting the long-term predictions of space debris evolutionary models, in: C. Bonnal (Ed.), 3rd European workshop on space debris modelling and remediation, 2014.

[72] D. A. Liedahl, A. M. Rubenchik, S. B. Libby, S. Nikolaev, C. R. Phipps, Pulsed laser interactions with space debris: Target shape effects, Advances in Space Research 52 (5) (2013) 895–915. doi:10.1016/j.asr.2013.05.019.

[73] D. A. Liedahl, S. B. Libby, A. M. Rubenchik, C. R. Phipps, Momentum transfer by laser ablation of irregularly shaped space debris, in: International symposium on high power laser ablation 2010, AIP Conference Proceedings, AIP, 2010, pp. 772–779. doi:10.1063/1.3507171.

[74] R. Soulard, M. N. Quinn, T. Tajima, G. Mourou, ICAN: A novel laser architecture for space debris removal, Acta Astronautica 105 (1) (2014) 192–200. doi:10.1016/j.actaastro.2014.09.004.

[75] C. Jacquelard, CLEANSPACE: Small debris removal by laser illumination and complementary technologies, in: C. Bonnal (Ed.), 3rd European workshop on space debris modelling and remediation, 2014.